Physics by Geometry

Unit 2. Vibration, Resonance, and Wave Motion

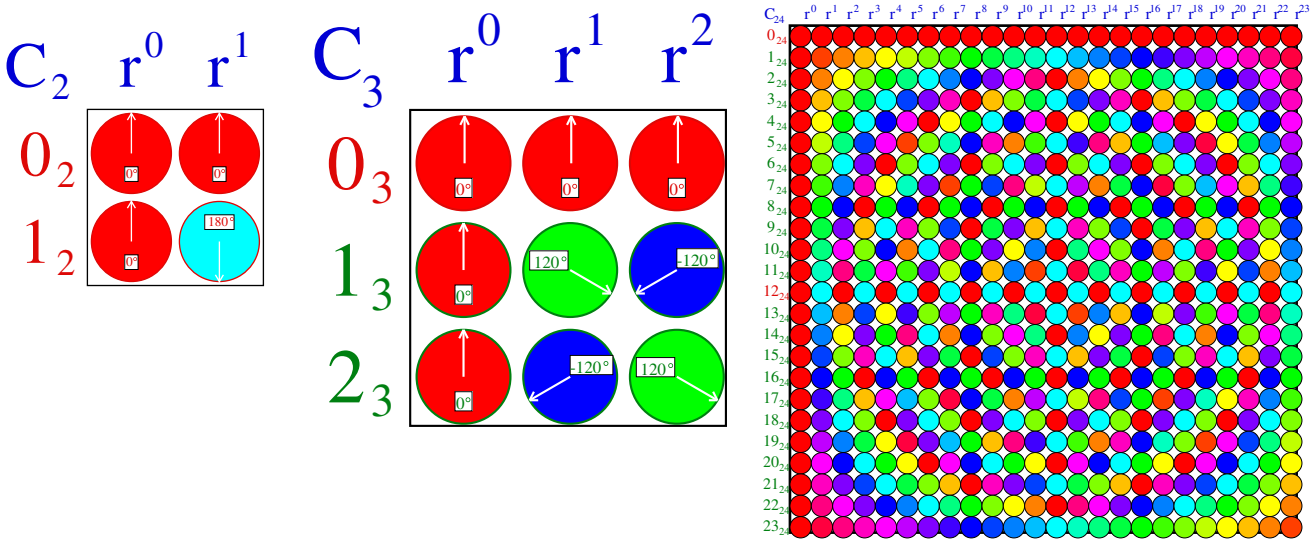

An Honors Course of Study

by

Bill Harter

Department of Physics

University of Arkansas

Fayetteville

Hardware and Software by

HARTER-Soft

Elegant Educational Tools Since 2001

Road Map for Physics Colloquium (3/25/03)-version

Euclid-Aristotelean World

Newton-Hamilton Classical World

(Think Bang-Bang particles ! Waves are Illusory.)

Concepts and Effects

Velocity (1-and-2-particles)
Momentum (1-and-2-particles)

Kinetic Energy
Potential Energy
Force
Force & PE Fields
(n-particles)
Friction

Ways to visualize

Velocity-velocity plots
Space-time and space-space
Energy shell (ellipse)
Matrix rotation & reflection
F versus space
PE versus space

Multi-velocity diagrams

Maxwell-Lorentz View of Classical and Quantum Worlds

(Think resonance! Nature works by persuasion)

Vibration
Action and phase
Hysteresis
1-Particle resonance
2-Particle resonance
n-Particle resonance (Waves)

Wave dispersion

Phasors
Momentum versus coordinate plot
F versus time & work plots
Lorentzian functions
Smith charts

Multiple Phasors

Frequency vs. wavevector plots

Einstein-Planck Relativity-Quantum World

(Think waves! Particles are Illusory.)

Space-Time by Wave Interference
Doppler shifts tell all
Energy Momentum Dispersion
Matter waves vs. No-Matter waves
What is matter?
Why Schrodinger was wrong
Waves in accelerated frames
Waves in nano-structures
Spin and quantum angular momentum
Correlation ("Entanglement")
Bose vs. Fermi

Minkowski Spacetime graph
Hyperbolic geometry
Epstein x-proper time graph

Dispersion graphs
Wavevector geometry
Angular momentum cones
RE surfaces

The U(2) spinor slide rule

Euclid to Einstein and Beyond: Geometry and Physics

UNIT 2. VIBRATION, RESONANCE AND WAVE MOTION 5

Unit 2. Vibration, Resonance and Wave Motion

Introduction

Unit 1 began with a car crash. Bang! Wham! Pow! Two superballs careen off each other onto the floor or ceiling. Huge forces quickly transfer enormous amounts of momentum and energy between the participants. Seeing this may be a little like watching violent US movies and TV. It looks like the world is just a lot of punching bags endlessly pounding each other.

Now we consider a view of the world that is more like French and English movies. Here the participants rarely if ever actually hit each other. Instead they sit for long periods of thought and reflection and engage in the gentle art of persuasion and being persuaded.

Thought! Reflection!? Mon Dieu! How unpatriotic! But, as we hope to show, this is a far better analogy for picturing the physics of the world than is an endless series of boring car crashes. The gentle art of persuasion found deep inside our physics is called *resonance* and resonance is the single most important physical process in the entire world, as we presently know it. Let's think about it.

We hear by resonance, we speak using resonance, and we see only by having delicate resonant processes in our eyes. Without resonance to amplify tiny vibrating forces, we are blind, deaf, and dumb. Resonance has been necessary to run our AC power grid. Communications have relied on resonance since early telegraphs. Without resonance there are no radios, radar, computers, TV (God forbid!), or cell phones. (God doubly forbid!) Recently, ultra-accurate clocks and the GPS (global positioning system) rely on resonant process of unimaginable quality and finesse.

Still, all that is not the half of it. What this unit is preparing are ways to see the role of resonance at the fundamental quantum level where everything, and we do mean *every*thing is resonating. Simply put, if something doesn't resonate, it just doesn't exist! So here we will also be introducing the most basic process of *quantum* or *Planck-DeBroglie mechanics*. We start by using classical coupled pendulums as one of our many analogies to quantum resonance.

Resonance requires oscillation. The simplest oscillation is *harmonic oscillation*, that is, oscillation whose frequency is the same for all amplitudes. So, the simplest resonance requires harmonic oscillation. Otherwise, it's usually too hard to stay in tune! Our inside-Earth-orbiting neutron starlet (Sec. 1.6(e)) and inside-asteroid-orbiting "astroidonaut" did harmonic oscillation as do sub-superballs with linear force functions $F(\mathbf{r})=-k\mathbf{r}$. (Recall, that linear-force RumpCo. sub-balls refuse to make car-crashes spectacular in Fig. 1.7.7. They're looking for some loving resonance, not just a bang!)

As we will see resonance can give a response millions or billions of times more than one lousy bang. The whole world depends on this beautiful and fascinating process. So get ready to learn about some things that are very fundamental. Also, prepare to see some very applied physics.

The engineering applications of resonance involve its ability to store and amplify signals, waves, and energy. If the energy comes in the form of sound waves their properties are described by one of the oldest physical sciences, that of *acoustics*. Long before electronic amplifiers were invented, the great churches and concert halls relied on acoustics to design better ways for speakers and performers to be heard. Controlling resonance was and still is an important part of good acoustics.

But even before we could assemble crowds in a hall, we had to evolve ways to speak. Again, resonance is essential. To illustrate this, try to pronounce the word “good” while smiling. You’ll find it much easier to say “bad” with a smile, but the word “good” comes as “gud” or “gad” and more like a Southern drawl than proper English!

The reason for this is that “good” requires a larger lower frequency component that in turn needs the amplification provide by an elongated mouth formed to a tubular resonator. It is unfortunate for all the smiling car dealers, and perhaps the whole human race, that the physics of resonance prevents “good” from coming out right with a smile!

The word “good” sounds fine if one’s mouth is shaped as it is when beginning a kiss! Perhaps reproductive persuasive dynamics trump those of diplomacy in linguistic evolution. Certainly insect, animal, and bird calls use it more for reproductive advantage than for diplomacy or business. These are but a few examples of how our world is built on resonant processes that are often not so obvious.

But, at the deepest levels of nature resonance seems to be the main game in town. And unlike practically any game we’ve ever imagined this one seems, at first, less obvious than anything ever has been before! But after you see how it works you will wonder why it took us so long to “get it.”

So get ready for the first secrets of the ultimate cosmic quantum game.

-- The Purest Light and a Resonance Hero – Ken Evenson (1932-2002) --

When travelers punch up their GPS coordinates they owe a debt of gratitude to an under sung hero who, alongside his colleagues and students, often toiled 18 hour days deep inside a laser laboratory lit only by the purest light in the universe.

Ken was an "Indiana Jones" of modern physics. While he may never have been called "Montana Ken," such a name would describe a real life hero from Bozeman, Montana, whose extraordinary accomplishments in many ways surpass the fictional characters in cinematic thrillers like *Raiders of the Lost Arc*.

Indeed, there were some exciting real life moments shared by his wife Vera, one together with Ken in a canoe literally inches from the hundred-foot drop-off of Brazil's largest waterfall. But, such outdoor exploits, of which Ken had many, pale in the light of an in-the-lab brilliance and courage that profoundly enriched the world.

Ken is one of few researchers and perhaps the only physicist to be twice listed in the *Guinness Book of Records*. The listings are not for jungle exploits but for his lab's highest frequency measurement and for a speed of light determination that made *c* many times more precise due to his lab's pioneering work with John Hall in laser resonance and metrology†.

The meter-kilogram-second (mks) system of units underwent a redefinition largely because of these efforts. Thereafter, the speed of light *c* was set to $299{,}792{,}458 ms^{-1}$. The meter was defined in terms of *c*, instead of the other way around since his time precision had so far trumped that for distance. Without such resonance precision, the Global Positioning System (GPS), the first large-scale wave space-time coordinate system, would not be possible.

Ken's courage and persistence at the Time and Frequency Division of the Boulder Laboratories in the National Bureau of Standards (now the National Institute of Standards and Technology or NIST) are legendary as are his railings against boneheaded administrators who seemed bent on thwarting his best efforts. Undaunted, Ken's lab painstakingly exploited the resonance properties of metal-insulator diodes, and succeeded in literally counting the waves of near-infrared radiation and eventually visible light itself.

Those who knew Ken miss him terribly. But, his indelible legacy resonates today as ultra-precise atomic and molecular wave and pulse quantum optics continue to advance and provide heretofore unimaginable capability. Our quality of life depends on their metrology through the Quality and Finesse of the resonant oscillators that are the heartbeats of our technology.

Before being taken by Lou Gehrig's disease, Ken began ultra-precise laser spectroscopy of unusual molecules such as HO_2, the radical cousin of the more common H_2O. Like Ken, such radical molecules affect us as much or more than better known ones. But also like Ken, they toil in obscurity, illuminated only by the purest light in the universe.

In 2005 the Nobel Prize in physics was awarded to Glauber, Hall, and Hensch†† for laser optics and metrology.

† K. M. Evenson, J.S. Wells, F.R. Peterson, B.L. Danielson, G.W. Day, R.L. Barger and J.L. Hall, Phys. Rev. Letters 29, 1346(1972).

†† *The Nobel Prize in Physics, 2005*. http://nobelprize.org/

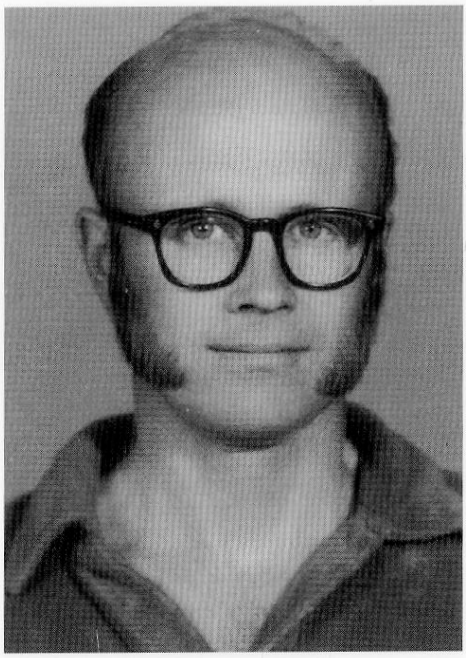

PAULINIA, BRASIL 1976

THE SPEED OF LIGHT IS
299,792,458 METERS PER SECOND!

Kenneth M. Evenson – 1932-2002

Chapter 1 Keep the phase, baby! Resonant energy transfer

Instead of trying to transfer energy in a single bang like a superball collision, let's se how it's done steadily by resonance. Imagine two big pendulum bobs, each of mass $M = 1000\ kg$, hanging from ropes, each of length $L=10\ meters$, and swinging back and forth with an amplitude of $A_1=10\ cm= A_2$, or so. First, let's review the properties of a single pendulum, the common tree swing.

(a) Swing-hi-swing-lo: A pendulum oscillator

If you've ever played with a big tall pendulum you may have noticed how easy it is to push it a little bit off center. (Recall or imagine pushing someone bigger than you on a tall swing.) If you keep pushing off-and-on in synchrony with the swing, pretty soon it's zooming. That's *resonance*! If the swing is very very tall ($L\to\infty$) it's like having a frictionless track. (That's *zero*-frequency resonance!) Resonance frequency ω of an L-long pendulum of mass M depends on its force $F(x)$ or energy $U(x)$ at small distances x off-center. We now do some geometry using energy in Fig. 1.1a and force vectors in Fig. 1.1b.

In Fig. 1.1a, gravity's potential energy Mgh varies with horizontal push distance x as seen by a geometric mean construction. (Recall Fig. 1.6.12(a).) It has a quadratic x-potential for low x. $(x<<L)$

$$U(x) = Mgh = \frac{1}{2}\frac{Mg}{L}x^2 \qquad (1.1)$$

A quadratic potential $U(x)=\frac{1}{2}kx^2$ has the linear force $F(x)=-kx$ of a harmonic oscillator with $k=Mg/L$.

$$F(x) = -\frac{dU(x)}{dx} = -\frac{Mg}{L}x \qquad (1.2)$$

Oscillator *angular* frequency ω follows using the "starlet" formula $\omega=\sqrt{k/m}$ from (1.6.42).

$$\omega = \sqrt{\frac{k}{M}} = \sqrt{\frac{g}{L}} = 2\pi\nu, \qquad \nu = \frac{1}{2\pi}\sqrt{\frac{g}{L}} = \frac{\omega}{2\pi} \qquad (1.3)$$

The frequency ν of an $L=10\ meter$ swing is about $1/6.3\ Hz$, or τ=6.3 *seconds* per swing. It's independent of mass M, and for low x, independent of amplitude x, too. Fat people swing as fast and high as skinny ones. Galileo made a big deal of this, but probably not because he was fat. It's important for resonance to have frequency not change with amplitude. It meant pendulums could (and did) improve clock precision.

In Fig. 1.1b, gravitational pendulum restoring force varies linearly with horizontal push distance x as seen by the vector construction. But, like Fig. 1.1a, it's linear only if amplitude x is a lot smaller than lever length L. While the formula $F(x)=-(Mg/L)x$ for force along the circular path is exact, that path is not linear and distance $x=L\sin\Theta$ never exceeds L. The exact angular force function : $F_\Theta=-Mg\sin\Theta$ is *non*-linear. Only for small angles $(\sin\Theta\sim\Theta)$ does it approach the desired linear one $(F_\Theta\sim-Mg\Theta)$.

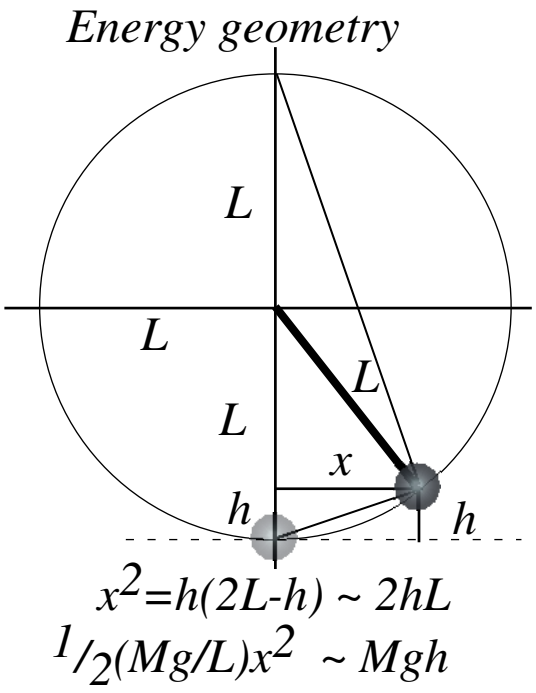

Fig. 1.1(a) Pendulum energy mean geometry

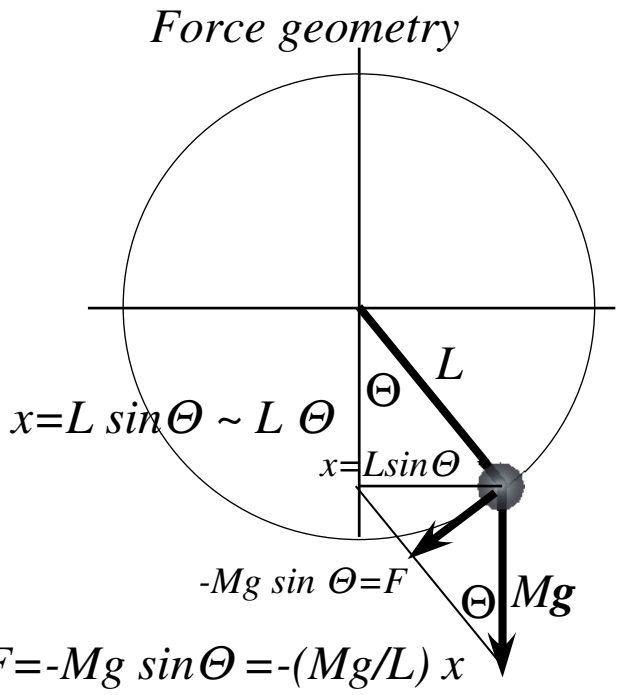

Fig. 1.1(b) Pendulum force vector geometry

(b) Energy transfer: Weakly coupled pendulum oscillators

Imagine we have a pair of identical big and tall swinging pendulums connected by a very weak rubber band or spring as shown in Fig. 1.2 below. How might the tiny spring start to drain energy out of one pendulum and into the other? At what rate is energy transferred? Through this simple example we see a little-appreciated principle of resonance with great and universal significance.

Here we assume the connecting spring constant k_{12} is small as is its transmitted force F_{12}.

$$F_{12} = F_{\text{on 1 due to 2}} = -k_{12}(x_1 - x_2) = -F_{\text{on 2 due to 1}} \qquad (1.4)$$

Each pendulum swings at frequency ω. amplitudes A_1 and A_2 and phases ρ_1 and ρ_2 are approximately constant. Only the phase difference or *relative phase* $\rho = \rho_1 - \rho_2$ is of interest here so we stick it on x_1.

$$x_1 = A_1 \cos(\omega t - \rho)\,, \quad (1.5a) \qquad x_2 = A_2 \cos(\omega t - 0)\,, \quad (1.5b)$$

The results are plotted in Fig. 1.3(a-d) for relative phase angles $\rho = 0°, 70°, 180°,$ *and* $-60°$. Note the differences in the ellipse plots of x_2 *versus* x_1 like orbit plots in Unit 1 Fig. 9.10. Here the area of the ellipse determines the work done by x_2 on x_1. Energy or work is area $\int F_{12}\,dx_1$ under a force function as given by (7.5a) in Unit 1. Here power loop integral $\int F_{12}\,dx_1$ repeats with each oscillator swing cycle giving k_{12} times the area of the $x_2(x_1)$-ellipse. For now we say the k_{12}-spring is too weak for this to have a noticeable effect on amplitudes A_1 or A_2 or phase lag angle ρ. In Ch. 5 we find what that effect is.

Before studying that force and energy dynamics, let us get some plots of the position versus time curves for the two connected pendulums such as are shown in Fig. 1.2. These are just sine (or cosine) curves shifted by their respective phase lags. You should notice that a function *cos(ωt-ρ)* is shifted ρ/ω radians *back* in time. This is unlike most function translation where *f(x-a)* shifts *f(x) forward* by *a* units in *x*. It is due to the fact that we make our clocks go *clockwise* which is a *negative* angular rotation. The phase space plot is made to have positive velocity *V/ω*-axis be *up*.

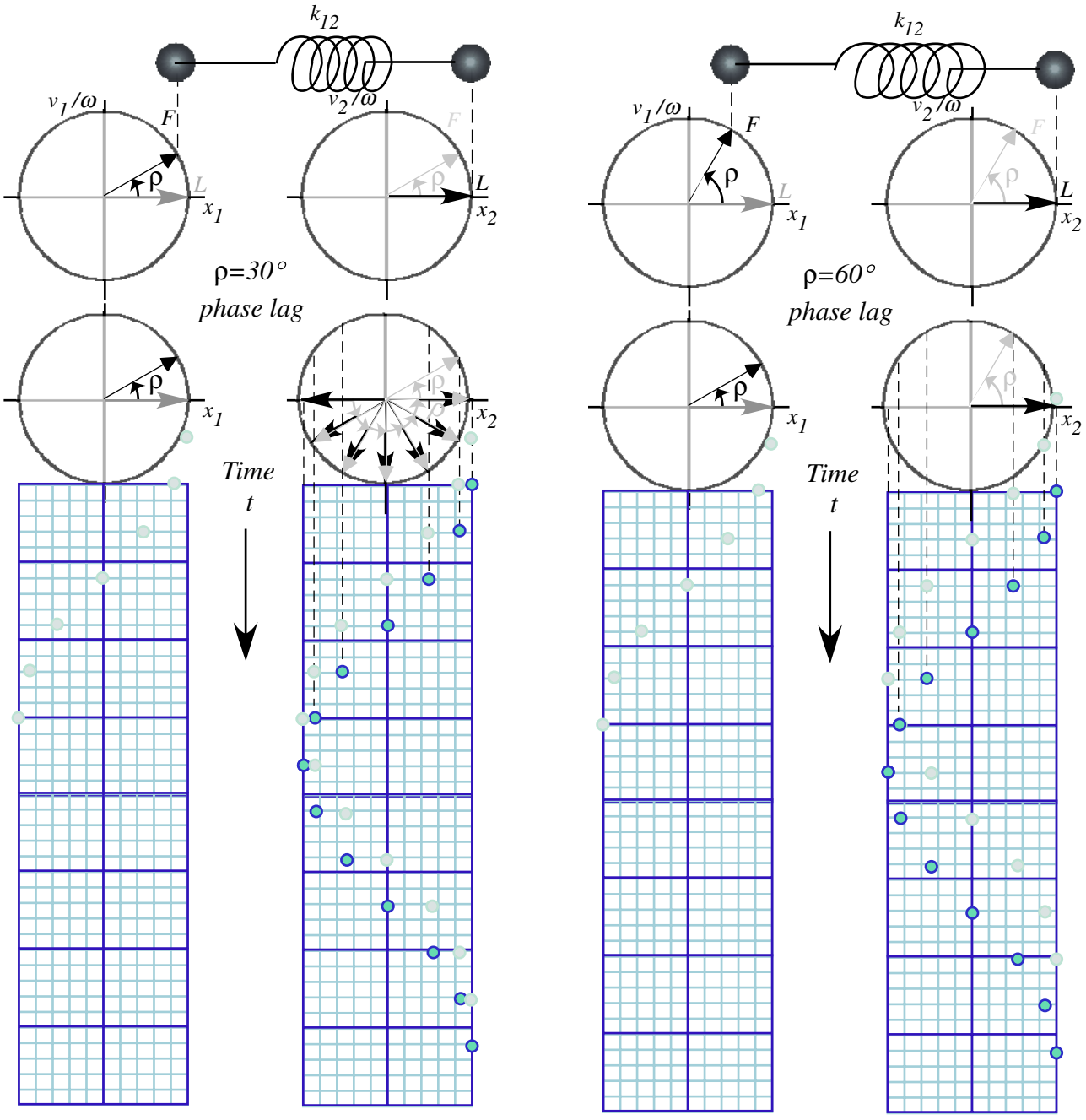

Fig. 1.2 Phasor and time plots of phased pendulum oscillation (a) ρ=30° phase lag, (a) ρ=60° phase lag

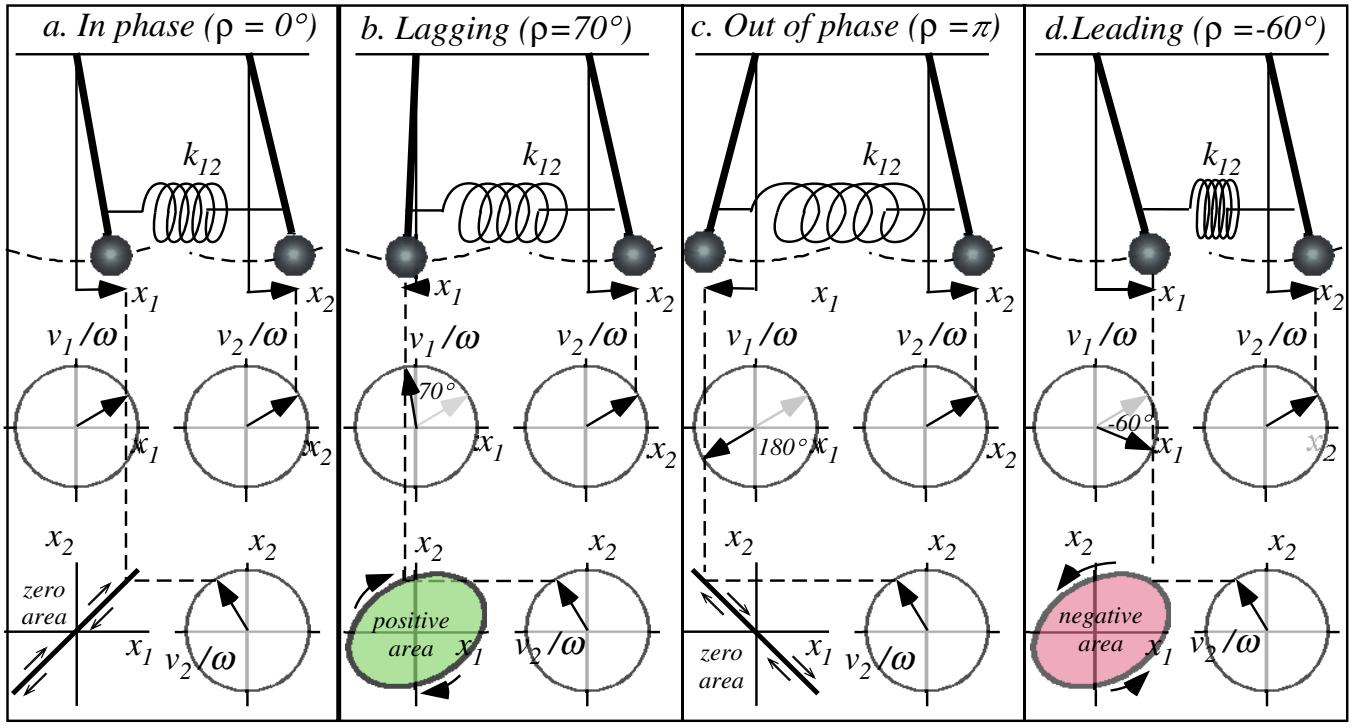

Fig. 1.3 Four classes (a) "in", (b) "lag", (c) "out", (d) "lead" of relative phase for two oscillators.

As long as the big pendulums swing with the same amplitude and phase, they will transfer the same amount of energy each cycle. If x_1's phasor clock lags behind that of x_2 by any angle from $\rho>0$ to $\rho<\pi$, then pendulum-1 gains while pendulum-2 loses, but if x_1's phasor leads $(-\pi>\rho>0)$, then pendulum-1 becomes a donor and pendulum-2 is a receiver of energy. Only for the cases of in-phase motion $(\rho=0)$ in Fig. 1.3(a) or π-out-of-phase motion $(\rho=\pi)$ in Fig. 1.3(c), is no energy transferred.

Zero energy transfer seems strange (particularly for ρ=π) given that the connecting spring is constantly pushing or pulling. Fig. 1.4(a) shows how energy gained during the upstroke is taken back by the return stroke. Only if lag angle is between π and zero, as in Fig. 1.4(b), does the returning spring leave behind some of the energy it gained coming in. ($\int x_2 dx_1$ is minus if x_2 *or else* dx_1 is negative.)

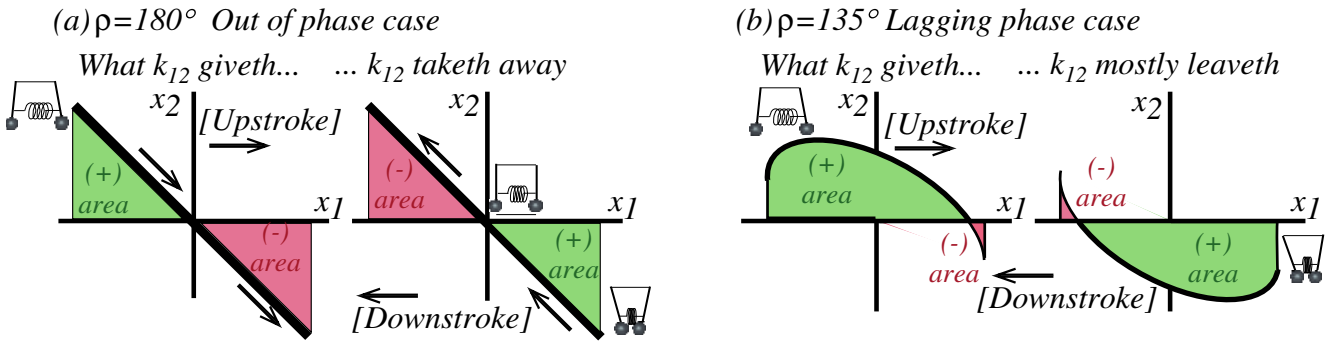

Fig. 1.4 Work-cycle area plots for (a) Out-of-phase (ρ=180°) case (b) Lagging phase (ρ=135°) case.

The phase-lag-sine-sign-rule: To lead takes energy!

If pendulum-1 leads pendulum-2, as in Fig. 1.3(d), its work-cycle area is swept out in an anti-clockwise direction giving an energy deficit for pendulum-1 who now pays pendulum-2 each cycle. The relation between lag angle ρ in (1.5b) and sign and value of energy flow needs to be derived. First, we do an algebraic approach. Work integral $W_{12}(t) = \int F_{12}\,dx_1$ is as follows using (1.4) and (1.5).

$$Work(t)_{on1\,by\,2} = \int F_{on1\,by\,2}dx_1 = \int_0^t F_{12}v_1 dt = \int_0^t -k_{12}(x_1 - x_2)v_1 dt \quad \text{where: } v_1 = \frac{dx_1}{dt} = -A_1\omega\sin(\omega t - \rho) \qquad (1.6a)$$

$$Work(\tau)_{on\,1by\,2} = K - k_{12}A_1A_2\omega\int_0^{2\pi/\omega}\cos(\omega t)\sin(\omega t - \rho)dt = k_{12}\int_0^{2\pi/\omega} x_2 dx_1 \quad \text{where: } \tau = \frac{2\pi}{\omega} \text{ is } period \qquad (1.6b)$$

The *K* term for pendulum-1 integral $\int x_1 dx_1$ is, for a *full period* τ, exactly zero for any phase lag angle ρ.

$$K = k_{12}\omega\int_0^{2\pi/\omega} dt\,A_1^2\cos(\omega t - \rho)\sin(\omega t - \rho) = \frac{1}{2}k_{12}A_1^2\omega\int_0^{2\pi/\omega} dt\sin 2(\omega t - \rho) = 0 \qquad (1.7)$$

Now $\sin(\omega t - \rho) = \sin\omega t\cos\rho - \cos\omega t\sin\rho$ gives a zero integral plus a $\sin\rho$ times an integral $\int_0^{2\pi/\omega}\cos^2\omega t = \pi/\omega$.

$$Work(\tau)_{on\,1by\,2} = -k_{12}A_1A_2\omega\int_0^{2\pi/\omega}\cos(\omega t)(\sin\omega t\cos\rho - \cos\omega t\sin\rho)dt = \pi\,k_{12}A_1A_2\sin\rho \qquad (1.8)$$

Energy flow per cycle goes as a sine of phase lag angle ρ. Compare it to oscillator total energy $\frac{1}{2}A\omega^2$.

$$Energy_{pendulum1} = \frac{1}{2}k_1A_1^2 = \frac{1}{2}M\omega^2A_1^2 \qquad (1.9a) \qquad Energy_{pendulum\,2} = \frac{1}{2}k_2A_2^2 = \frac{1}{2}M\omega^2A_2^2 \qquad (1.9a)$$

Power transfer is work-per-cycle (1.8) times number of cycles per second or frequency $\nu = 2\pi\omega$.

$$Power_{to\ 1from\ 2} = 2\pi^2\,\omega\,k_{12}A_1A_2\sin\rho \qquad (1.10)$$

Such a sweet and powerful relation deserves a geometric construction. An attempt is made in Fig. 1.5 for the case of equal amplitudes $A_1 = A = A_2$. Each step draws a different time snapshot in a cycle in which "Follower" pendulum-1 lags behind the "Leader" pendulum-2 by a constant angle $\rho = 60°$. At first, the fearless Leader *L* is stationary $(v_2 = 0)$ at its maximum righthand point $x_2 = A$ and tugging on Follower *F* who is back at $x_1 = A\cos\rho$ with velocity $v_1 = A\omega\sin\rho$. A little later at time $t = \rho/2\omega$ the Leader is starting back with velocity $v_2 = -A\omega\sin\rho/2$ at $x_2 = A\cos\rho/2$. Then x_2 equals the off-center distance $x_1 = A\cos\rho/2$ of the follower who is coming forward with velocity $v_2 = +A\omega\sin\rho/2$. This is the work-ellipse $+45°$ apogee point at major axis $a = \sqrt{2}A\cos\rho/2$. There the k_{12} spring stops pulling and starts pushing. Later at $t = \rho/\omega$ comes a $-45°$ perigee point or minor axis $b = \sqrt{2}A\sin\rho/2$. The area of the resulting ellipse is πab. Work is k_{12} times this.

$$Work(\tau)_{on\,1by\,2} = k_{12}\,\pi ab = k_{12}\,\pi\,2A^2\sin\rho/2\cos\rho/2 = \pi\,k_{12}\,A^2\sin\rho \qquad (1.11)$$

This geometric result equals the algebraic one in (1.8) for $A_1 = A = A_2$. But, how do we do a $A_1 \neq A_2$ case?

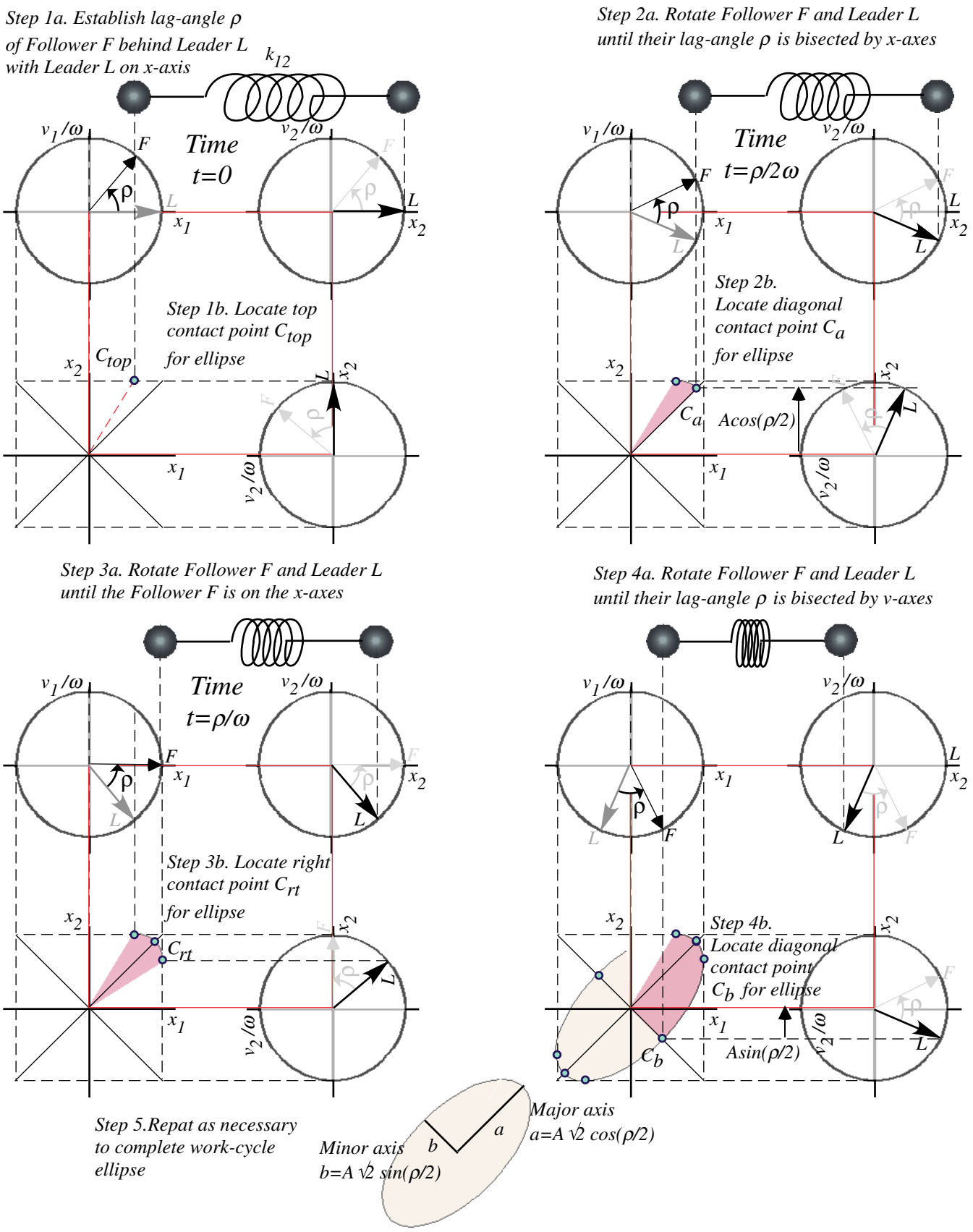

Fig. 1.5 Work-cycle geometry for two weakly-coupled oscillators

Also, shouldn't work stop increasing and start decreasing after the apogee when $k_{12}(x_1-x_2)$ goes negative? These two questions are related and help us understand an oscillator energy shell game that might seem, at first, to be as convoluted as an Enron accounting scandal.

First, the $Work(\tau)_{on\,1by\,2}$ expression averages a *whole period* $\tau=2\pi/\omega$ ignoring *W* fluctuations.

$$Work(t)_{on\,1\,by\,2} = k_{12}\int_0^t x_2 dx_1 - k_{12}\int_0^t x_1 dx_1 \;= k_{12}\int_0^t x_2 dx_1 - k_{12}\frac{x_1^2}{2} \qquad (1.12)$$

The *K*-term $K = k_{12}\int x_1 dx_1 = -k_{12}x_1^2/2$ in (1.6b) adds an oscillation to the elliptic loop area $A = k_{12}\int x_2 dx_1$ as seen in Fig. 1.6 below. $Work(t)_{on\,1\,by\,2}$ in (1.12) has both *K* and *A* terms. The *K*-term subtracts a *45°* right triangle just so that when $k_{12}(x_1-x_2)$ changes sign, as it's doing in Fig. 1.6(a), so also does the growth of instantaneous work $W=K+A$. Total work *W* goes down briefly as it is in Fig. 1.6(b) even as ellipse area *A* is still growing, but then the thieving *K*-triangle spits back its area in Fig. 1.6(c) and *A* starts grabbing area below the x_1 axis in Fig. 1.6(d). Together this makes *W* surge ahead in Fig. 1.6(e). Then *K* again eats some more area but again spits it back. But, finally the effect of *K* for a full period is *zero*.

Elliptical area-sweeping represented by *A* or *W* does not accumulate area at a constant rate like the Kepler area sweeps in (1.16) below that are *angular* sweeps by a *radius* line. Here the *A*-sweep in Fig. 1.5 is by a Cartesian *vertical* $x_2=y$-line. The *A*-sweep first gobbles area voraciously and then gives some back and then becomes voracious again but has to give some back, again, during each period. This bi-cyclic binge-and-purge behavior of *A* is tempered somewhat by the thieving *K*-triangle which partially "starves" *A* and spits energy back with almost, but not quite, the same bi-cyclic schedule.

As we see in Fig. 1.6, *K* is too late each time to make *W* eat its area at a constant rate. To see this with algebra, we work out the *W*-integral (1.6) or (1.12) completely as a function of time.

$$\begin{aligned} Work(t)_{on\,1\,by\,2} &= k_{12}A_1^2\omega\int_0^t \cos(\omega t-\rho)\sin(\omega t-\rho)dt - k_{12}A_1A_2\omega\int_0^t \cos(\omega t)\sin(\omega t-\rho)dt \\ &= k_{12}A_1A_2\frac{\omega t}{2}\sin\rho + k_{12}\frac{A_1A_2}{4}\cos(2\omega t-\rho) - k_{12}\frac{A_1^2}{4}\cos(2\omega t-2\rho) + const. \end{aligned} \qquad (1.13)$$

(The constant term is $k_{12}(A_1^2-A_1A_2)/4$.). The first term is the constant area growth that a Kepler ellipse might predict. With $A_1=A_2$, the oscillating terms might cancel each other were not that the *K*-part (last term) is late by 2ρ or *twice* the phase lag ρ of follower x_1 and the other term. So feast-to-famine is unavoidable.

Finally, let us see how geometry treats the case of unequal $(A_1\neq A_2)$ amplitudes. We have been plotting force F_{12} versus x_1 to represent work by area under the curve. It happened that the force was proportional to the coordinate x_2 so we plotted that instead. But, when you plot things of different dimension you may scale them however you wish. This means you can turn what might have been an ellipse into a circle as we do for our phasor plots. We may do the same with F_{12} versus x_1 plots.

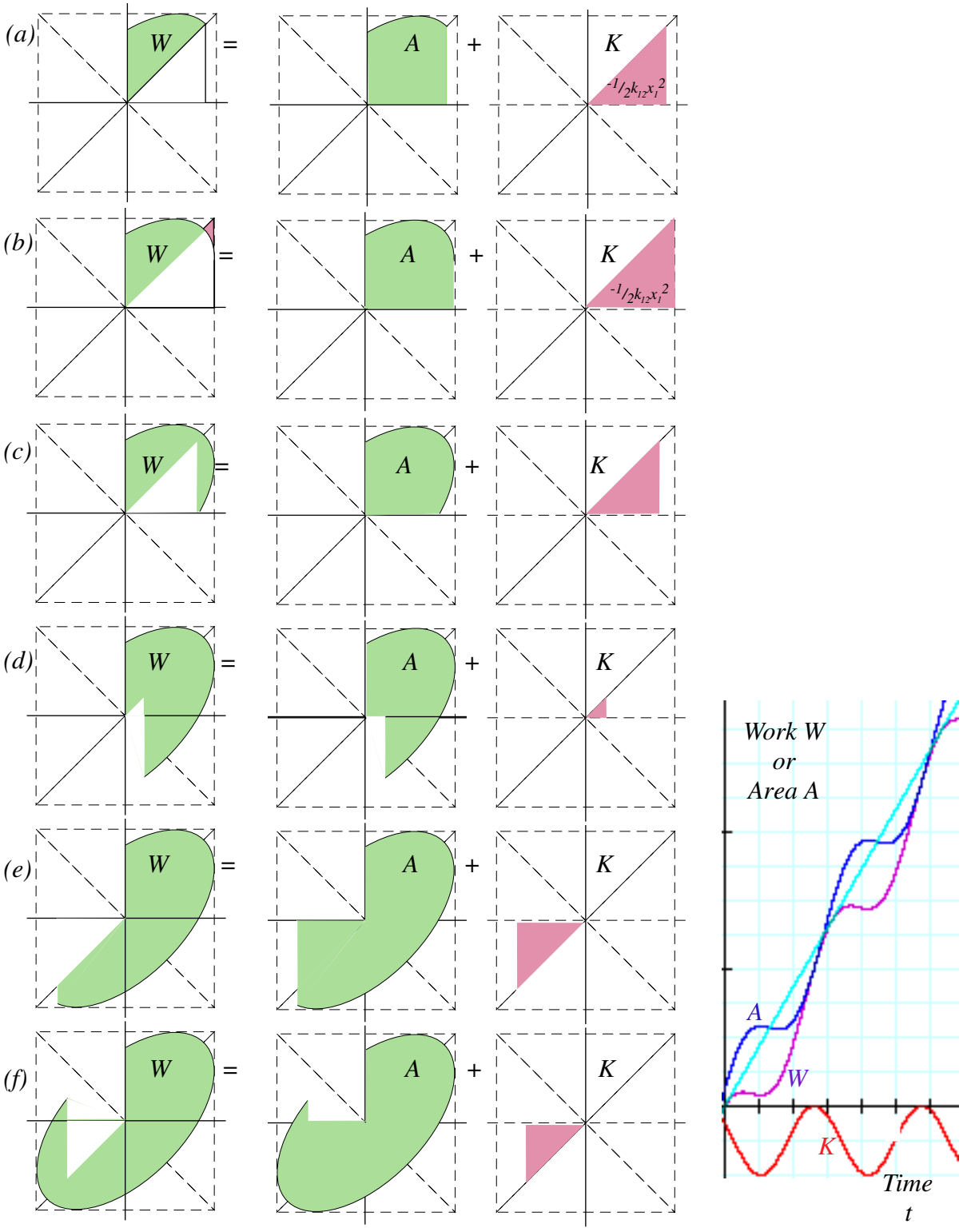

Fig. 1.6 Work-area F_{12} versus x_1 plot-W made from sum of x_2 versus x_1 plot A and x_1 versus x_1 plot K.

An ellipse-in-a-square has its axes on the ±45° diagonals of the square. But, rescaling a dimension of an ellipse-in-a-square results in an ellipse-in-a-rectangle whose axes are *not* on a rectangle diagonal.

This is shown by Fig. 1.7(b) in which the A_1 amplitude is twice that of the A_2 amplitude, and the ellipse axis is clearly off the rectangle's diagonal. Calculating the new ellipse inclination is an interesting geometry problem that we will consider below. But, this isn't needed to see that the lag-sine-rule (1.8) is derived by geometry for any amplitude A_1 or A_2. Scaling *one* amplitude scales area by the same amount.

(c) Boxing ellipses

You can put a rectangular box at any angle relative to an ellipse so that all four sides of the box are ellipse tangents as shown in Fig. 1.8. If the ellipse has major-by-minor *(a-by-b)*-radii then the box parallel to ellipse axes is a *(2a-by-2b)*-rectangle as indicated in Fig. 1.8(a). A box tipped at $\varphi=30°$ to the ellipse axes is fatter as shown in Fig. 1.8(b). A box at $\varphi=45°$ to the ellipse axes is a perfect square as shown in Fig. 1.8(c). Note, all boxes in Fig. 1.8 share a diagonal diameter $R=\sqrt{(a^2+b^2)}$ of a circle that inscribes them including the skinniest $\varphi=0°$ *(2a-by-2b)*-box (a) or fattest $\varphi=45°$ $(\sqrt{2}a\text{-by-}\sqrt{2}a)$ box (c).

Another way to view this is to tip the ellipse while keeping it against a corner wall and floor frame as shown in Fig. 1.9. The center of the ellipse stays on a circle of the same radius $R=\sqrt{(a^2+b^2)}$ because total energy must be the same no matter what box frame or φ we use to frame an elliptic orbit. (Energy of an elliptic starlet orbit in Unit 1 Fig. 9.10 is the same viewed from any latitude φ.)

$$\begin{aligned} E &= \frac{1}{2}mv_1^2 + \frac{1}{2}m\omega^2x_1^2 + \frac{1}{2}mv_2^2 + \frac{1}{2}m\omega^2x_2^2 \\ &= \frac{1}{2}m\left(-\omega A_1\sin(\omega t-\rho)\right)^2+\frac{1}{2}m\omega^2\left(A_1\cos(\omega t-\rho)\right)^2+\frac{1}{2}m\left(\omega A_2\sin(\omega t)\right)^2+\frac{1}{2}m\omega^2\left(A_2\cos(\omega t)\right)^2 \\ &= \frac{1}{2}mA_1{}^2\omega^2\left(\sin^2(\omega t-\rho)+\cos^2(\omega t-\rho)\right) + \frac{1}{2}mA_2{}^2\omega^2\left(\sin^2(\omega t)+\cos^2(\omega t)\right) \end{aligned} \quad (1.14)$$

Each φ-ellipse has different box components $x_1=A_1\cos(\omega t-\rho)$ and $x_2=A_2\cos(\omega t)$ but the *same total energy*.

$$E=\frac{1}{2}m\omega^2\left(A_1{}^2+A_2{}^2\right)=\frac{1}{2}m\omega^2R^2=\frac{1}{2}m\omega^2\left(a^2+b^2\right) \quad (1.15)$$

Each φ-ellipse orbit also has constant *angular momentum* $L=|\mathbf{rxp}|=m|\mathbf{rxv}|$.

$$\begin{aligned} L &= mx_1v_2 - mx_2v_1 \\ &= m\left(A_1\cos(\omega t-\rho)\right)\left(-\omega A_2\sin(\omega t)\right)-m\left(A_2\cos(\omega t)\right)\left(-\omega A_1\sin(\omega t-\rho)\right) \\ &= m\omega A_1A_2\left(\cos(\omega t)\sin(\omega t-\rho)-\sin(\omega t)\cos(\omega t-\rho)\right) = -m\omega A_1A_2\sin\rho \end{aligned} \quad (1.16a)$$

Angular momentum L is proportional to ellipse area πab as is work-per-cycle in the lag-sine-rule (1.8).

$$L=-m\omega A_1A_2\sin\rho=-m\omega ab\sin\frac{\pi}{2}=-m\omega ab \quad (1.16b)$$

Area $|\mathbf{rxv}|$ is constant so equal area $|\mathbf{rx}d\mathbf{r}|=|\mathbf{rxv}|dt$ is swept each time interval dt. *(Kepler's law)*.

Phase lag angle ρ varies with angle φ and ρ is $\pi/2$ for $\varphi=0$. Clockwise or *left*-handed. rotation (viewed as *negative* motion in the Northern hemisphere) gives negative L in (1.16) but *positive* power in (1.10). *Right*-handed rotation yields *negative* work and power. (Is there political analogy here?)

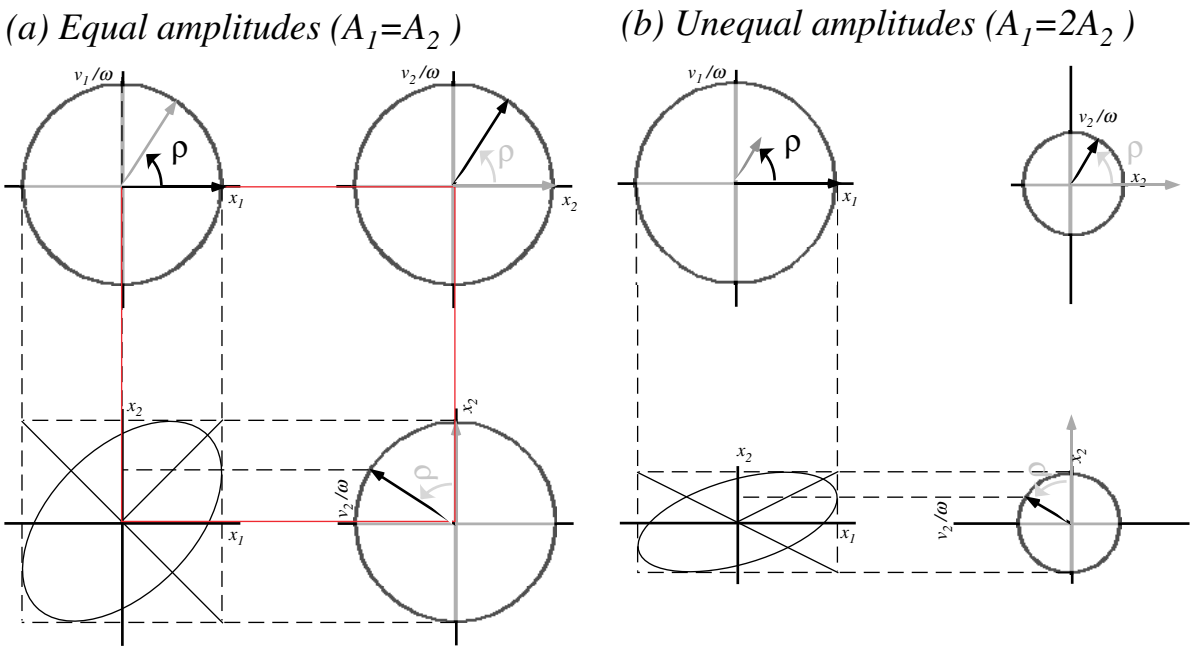

Fig. 1.7 Comparing equal-amplitude resonance (a) to a more generic case (b).

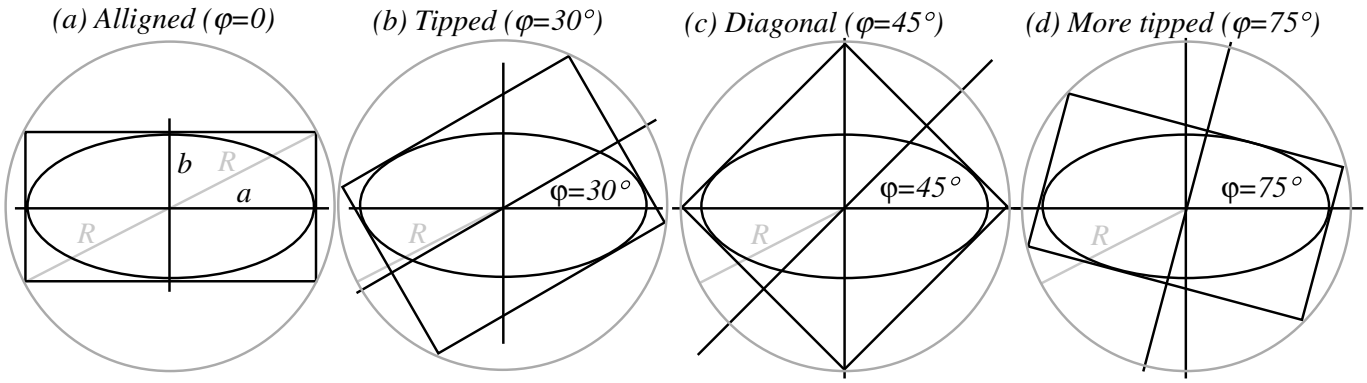

Fig. 1.8 Different tipped boxes for the same ellipsehave the same diagonal radius R.

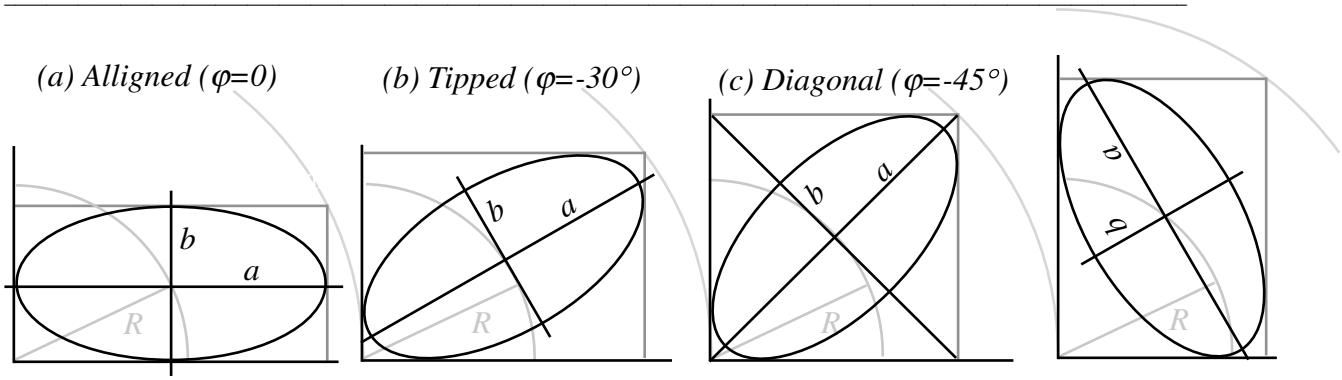

Fig. 1.9 "Cornered" ellipse rotated by various angles maintains central radius R.

The difference $D = E_1 - E_2$ between the energy E_1 in one oscillator and the energy E_2 in the other is an important quantity like total energy $E = E_1 + E_2$ (1.15) and angular momentum L (1.16).

$$\begin{aligned} D &= \frac{1}{2}mv_1^2 + \frac{1}{2}m\omega^2 x_1^2 - \frac{1}{2}mv_2^2 - \frac{1}{2}m\omega^2 x_2^2 \\ &= \frac{1}{2}m\omega^2\left(A_1^2 - A_2^2\right) \end{aligned} \qquad (1.17)$$

To express this in terms of the tipping angle φ we will make use of a geometric construction in Fig. 1.10 of an ellipse's box tangents. The oscillation energy in the u_1-axis tipped by φ from x_1 is a sum of energy $^1/_2 m\omega^2(a\cos\varphi)^2$ from x_1-component $a\cos\varphi$ and energy $^1/_2 m\omega^2(b\sin\varphi)^2$ from x_2-component $b\sin\varphi$ while oscillation associated with the u_2-axis tipped by φ from x_2 has the sum of energy $^1/_2 m\omega^2(a\sin\varphi)^2$ from x_1-component $a\sin\varphi$ and energy $^1/_2 m\omega^2(b\cos\varphi)^2$ from x_2-component $b\cos\varphi$.

$$\begin{aligned} A_1^2 &= (a\cos\varphi)^2 + (b\sin\varphi)^2 \\ A_2^2 &= (a\sin\varphi)^2 + (b\cos\varphi)^2 \end{aligned} \qquad (1.18)$$

Taking the difference (1.17) gives the third oscillator quantity D in angular form.

$$D = \frac{1}{2}m\omega^2\left(A_1^2 - A_2^2\right) = \frac{1}{2}m\omega^2\left(a^2 - b^2\right)\left(\cos^2\varphi - \sin^2\varphi\right) = \frac{1}{2}m\omega^2\left(a^2 - b^2\right)\cos 2\varphi \qquad (1.19a)$$

$$= \frac{1}{2}m\omega^2\left(a^2 - b^2\right) \quad \text{for:} \quad \varphi = 0 \qquad (1.19b)$$

$$= 0 \quad \text{for:} \quad \varphi = \pm\frac{\pi}{4} \qquad (1.19c)$$

The horizontal x_1-oscillation along the a-axis of the ellipse has a phase angle exactly $\rho = 90°$ behind the vertical x_2-oscillation along the b-axis. This makes the amplitudes in (1.18) add *in quadrature*, that is, like the two sides of a right triangle. If x_1-oscillation and x_2-oscillation were in phase then we would have $A_1^2 = (a\cos\varphi + b\sin\varphi)^2$ and $A_2^2 = (a\sin\varphi + b\cos\varphi)^2$, but if a-oscillation and b-oscillation were 180° out of phase then we would have $A_1^2 = (a\cos\varphi - b\sin\varphi)^2$ and $A_2^2 = (a\sin\varphi - b\cos\varphi)^2$.

For a tipped ellipse the horizontal and vertical oscillations have some phase angle ρ other than one of the four E, W, N, or S compass points of heading *0°*, *180°*, *90°*, or *270°=-90°*, respectively. This was shown already in Fig. 1.3. Now we will precisely quantify just how the all-important phase lag angle ρ varies with the tipping angle φ of an ellipse relative to its defining oscillators.

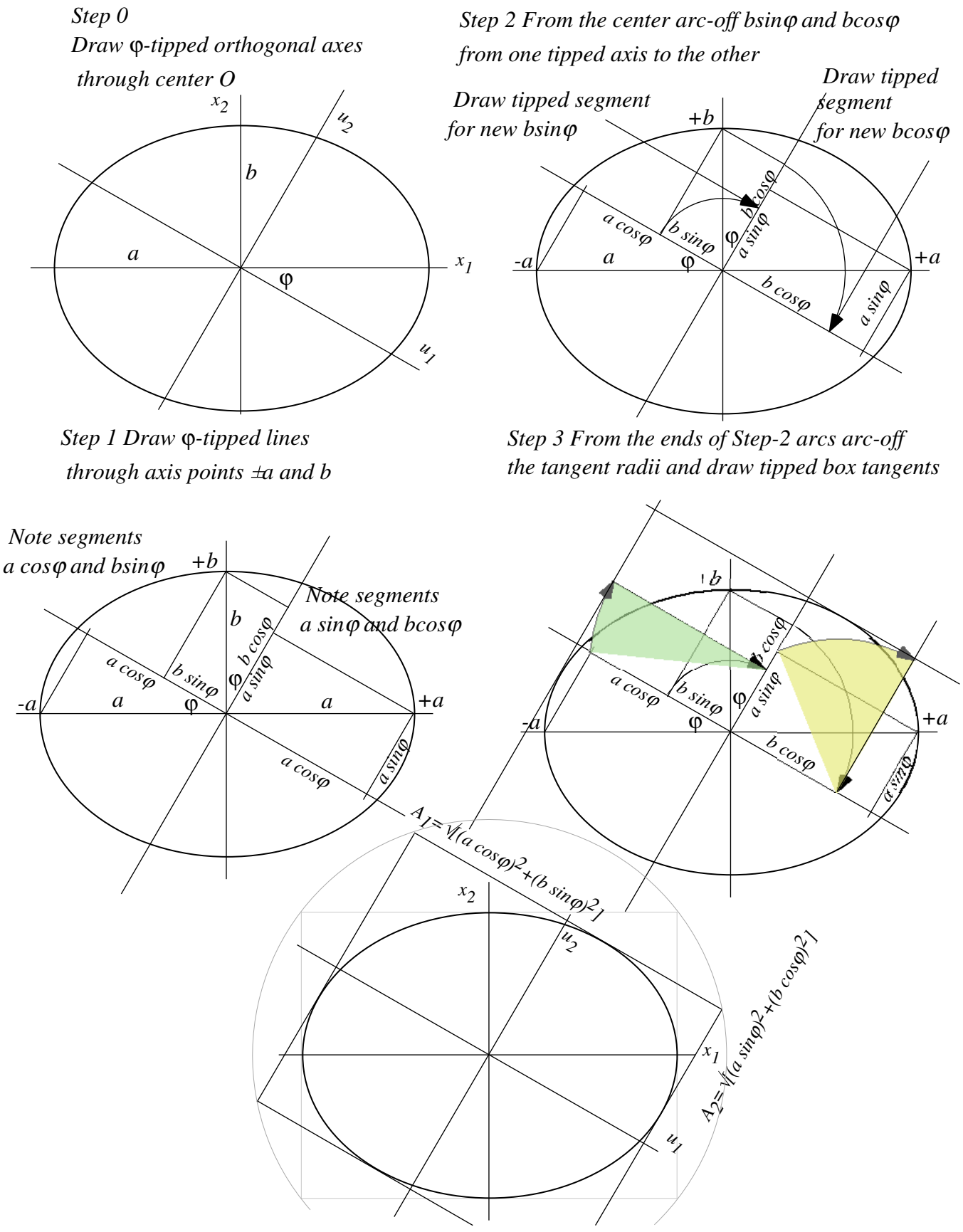

Fig. 1.10 Construction of φ-tipped amplitudes and box-tangents for ellipse.

(d) Relative phase angle ρ versus relative tipping angle φ.

Fig. 1.11 shows a horizontal x_1-oscillation and vertical x_2-oscillation that are 90° out of phase and making an *(a-by-b)*-ellipse. This is compared directly with a φ*=-30°*-tipped u_1-oscillation and φ*+90°=60°*-tipped u_2-oscillation that are 57° out of phase and *making the very same (a-by-b)*-ellipse. To understand this diagram and construction is to better understand the clockwork relation between any pair of quantum states in the universe! It's certainly an important piece of geometry.

The chosen *(a-by-b)*-ellipse has *a=2* and *b=1*. With φ*=-30°*-tipping, amplitudes (1.18) are

$$A_1^2 = (a\cos\varphi)^2 + (b\sin\varphi)^2 = \left(2\cdot\frac{\sqrt{3}}{2}\right)^2 + \left(1\cdot\frac{1}{2}\right)^2 = \frac{13}{4}, \qquad A_1 = \frac{\sqrt{13}}{2}$$
$$A_2^2 = (a\sin\varphi)^2 + (b\cos\varphi)^2 = \left(2\cdot\frac{1}{2}\right)^2 + \left(1\cdot\frac{\sqrt{3}}{2}\right)^2 = \frac{7}{4}, \qquad A_2 == \frac{\sqrt{7}}{2} \tag{1.20a}$$

With these amplitudes we calculate total energy *E*, energy difference *D*, and angular momentum *L*. Total energy is proportional to the total area $\pi A_1^2 + \pi A_2^2$ of the two tipped phasors in Fig. 1.11 or area πR^2.

$$E = \frac{1}{2}m\omega^2\left(A_1^2 + A_2^2\right) = \frac{1}{2}m\omega^2\left(a^2+b^2\right) = \frac{1}{2}m\omega^2 R^2$$
$$= \frac{1}{2}m\omega^2\left(\frac{13}{4}+\frac{7}{4}\right) = \frac{1}{2}m\omega^2\left(2^2+1^2\right) = \frac{1}{2}m\omega^2(5) \tag{1.20b}$$

The angular momentum *L* and also work-per-cycle *W* depends on the sine of the phase-lag-angle and while *L* and *W*, like *E* above, must each be the same for the two oscillator pairs, the lag angle differs.

$$L = -m\omega A_1 A_2 \sin\rho = -m\omega ab = -W$$
$$= -m\omega\sqrt{\frac{13}{4}}\sqrt{\frac{7}{4}}\sin\rho = -m\omega 2\cdot 1 = 2\,, \quad \text{or: } \sin\rho = \frac{2\cdot 4}{\sqrt{13\cdot 7}} \tag{1.20c}$$

This give a tipped lag angle of $sin^{-1}(8/\sqrt{91})$=56.996°. That is consistent with the angle 57° angle obtained by geometric construction in Fig. 1.11. It's quite a bit less than the *90°* lag between *a-and-b* horizontal-vertical oscillators that give the same ellipse.

Finally we compare the energy difference *D*-function (1.19) for the two pairs of oscillators.

$$D = \frac{1}{2}m\omega^2\left(A_1^2 - A_2^2\right) = \frac{1}{2}m\omega^2\left(a^2-b^2\right)\cos 2\varphi$$
$$= \frac{1}{2}m\omega^2\left(\frac{13}{4}-\frac{7}{4}\right) = \frac{1}{2}m\omega^2\left(2^2-1^2\right)\cos(2\cdot 30°) \tag{1.20da}$$
$$= \frac{1}{2}m\omega^2 \quad \left(\frac{6}{4}\right) = \frac{1}{2}m\omega^2 \quad (3)\cdot\frac{1}{2} \qquad = \frac{1}{2}m\omega^2\frac{3}{2}$$

Both the *D* and *L* are functions of a relativity angle. For *D* it is the tipping angle φ in oscillator coordinate space. For *L* it is the relative phase lag-angleρ or phase-space tipping. These are important insights.

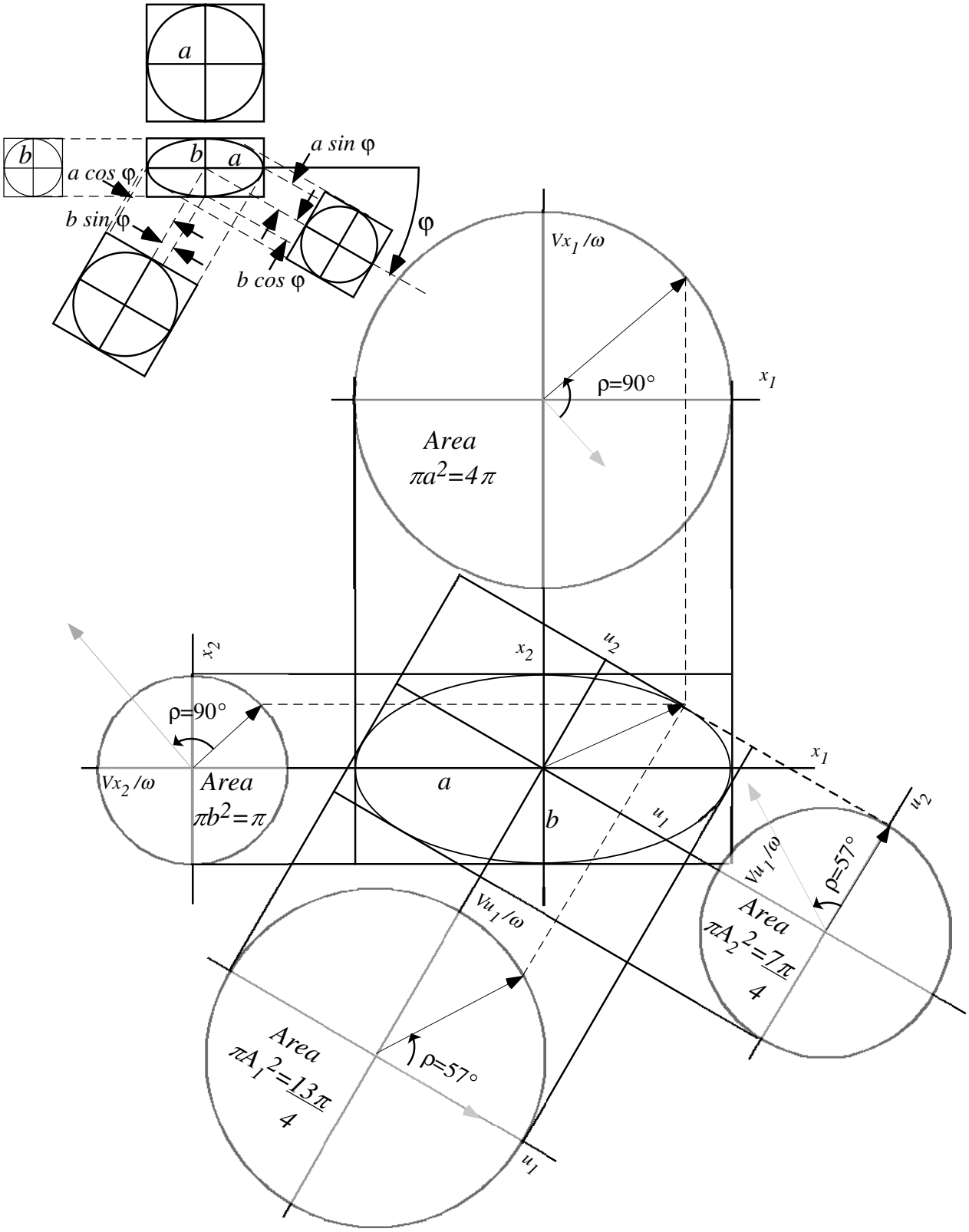

Fig. 1.11 Untipped (a-by-b) ellipse of (x_1,x_2)-phasors, (A_1-by-A_2) ellipse, φ=30°-tipped (u_1,u_2)-phasors.

Chapter 2 Ellipse orbit vector and matrix relations

The construction in the preceding Fig. 1.11 neglects the geometry of oscillator velocity, acceleration, and other kinematic quantities that help greatly in understanding ellipse geometry. Vector algebra as well as matrix algebra helps to make calculation and visualization easier as shown in Unit 1 for superball velocity ellipse mechanics (Ch.4 Fig. 4.10) and for oscillator orbits (Ch. 9 fig. 9.10).

(a) Vector mechanics of elliptic oscillator orbits

Oscillator orbits have a peculiar property. According to (1.9.5) their position $\mathbf{r}(t)$, velocity $\mathbf{v}(t)/\omega$, acceleration $\mathbf{a}(t)/\omega^2$, and jerk $\mathbf{j}(t)/\omega^3$, etc., all follow the same elliptical $\frac{x^2}{a^2}+\frac{y^2}{b^2}=1$ path if scaled by ω.

$$\mathbf{r}(t)=\begin{pmatrix} a\cos(\omega t)\\ b\sin(\omega t)\end{pmatrix},\quad \frac{\mathbf{v}(t)}{\omega}=\begin{pmatrix} -a\sin(\omega t)\\ b\cos(\omega t)\end{pmatrix},\quad \frac{\mathbf{a}(t)}{\omega^2}=\begin{pmatrix} -a\cos(\omega t)\\ -b\sin(\omega t)\end{pmatrix},\quad \frac{\mathbf{j}(t)}{\omega^3}=\begin{pmatrix} a\sin(\omega t)\\ -b\cos(\omega t)\end{pmatrix},$$
$$=\begin{pmatrix} a\cos\left(\omega t+\frac{\pi}{2}\right)\\ b\sin\left(\omega t+\frac{\pi}{2}\right)\end{pmatrix},\quad =\begin{pmatrix} a\cos\left(\omega t+\frac{2\pi}{2}\right)\\ b\sin\left(\omega t+\frac{2\pi}{2}\right)\end{pmatrix},\quad =\begin{pmatrix} a\cos\left(\omega t+\frac{3\pi}{2}\right)\\ b\sin\left(\omega t+\frac{3\pi}{2}\right)\end{pmatrix}, \qquad (2.1)$$

Each is *90°* ahead in angle or *90° behind* in time phase. The next derivative, inauguration $\mathbf{i}(t)/\omega^4$, in the sequence above will be identical to position $\mathbf{r}(t)$. So the sequence of vectors repeats after four quadrants.

Fig. 2.1 uses an *(a,b)*-circle construction from Fig. 3.4 of Unit 1 to construct each quadrant vector of position $\mathbf{r}(t)$ *(Step-0)*, velocity $\mathbf{v}(t)/\omega$ *(Step-1)*, acceleration $\mathbf{a}(t)/\omega^2$ *(Step-2)*, and jerk $\mathbf{j}(t)/\omega^3$ *(Step-3)*. The $(\omega t+n\pi/2)$-phase radius *(Step-n)* is from (2.1).

In Step-1 the velocity vector $\mathbf{v}(t)/\omega$ is copied to sit head-to-tail on the position vector . It is seen that $\mathbf{v}(t)/\omega$ is tangent to the ellipse at $\mathbf{r}(t)$, as it should be in order to represent velocity correctly and be the rate of change of position. Note: acceleration $\mathbf{a}(t)$ equals $-\omega^2\,\mathbf{r}(t)$ and restates $\mathbf{F}(t) = M\,\mathbf{a}(t) = -k\,\mathbf{r}(t)$.

Tangency relations for elliptical oscillator orbits apply *vice-versa*, that is, position vector $\mathbf{r}(t)$ is tangent to the ellipse at velocity point $\mathbf{v}(t)/\omega$. Thus we can work this construction in reverse as well as forward. The reverse construction shown at the bottom of Fig. 2.1 starts with a tangent line direction $\mathbf{v}(t)$, such as the construction in Fig. 1.10, and locates the position point of contact $\mathbf{r}(t)$. So geometric *integration* (finding $\mathbf{r}(t)$ given $\mathbf{v}(t)$) for elliptic oscillator orbits is as easy as geometric *differentiation* (finding $\mathbf{v}(t)$ given $\mathbf{r}(t)$). (The construction in Fig. 1.10 also gives tangents for a particular tipping angle φ or ωt but only approximate location of tangent *contact* points.) Area of the **r**-**v** parallelogram equals $|\mathbf{r}\times\mathbf{v}|$ and is proportional to the angular momentum L in (1.16) that is a Kepler-law constant.

$$L=|\mathbf{r}\times\mathbf{p}|=m|\mathbf{r}\times\mathbf{v}| = m\,|\,\mathbf{r}\,|\,|\,\mathbf{v}\,|\sin\angle_{\mathbf{r}}^{\mathbf{v}}$$

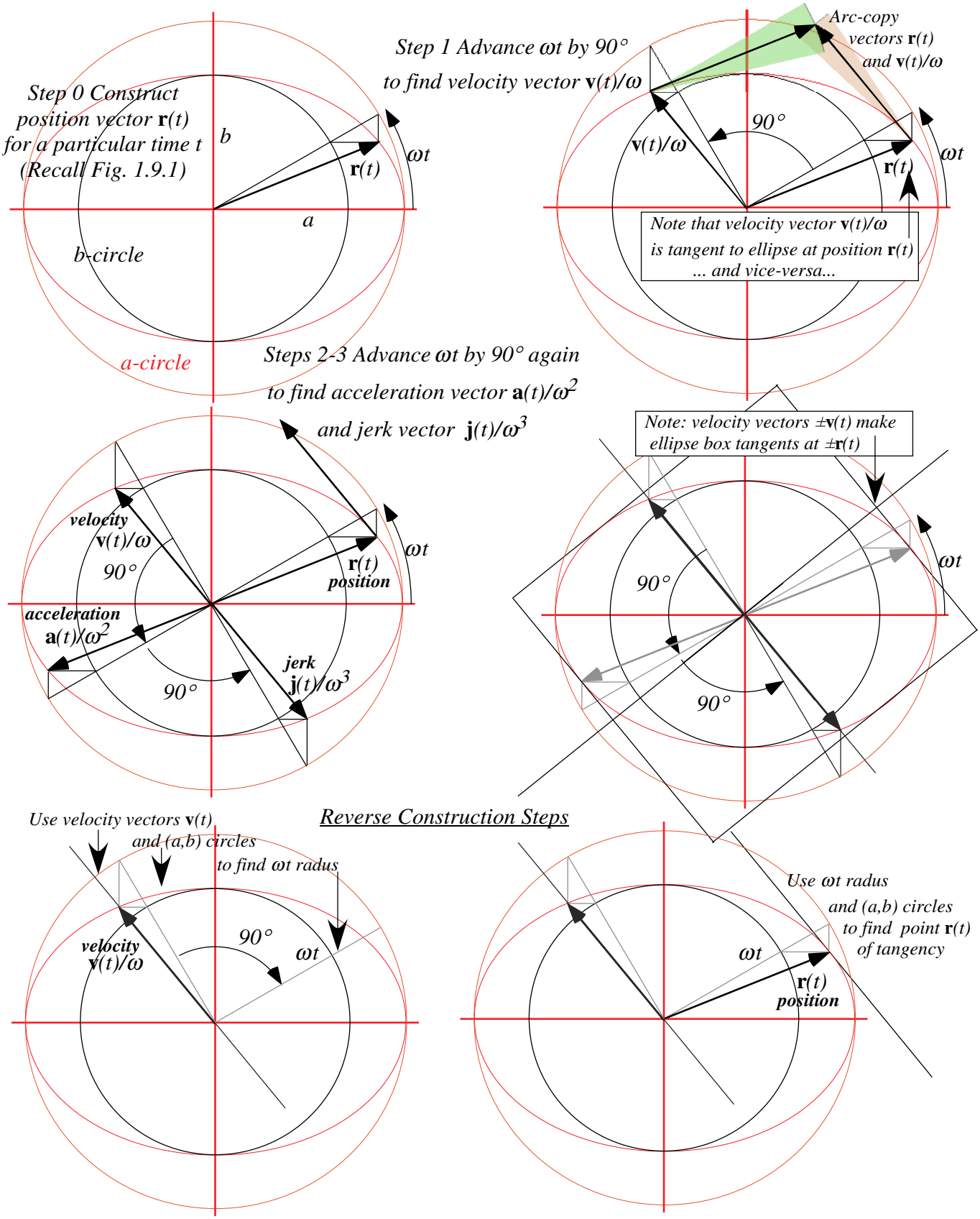

Fig. 2.1 Construction of ellipse box tangents using position, velocity, acceleration and jerk vectors.

(b) Ellipses and matrix operations: Quadratic forms

Ellipse equation $\frac{x^2}{a^2}+\frac{y^2}{b^2}=1$ can be expressed by a matrix $\mathbf{Q}=\begin{pmatrix}1/a^2 & 0\\ 0 & 1/b^2\end{pmatrix}$ and vectors $\mathbf{r}=\begin{pmatrix}x\\ y\end{pmatrix}=\begin{pmatrix}x & y\end{pmatrix}$.

$$\begin{pmatrix}x & y\end{pmatrix}\bullet\begin{pmatrix}\frac{1}{a^2} & 0\\ 0 & \frac{1}{b^2}\end{pmatrix}\bullet\begin{pmatrix}x\\ y\end{pmatrix}=1=\begin{pmatrix}x & y\end{pmatrix}\bullet\begin{pmatrix}\frac{x}{a^2}\\ \frac{y}{b^2}\end{pmatrix}=\frac{x^2}{a^2}+\frac{y^2}{b^2}\qquad\text{or:}\qquad \mathbf{r}\bullet\mathbf{Q}\bullet\mathbf{r}=1 \tag{2.2a}$$

We use dot product introduced (10.30) and matrix product introduced in (5.2) of Unit 1. One advantage of matrix notation **r•Q•r**=*1* is it describes *tipped* ellipses $Ax^2+Bxy+Byx+Cy^2=1=Ax^2+2Bxy+Cy^2$, too.

$$\begin{pmatrix}x & y\end{pmatrix}\bullet\begin{pmatrix}A & B\\ B & C\end{pmatrix}\bullet\begin{pmatrix}x\\ y\end{pmatrix}=1=\begin{pmatrix}x & y\end{pmatrix}\bullet\begin{pmatrix}Ax+By\\ Bx+Cy\end{pmatrix}=Ax^2+2Bxy+Cy^2\quad\text{or:}\quad \mathbf{r}\bullet\mathbf{Q}\bullet\mathbf{r}=1 \tag{2.2b}$$

Mathematicians call **r•Q•r** a *quadratic form QF*. Physics uses QF's (metric $ds^2=g_{mn}dx^m dx^n$, energy, etc.) a lot.

Matrix $\mathbf{Q}=\begin{pmatrix}1/a^2 & 0\\ 0 & 1/b^2\end{pmatrix}$ operates on vector $\mathbf{r}=\begin{pmatrix}x\\ y\end{pmatrix}$ to give a vector **p** *perpendicular* to ellipse tangent $\dot{\mathbf{r}}=\frac{d\mathbf{r}}{d\varphi}$.

$$\mathbf{p}=\mathbf{Q}\bullet\mathbf{r}==\begin{pmatrix}\frac{1}{a^2} & 0\\ 0 & \frac{1}{b^2}\end{pmatrix}\bullet\begin{pmatrix}x\\ y\end{pmatrix}=\begin{pmatrix}\frac{x}{a^2}\\ \frac{y}{b^2}\end{pmatrix}=\begin{pmatrix}\frac{\cos\phi}{a}\\ \frac{\sin\phi}{b}\end{pmatrix}\quad\text{where:}\quad\begin{matrix}x=r_x=a\cos\phi=a\cos\omega t\\ y=r_y=b\sin\phi\ \ =b\sin\omega t\end{matrix} \tag{2.3a}$$

$$\dot{\mathbf{r}}\bullet\mathbf{p}=0=\begin{pmatrix}\dot{r}_x & \dot{r}_y\end{pmatrix}\bullet\begin{pmatrix}p_x\\ p_y\end{pmatrix}=\begin{pmatrix}-a\sin\phi & b\cos\phi\end{pmatrix}\begin{pmatrix}\frac{\cos\phi}{a}\\ \frac{\sin\phi}{b}\end{pmatrix}\quad\text{where:}\quad\begin{matrix}\dot{r}_x=-a\sin\phi\\ \dot{r}_y=b\cos\phi\end{matrix}\quad\text{and:}\quad\begin{matrix}p_x=\frac{1}{a}\cos\phi\\ p_y=\frac{1}{b}\sin\phi\end{matrix} \tag{2.3b}$$

Also, the resulting **p**-vector lies on the ellipse of the *inverse quadratic form* $Q^{-1}F$ **r•Q^{-1}•r**=*1* whose axes are the inverses *(1/a,1/b)* of the original **Q**-ellipse. This is shown by the equations below and in Fig. 2.2.

$$\begin{pmatrix}p_x & p_y\end{pmatrix}\bullet\begin{pmatrix}a^2 & 0\\ 0 & b^2\end{pmatrix}\bullet\begin{pmatrix}p_x\\ p_y\end{pmatrix}=1=\begin{pmatrix}p_x & p_y\end{pmatrix}\bullet\begin{pmatrix}a^2p_x\\ b^2p_y\end{pmatrix}=a^2p_x+b^2p_y\quad\text{or:}\quad\mathbf{p}\bullet\mathbf{Q}^{-1}\bullet\mathbf{p}=1 \tag{2.4}$$

The original vector **r**, obtained by inverse operation **Q^{-1}•p** on **p** is perpendicular to the $Q^{-1}F$ ellipse tangent.

$$\mathbf{r}=\mathbf{Q}^{-1}\bullet\mathbf{p}==\begin{pmatrix}a^2 & 0\\ 0 & b^2\end{pmatrix}\bullet\begin{pmatrix}p_x\\ p_y\end{pmatrix}=\begin{pmatrix}a^2p_x\\ b^2p_y\end{pmatrix}=\begin{pmatrix}a\cos\phi\\ b\sin\phi\end{pmatrix}\quad\text{where:}\quad\begin{matrix}p_x=\frac{1}{a}\cos\phi\\ p_y=\frac{1}{b}\sin\phi\end{matrix} \tag{2.5a}$$

$$\dot{\mathbf{p}}\bullet\mathbf{r}=0=\begin{pmatrix}\dot{p}_x & \dot{p}_y\end{pmatrix}\bullet\begin{pmatrix}r_x\\ r_y\end{pmatrix}=\begin{pmatrix}-\frac{1}{a}\sin\phi & \frac{1}{b}\cos\phi\end{pmatrix}\begin{pmatrix}a\cos\phi\\ b\sin\phi\end{pmatrix}\quad\text{where:}\quad\begin{matrix}\dot{p}_x=-\frac{1}{a}\sin\phi\\ \dot{p}_y=\frac{1}{b}\cos\phi\end{matrix}\quad\text{and:}\quad\begin{matrix}r_x=a\cos\phi\\ r_y=b\sin\phi\end{matrix} \tag{2.5b}$$

Note that vectors **p** and **r** maintain a *unit mutual projection*, that is, their dot-product **p•r** *always* is 1.

$$\mathbf{p}\bullet\mathbf{r}=1=\begin{pmatrix}p_x & p_y\end{pmatrix}\bullet\begin{pmatrix}r_x\\ r_y\end{pmatrix}=\begin{pmatrix}\frac{1}{a}\cos\phi & \frac{1}{b}\sin\phi\end{pmatrix}\begin{pmatrix}a\cos\phi\\ b\sin\phi\end{pmatrix}=\mathbf{p}\bullet Q^{-1}\bullet\mathbf{p}=1=\mathbf{r}\bullet Q\bullet\mathbf{r} \tag{2.5c}$$

What gorgeous geometric-algebraic symmetry! It works for tipped ellipses, too. We scale our ellipse plots by the geometric mean $S=\sqrt{(ab)}$ so that minor radius $b/S=\sqrt{(b/a)}$ is the inverse of major radius $a/S=\sqrt{(a/b)}$, that is $b_S=1/a_S$. So to get the inverse ellipse, just switch axes (or rotate by *90°*)! This shows the symmetry.

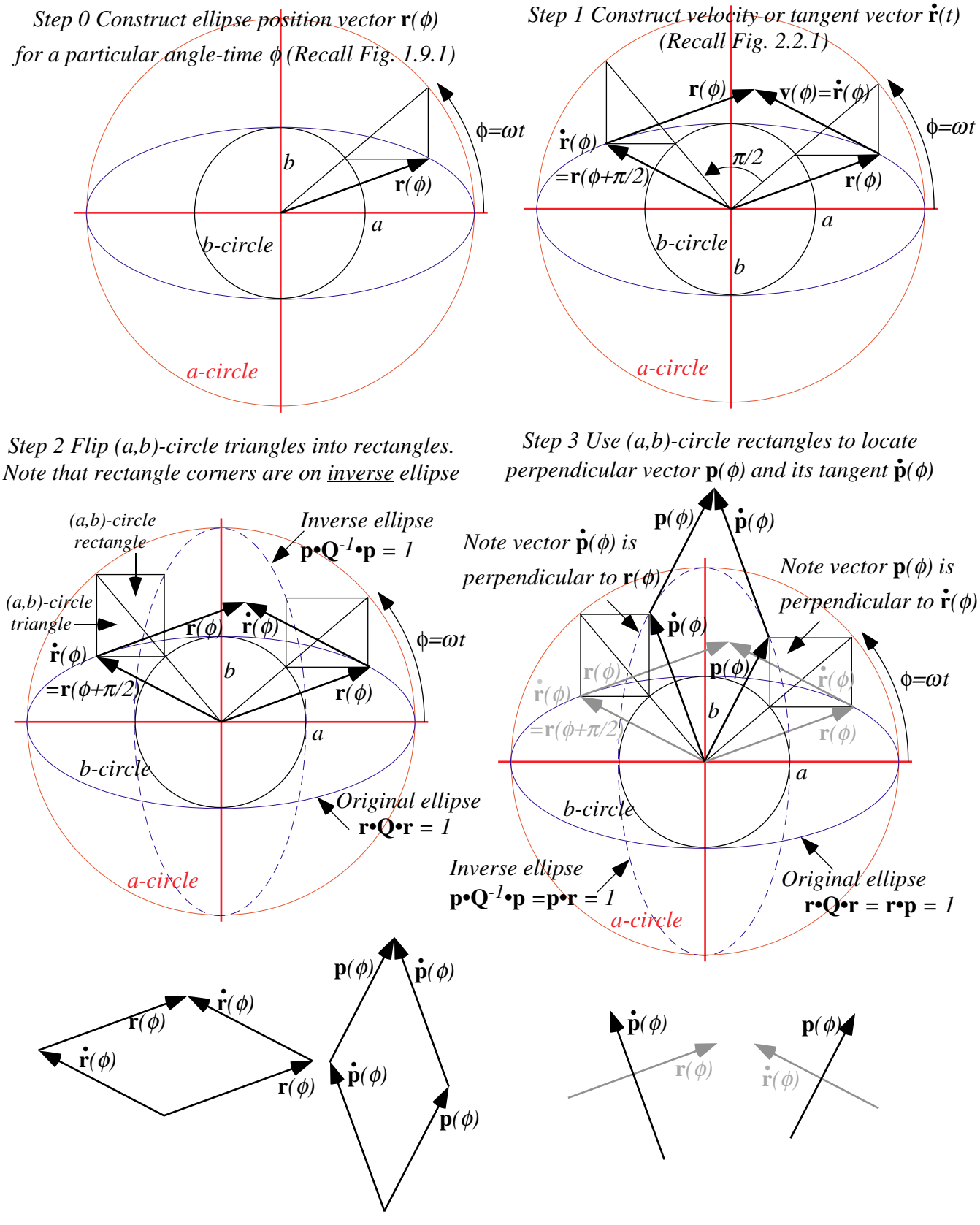

Fig. 2.2 Quadratic form and orbit geometry. From ellipse orbit $\mathbf{r}(\phi)$ *and velocity tangent* $\dot{\mathbf{r}}(\phi) = d\mathbf{r}(\phi)/d\phi$, *constructs the inverse or "perpendicular" ellipse* $\mathbf{p}(\phi)$ *and its velocity tangent* $\dot{\mathbf{p}}(\phi) = d\mathbf{p}(\phi)/d\phi$. *(Here* $\omega=1$*)*

Tipped boxes and phasor clockwork

Before studying tipped-ellipse equations for coupled-oscillator analysis, let us review geometry of tipped-tangent ellipse boxes. A tangent vector $\dot{\mathbf{r}}(\phi)$ in *Step 2* of Fig. 2.2 (upper left) lies on one corner of an *(a,b)*-circle rectangle and $\dot{\mathbf{p}}(\phi)$ lies on the opposite corner in *Step 3*. Between $\dot{\mathbf{r}}(\phi)$ and $\dot{\mathbf{p}}(\phi)$ passes the radial diagonal at angle ϕ+*90°* that connects the other two rectangle corners.

A *90°* clockwise rotation of the $\dot{\mathbf{r}}(\phi)$ - $\dot{\mathbf{p}}(\phi)$ rectangle gives the $\mathbf{r}(\phi)$ - $\mathbf{p}(\phi)$ rectangle at *phase angle* ϕ in *Step 3* of Fig. 2.2. The vectors $\dot{\mathbf{r}}(\phi)$ and $\mathbf{p}(\phi)$ define tangent and normal to point $\mathbf{r}(\phi)$ on the *Q*-ellipse. They also are parallel to sides of an ellipse box with a *tipping angle* φ. We now relate phase angle-ϕ to tipping angle-φ, slope angle $\angle^{\mathbf{r}}$ of position $\mathbf{r}(\phi)$, and slope angle $\angle^{\dot{\mathbf{r}}}$ of tangent (velocity) $\dot{\mathbf{r}}(\phi)$.

Below is a summary of the slope angles of the position $\mathbf{r}(\phi)$, velocity $\dot{\mathbf{r}}(\phi)$, and perpendicular or normal vector $\mathbf{p}(\phi)$ using (2.3) through (2.5). The geometric relations are constructed in Fig. 2.3.

$$\textit{Slope of tangent contact position } \mathbf{r}(\phi): \quad \tan\left(\angle^{\mathbf{r}}\right) = \frac{y}{x} = \frac{r_y}{r_x} = \frac{b\sin\phi}{a\cos\phi} = \frac{b}{a}\tan(\phi) \quad \text{or:} \quad \begin{matrix} \angle^{\mathbf{r}} = ATN\left(\frac{b}{a}\tan(\phi)\right) \\ \phi = ATN\left(\frac{a}{b}\tan\left(\angle^{\mathbf{r}}\right)\right) \end{matrix} \tag{2.6a}$$

$$\textit{Slope of tangent velocity vector } \dot{\mathbf{r}}(\phi): \quad \tan\left(\angle^{\dot{\mathbf{r}}}\right) = \frac{\dot{r}_y}{\dot{r}_x} = \frac{b\cos\phi}{-a\sin\phi} = \frac{-b}{a}\cot(\phi) \quad \text{or:} \quad \begin{matrix} \angle^{\dot{\mathbf{r}}} = ATN\left(\frac{-b}{a}\cot(\phi)\right) \\ \phi = ACT\left(\frac{a}{-b}\tan\left(\angle^{\dot{\mathbf{r}}}\right)\right) \end{matrix} \tag{2.6b}$$

$$\textit{Slope of tangent perpendicular } \mathbf{p}(\phi): \quad \tan\left(\varphi = \angle^{\mathbf{p}}\right) = \frac{p_y}{p_x} = \frac{a\sin\phi}{b\cos\phi} = \frac{a}{b}\tan(\phi) \quad \text{or:} \quad \begin{matrix} \varphi = ATN\left(\frac{a}{b}\tan(\phi)\right) \\ \phi = ATN\left(\frac{b}{a}\tan(\varphi)\right) \end{matrix} \tag{2.6c}$$

The object of the construction in Fig. 2.3 is to box an ellipse by a tangent rectangle at a given tipping angle φ of the tangent perpendicular vector $\mathbf{p}(\phi)$. Fig. 2.3 is a more precise tipped box than Fig. 1.10-11. The key relation is (2.6c) between phase angle $\phi=\omega t$ and the polar angle φ of the tangent perpendicular vector $\mathbf{p}(\phi)=\mathbf{Q}\bullet\mathbf{r}(\phi)$. If position **r**-vector is on an ellipse axis *(φ=0* or *$\varphi=\pi$)* then so is the **p**-vector (**p***(0)*=**r***(0)*). Otherwise, they are separated by one of those *(a,b)*-circle rectangles developed in *Step 2* of Fig. 2.2 and *Step 1* of Fig. 2.3 on the next page.

Each rectangle has a phase angle ϕ as its radial diagonal, and ϕ is found using a $\tan\phi = b\tan\varphi$ (2.6c) in *Step 0* of Fig. 2.3. The phase angles $\phi'_c = \phi_c + \pi/2$ and $\phi' = \phi + \pi/2$ in Fig. 2.3-*Step 0* are for two velocity vectors $\dot{\mathbf{r}}(\phi_c)$ and $\dot{\mathbf{r}}(\phi)$ that will lie along the φ-tipped ellipse box. In *Step 1* their companion position vectors for the tangent contact points $\mathbf{r}(\phi_c)$ and $\mathbf{r}(\phi)$ are easily found, too.

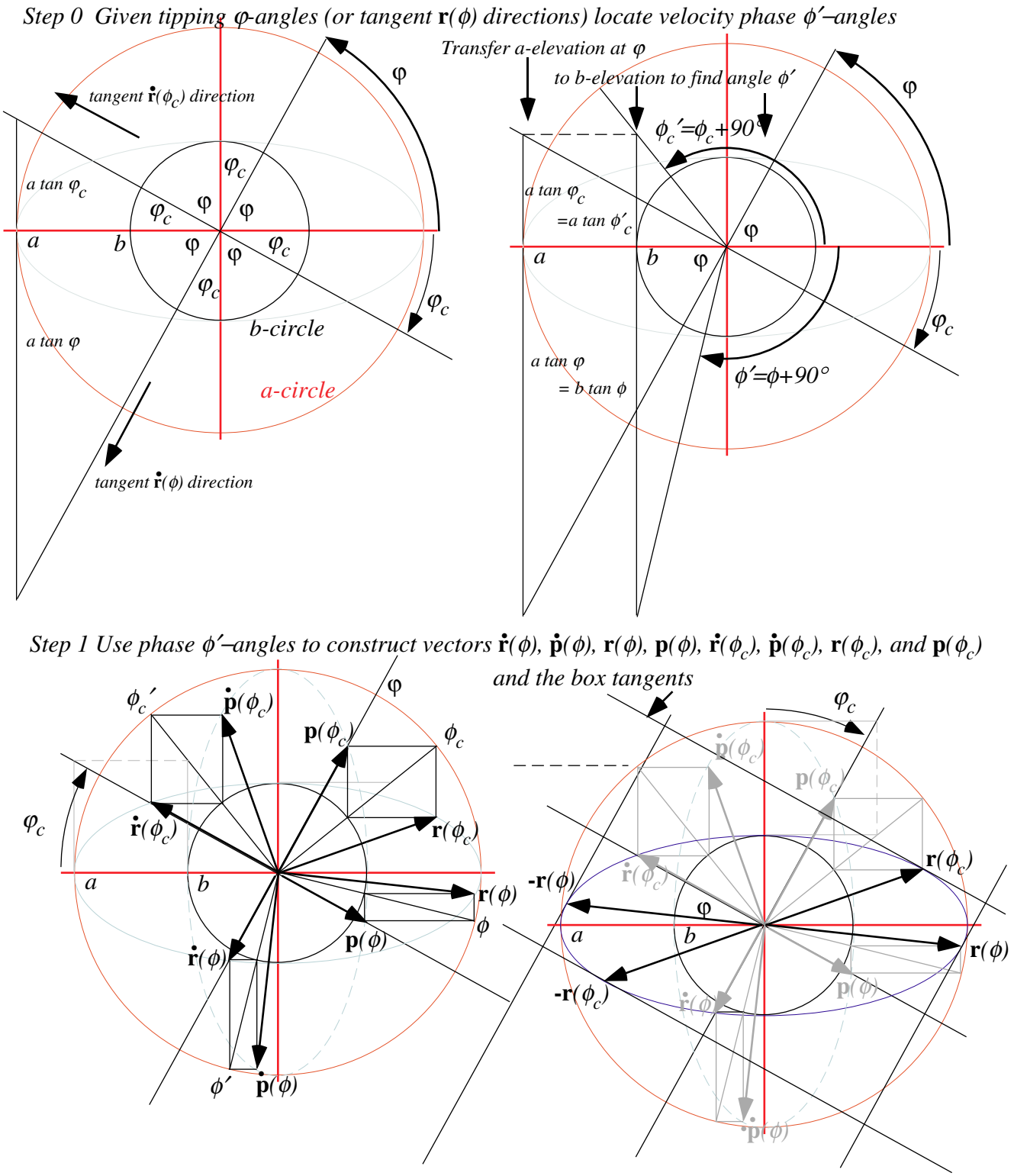

Fig. 2.3 Precise construction of ellipse tangent box with a given vertical inclination $\varphi=90°-\varphi_c$.

The next Fig. 2.4(a-b) uses the box tangents to compare φ-tipped (u_1,u_2)-axis phasor components with those of ellipse's own (x_1,x_2)-axes. Phasors rotate clockwise by a ϕ-angle all with the same rate ω.

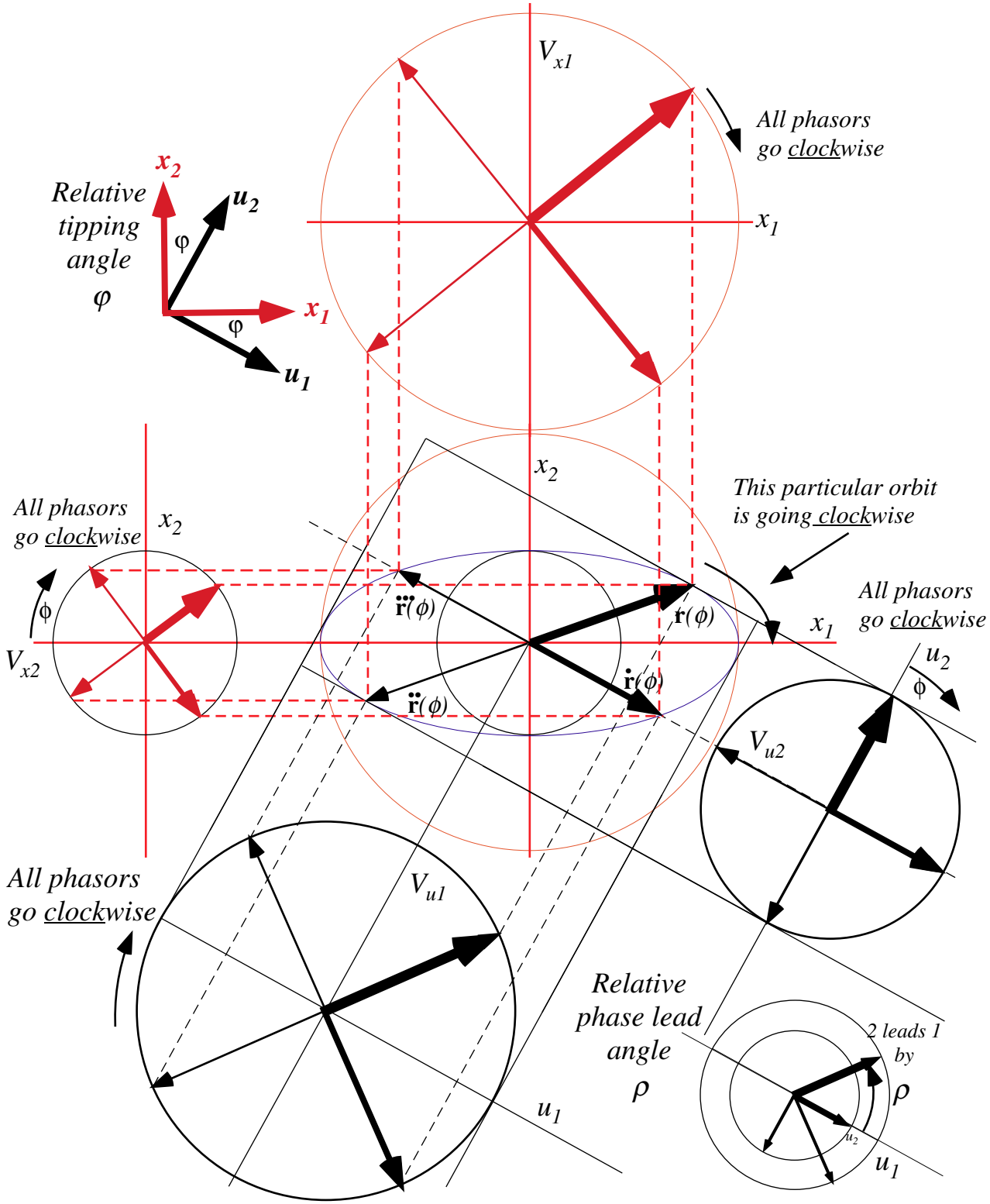

Fig. 2.4 (a) Two pairs of phasor components that make a clockwise orbit.

In Fig. 2.4(a) above the ellipse orbit also goes clockwise, but in the next Fig. 2.4(b) the ellipse orbit is *counter* clockwise even though the phasor rotation is clockwise there as it is above. Setting the x_2 phasor ahead of x_1 by $\pi/2$ (or u_2 ahead of u_1 by ρ) causes the orbit to be clockwise ((+) work *W* and (-) *L*)

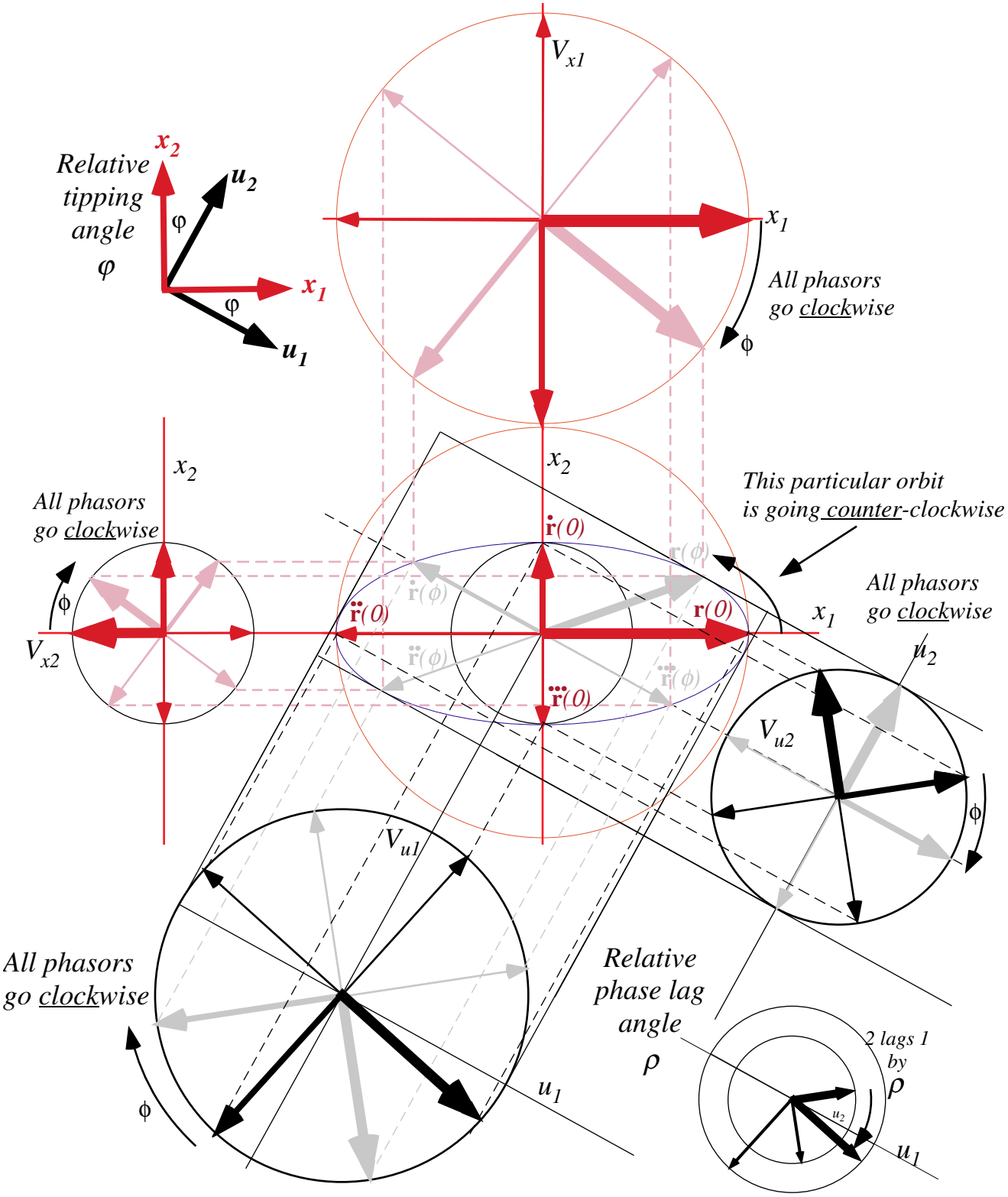

Fig. 2.4 (b) Two pairs of phasor components that make a counter-clockwise orbit.

It is important to see how the phasors are adjusted to make the orbits come out as they do. In the case above the x_2 phasor is *behind* x_1 by $\pi/2$ giving a *counter* clockwise orbital rotation. These are elementary examples of a wave going around a circular or elliptical enclosure. Very useful!

Special Tippings: a/b and 1/1

The perpendicular $\mathbf{p}(\phi)$ starts out at zero-phase $\phi=0$ in the same direction as the position radius vector $\mathbf{r}(\phi)$, and would remain so if $a=b$. But, if $a>b$, as in Fig. 2.5, the slope of perpendicular $\mathbf{p}(\phi) = Q \bullet \mathbf{r}(\phi)$ is greater by a/b than phase slope $\tan\phi$ while slope of position radius $\mathbf{r}(\phi)$ is less than ϕ by the same factor.

Fig. 2.5 *Step 0-1*shows a special case. The phase angle slope $\tan\phi$ is precisely that of the ellipse diagonal, that is, $\tan\phi = b/a$. By (2.6a) position radius has slope b^2/a^2. The tangent slope, given $\cot\phi = a/b$, equals -1 by (2.6b) so its perpendicular has slope is $+1$, that is, angle $45°$ in agreement with (2.6c). For *Step 2-3* the phase slope is instead $\tan\phi_c = a/b$ so the position radius has slope $+1$, its tangent has a slope $-b^2/a^2$, and its tangent perpendicular has a slope a^2/b^2. This is shown by geometric construction in Fig. 2.5 *Step 4* of a box tipped to $-b^2/a^2$ that touches the ellipse at the $45°$ line.

In Fig. 2.6, the phase angle slope is set to one ($\tan\phi=1$) so that the position radius rises up to the ellipse diagonal, that is, $\tan\angle\mathbf{r} = b/a$. A box tangent to the ellipse diagonal is tipped to $-b/a$ (2.6b) while the perpendicular slope (2.6c) is a/b. Applying matrix **Q** moves slope closer to the minor $(b=1/a)$-axis of the **Q**-ellipse by a factor a^2/b^2, while inverse matrix $\mathbf{Q}^{-1}$ moves slope closer to the major $(a=1/b)$-axis of the **Q**-ellipse by a factor b^2/a^2, that is, by the inverse factor.

This **Q**-matrix geometry is important. One of the matrices seems to want to sweep all vectors onto the *y*-axis while the other is just as determined to send every one to the *x*-axis. The *x*-axis and *y*-axis are the ellipse's own axes or, in partial-German, *eigen*-axes. The concept of *eigenvectors* which lie along eigen-axes is the single most important mathematical concept in quantum theory.

Step 0

Set phase-angle ϕ to diagonal of (a,b) of ellipse box. Using circle-(a,b) box, find ellipse position vector $\mathbf{r}(\phi)$ *and its tangent-perpendicular* $\mathbf{p}(\phi)$ *(Recall Fig. 2.2.2)*

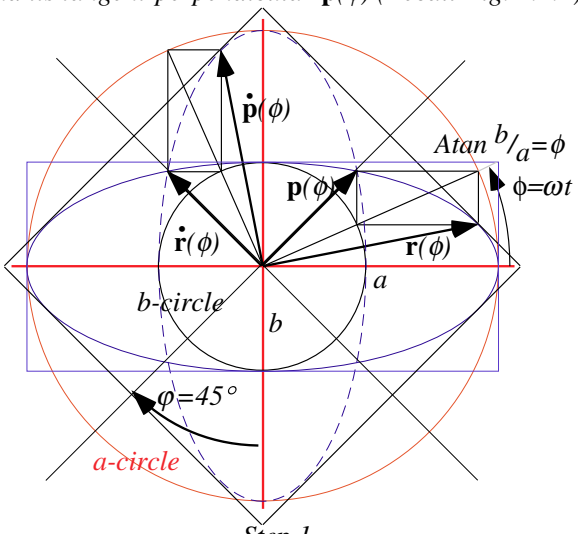

Step 1

Rotate Step-0 construction 90° to get velocity vector $\dot{\mathbf{r}}(\phi)$ *and its tangent-perpendicular* $\dot{\mathbf{p}}(\phi)$*. 45° contact box of <u>both</u> Q and* Q^{-1} *ellipses has axes* $\dot{\mathbf{r}}(\phi)$ *and* $\mathbf{p}(\phi)$

Step 2

Do Steps 0-2 for complimentary angle $\phi_c=\pi/2-\phi$

X-reflection of $\mathbf{r}(\phi)$ *and* $\mathbf{p}(\phi)$ *gives* $\dot{\mathbf{r}}(\phi_c)$ *and* $\dot{\mathbf{p}}(\phi_c)$

X-reflection of $\dot{\mathbf{r}}(\phi)$ *and* $\dot{\mathbf{p}}(\phi)$ *gives* $\mathbf{r}(\phi_c)$ *and* $\mathbf{p}(\phi_c)$

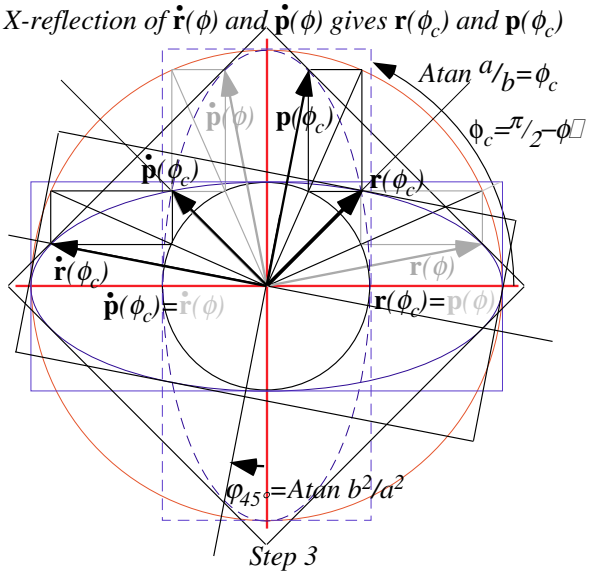

Step 3

Use velocity $\dot{\mathbf{r}}(\phi_c)$ *and its perpendicular* $\mathbf{p}(\phi_c)$ *to construct box tangent at 45° position* $\mathbf{r}(\phi_c)$*. 45° contact slope angle is* $\varphi_{45°}=\text{Atan } b^2/a^2$*.*

Fig. 2.3 Square with φ=45° tipping contacts both Q and Q^{-1} ellipses. Slope b^2/a^2 box contacts at 45°.

Step 1 Set phase-angle ϕ to 45°.Using circle-(a,b) box, find ellipse position vector $\mathbf{r}(\phi)$ *and* $\mathbf{p}(\phi)$ *and ellipsevelocity vector* $\dot{\mathbf{r}}(\phi)$ *and* $\dot{\mathbf{p}}(\phi)$

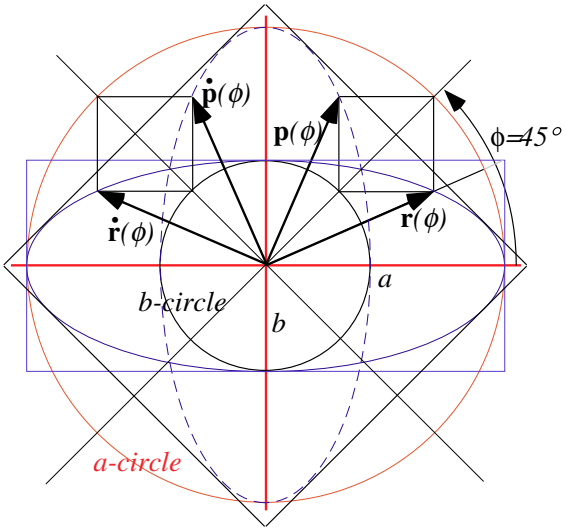

Step 2 Use velocity $\dot{\mathbf{r}}(\phi)$ *and its perpendicular* $\mathbf{p}(\phi)$ *to construct box tangent at position* $\mathbf{r}(\phi)$*. Contact slope angle is φ=Atan b/a.*

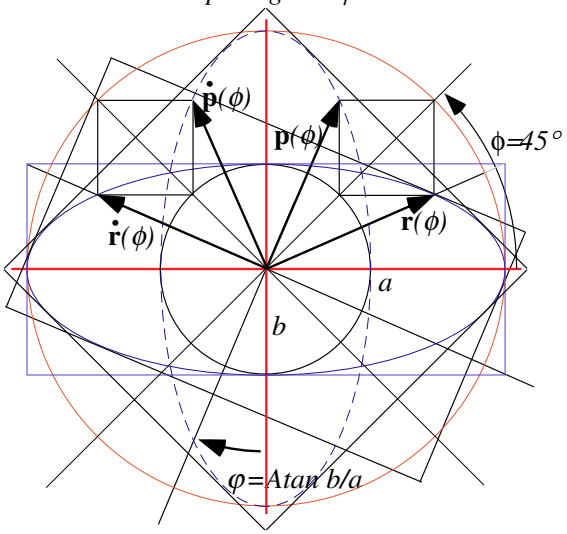

Fig. 2.4 Box with ϕ=45° phase angle contacts Q ellipse at its (a,b)-diagonal with slope-b/a.

Chapter 3 Strongly Coupled Oscillators and Beats

So far, two identical swinging pendulums were coupled by a k_{12}-spring so weak that it would take a long time to noticeably affect the motion of either one. We derived the sine-lag work-energy per-cycle transfer formula (1.8) and the power transfer formula (1.10) using geometry of phasors and ellipses.

$$Work(\tau)_{on\ 1\ by\ 2}=\pi k_{12}A_1\,A_2\,\sin\rho \qquad (1.8)_{\text{repeat}}$$

$$Power(\tau)_{on\ 1\ by\ 2}=2\pi^2\omega k_{12}A_1\,A_2\,\sin\rho \qquad (1.10)_{\text{repeat}}$$

Now finally, we will work out how a k_{12}-spring of arbitrary strength will affect each of the pendulum's motion. As before, we use geometry and algebra to help understand the resonance behavior.

(a) Elliptical potential energy bowls

The energy expression given back in (1.14) does not include the potential energy $^1/_2\,k_{12}(x_1\text{-}x_2)^2$ in the coupling spring. (We assumed k_{12} was tiny.) Now we add it in to get a total PE function $V(x_1,x_2)$.

$$\begin{aligned} V(x_1,x_2) &= PE_{osc\,1}+PE_{osc\,2}+PE_{coupling\,12} \\ &= \frac{1}{2}kx_1^2 \;+\frac{1}{2}kx_2^2 \;+\frac{1}{2}k_{12}\left(x_1-x_2\right)^2 \end{aligned} \qquad (3.1)$$

Here individual spring constants $k_1=k=m\omega^2=k_2$ are assumed the same for each pendulum-oscillator. A plot of this function in Fig. 3.1 reveals a beautiful bowl or *elliptical paraboloid*.

Imagine this is a bare-essentials ski bowl. (Ski Bare Valley!) A nearly overhead view such as Fig. 3.1(a) and a topographical map in Fig. 3.2 reveals elliptical *topography contours*, lines of equal altitude or potential energy. If potential $V(x_1,x_2)$ equals a constant E, that is a tipped ellipse equation.

$$V(x_1,x_2)=E=\frac{1}{2}kx_1^2 \;+\frac{1}{2}kx_2^2 \;+\frac{1}{2}k_{12}\left(x_1-x_2\right)^2 \text{ or: } \frac{k}{2E}\left(x_1^2+x_2^2\right)+\frac{k_{12}}{2E}\left(x_1-x_2\right)^2=1 \qquad (3.2)$$

This is a quadratic form or ellipse matrix equation with a *spring-force matrix* $\mathbf{K}=\begin{pmatrix} k+k_{12} & -k_{12} \\ -k_{12} & k+k_{12}\end{pmatrix}$.

$$\begin{aligned} V(x_1,x_2) &= \frac{k+k_{12}}{2}x_1^2+\frac{k+k_{12}}{2}x_2^2-k_{12}x_1x_2 \\ &= \frac{1}{2}\begin{pmatrix}x_1 & x_2\end{pmatrix}\bullet\begin{pmatrix} k+k_{12} & -k_{12} \\ -k_{12} & k+k_{12}\end{pmatrix}\bullet\begin{pmatrix}x_1\\ x_2\end{pmatrix} \quad \text{or:} \quad V=\frac{1}{2}\mathbf{x}\bullet\mathbf{K}\bullet\mathbf{x} \end{aligned} \qquad (3.3)$$

The NW and SE corners have more crowded topo-lines and steeper slope with greater force $F_k=-\frac{\partial V}{\partial x_k}$.

$$\begin{aligned} -F_1 &= \frac{\partial V(x_1,x_2)}{\partial x_1}=(k+k_{12})x_1-k_{12}x_2 \\ -F_2 &= \frac{\partial V(x_1,x_2)}{\partial x_2}=-k_{12}x_1+(k+k_{12})x_2 \end{aligned} \text{ or: } -\begin{pmatrix}F_1\\F_2\end{pmatrix}=\begin{pmatrix}\partial_1 V\\ \partial_2 V\end{pmatrix}=\begin{pmatrix} k+k_{12} & -k_{12} \\ -k_{12} & k+k_{12}\end{pmatrix}\bullet\begin{pmatrix}x_1\\x_2\end{pmatrix} \text{ or :-}\mathbf{F}=\frac{\partial V}{\partial \mathbf{x}}=\mathbf{K}\bullet\mathbf{x} \qquad (3.4)$$

Force $\mathbf{F}=-\mathbf{K}\bullet\mathbf{x}$ is along the *fall-line* and *perpendicular* to topo-lines. Vector-$\mathbf{F}$ is perpendicular to a $\mathbf{K}$-ellipse at point $\mathbf{x}$ as in Fig. 3.2 just like vector $\mathbf{p}=\mathbf{Q}\bullet\mathbf{r}$ is perpendicular to $\dot{\mathbf{r}}$ in *Step 2* of Fig. 2.2.

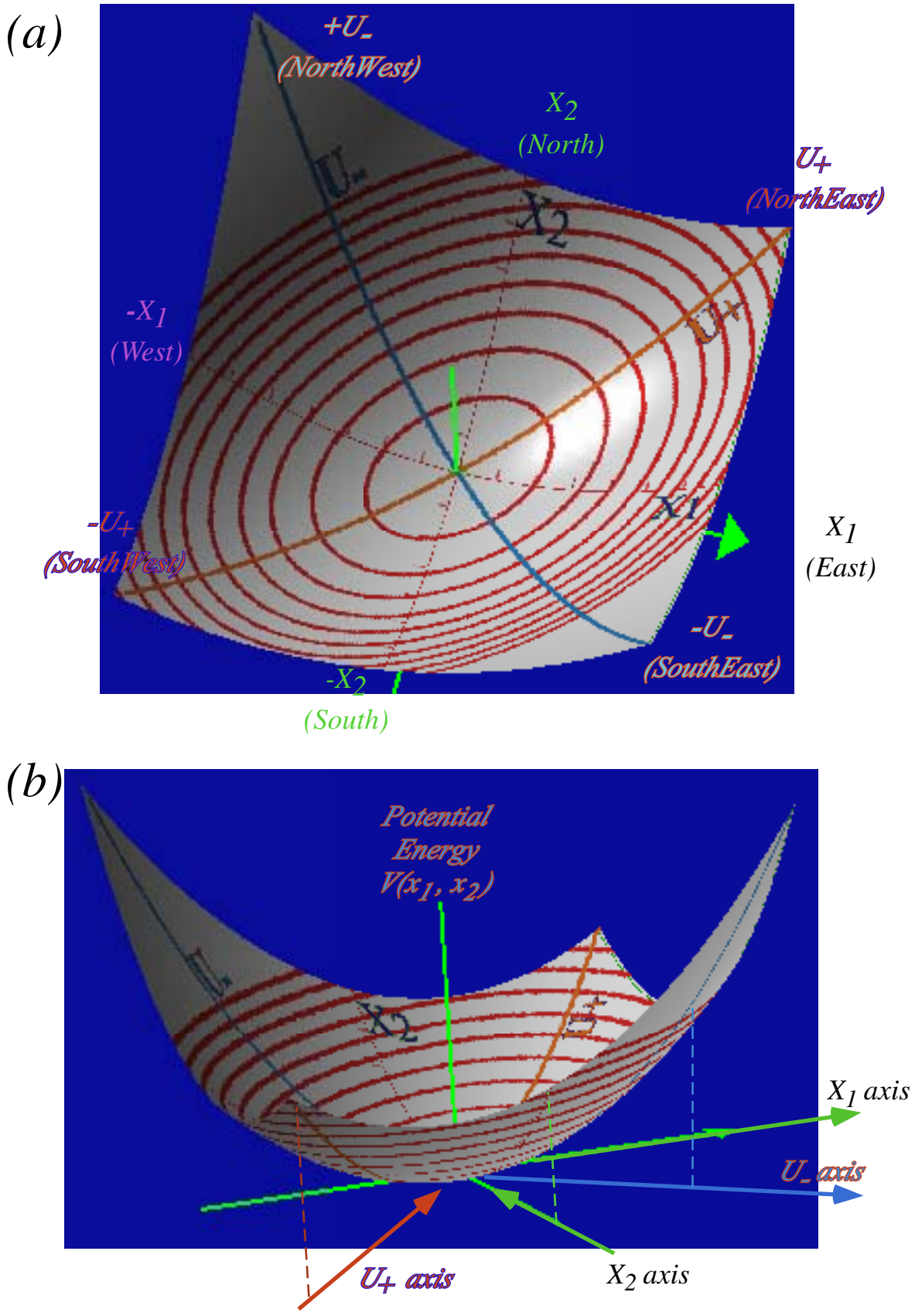

Fig. 3.1 Bare-Valley parabolic topography ($k=0.3$, $k_{12}=0.2$). (a) Elliptic contours (b) Coordinates

(b) Gradients and modes

An important idea of calculus is being shown by the elliptical topo-lines. The idea involves a vector whose *x* and *y* components (and *z* component if we're in 3D…and *t* component if we're in 4D spacetime…) are made of the *x* and *y* (and *z*, etc…) slopes or derivatives. There are several ways to write this operation that is called the *gradient* $\nabla V = \frac{\partial V}{\partial \mathbf{x}}$ of a function $V=V(\mathbf{x})$.

$$\nabla V = \frac{\partial V}{\partial \mathbf{x}} = \begin{pmatrix} \frac{\partial V}{\partial x} \\ \frac{\partial V}{\partial y} \end{pmatrix} = \begin{pmatrix} \partial_x V \\ \partial_y V \end{pmatrix} = \begin{pmatrix} \nabla_x V \\ \nabla_y V \end{pmatrix} \qquad (3.5)$$

I personally like the second way because it makes a nice shorthand for the old calculus formula $\frac{\partial(kx^2)}{\partial x} = 2kx$.

$$\frac{\partial(\mathbf{x} \bullet \mathbf{K} \bullet \mathbf{x})}{\partial \mathbf{x}} = 2\mathbf{K} \bullet \mathbf{x}\,, \qquad \frac{\partial(\mathbf{x} \bullet \mathbf{x})}{\partial \mathbf{x}} = 2\mathbf{x} \qquad (3.6)$$

(But be careful!) The main geometrical thing to remember about a gradient ∇V is that it gives a vector perpendicular to the *V* function it's acting upon as we showed in (3.4). The Bare Valley topography map in Fig. 3.2 shows this. And, minus the ∇V vector is the applied force that the mass or "skier" at position $\mathbf{x}$ will experience due to springs, gravity, or whatever is making things swing back and forth.

Bare Valley has its gentlest "beginner slopes" on the NE *(45°)* and SW *(225°)* sides and its steeper "advanced slopes" on the NW *(135°)* and SE *(315°)* corners while "intermediate slopes" are found at N*(90°)*, W*(180°)*, S*(270°)*, and E*(0°)*, unlike the usual compass headings with *0°* for North at the top of a map. The *45°* beginner coordinate u_+ and the *135°* advanced coordinate u_- are related to the *x* and *y* or East and North coordinates x_1 and x_2 by projecting on *45°* or *135°*. *(cos 45°=1/√2=sin 45°=sin135°= -cos135°)*

$$u_+ = \frac{x_1 + x_2}{\sqrt{2}} \qquad (3.7a) \qquad x_1 = \frac{u_+ - u_-}{\sqrt{2}} \qquad (3.7b)$$
$$u_- = \frac{-x_1 + x_2}{\sqrt{2}} \qquad\qquad x_2 = \frac{u_+ + u_-}{\sqrt{2}}$$

The energy equation (3.2) is one of an ellipse on (u_+, u_-) axes since $u_+^2 + u_-^2 = x_1^2 + x_2^2$ and $x_1 - x_2 = -\sqrt{2}u_-$.

$$V = \frac{k}{2}\left(x_1^2 + x_2^2\right) + \frac{k_{12}}{2}\left(x_1 - x_2\right)^2 = \frac{k}{2}\left(u_+^2 + u_-^2\right) + \frac{k_{12}}{2}\left(-\sqrt{2}u_-\right)^2 = \frac{k}{2}u_+^2 + \frac{k + 2k_{12}}{2}u_-^2 \qquad (3.2)_{redone}$$

This means the beginner-slope force constant *k* is lower than the advanced slope constant $k+2k_{12}$. So is beginner oscillation frequency ω_+ less than that the frequency ω_- something sliding on the advanced slope.

$$\omega_+ = \sqrt{\frac{k}{m}} \qquad (3.8a) \qquad \omega_- = \sqrt{\frac{k + 2k_{12}}{m}} \qquad (3.8b)$$

Fig. 3.2(a) shows the SLOW u_+ mode that goes NE *(45°)* to SW *(225°)* so x_1 and x_2 are *in* phase. Fig. 3.2(b) shows the FAST u_- mode that goes NW *(135°)* to SE *(315°)* so x_1 and x_2 are *π out of* phase.

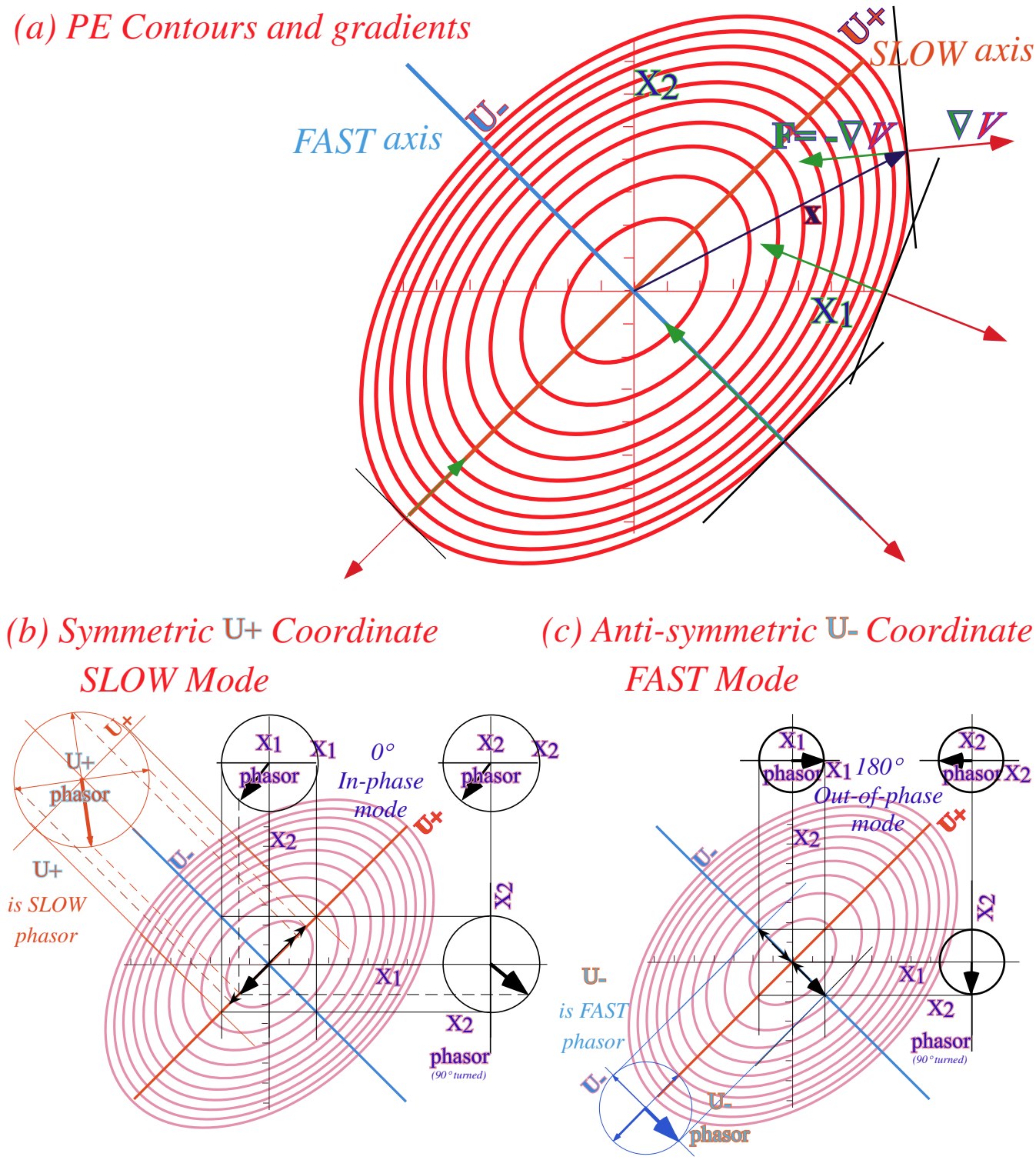

Fig. 3.2 (a) Force-potential of Bare Valley gives symmetric (+) or antisymmetric (-) vibration modes. (b) SLOW (+) mode goes on minimum shallow slope. (c) FAST (-) mode goes on maximum steep slope.

Now let's see what happens if we superimpose both these modes at once. We can do this and still have a valid motion because the force equations are *linear* ones. The result is shown in Fig. 3.3.

(c) Superposition principle and beats

An important idea of modern physics of linear resonance dynamics is the *superposition principle*, that you can simply add two valid motions together and get another one. Modes mix like paints that together can paint anything that happens in the world! It's an idea that is generally credited to Jean Baptiste Fourier's analysis, but it really goes back to Huygens and Leibenitz. It works well if mode frequencies are the same for all amplitudes as they are for *harmonic* oscillations under *linear* force laws.

By adding each of the U_+-*SLOW*-mode phasors in Fig. 3.2(a) to each of the U_--*FAST*-mode phasors in Fig. 3.2(b) we get the situation depicted in Fig. 3.3. The result, if the two modes were the same frequency, is no different from the mode pictures of previous figures like Fig. 2.4. The elliptic orbit would be drawn over and over because the phase lag $\rho = \theta_- - \theta_+$ of the SLOW U_+-mode phasor behind the FAST U_--mode phasor must then stay fixed since the modes are turning at the same rate.

However, that is not the case here. The *FAST* U_--mode phase θ_- soon runs ahead of the *SLOW* U_+-mode phase θ_+. As their phase lag $\rho = \theta_- - \theta_+$ changes so does the (x_1,x_2)-ellipse drawn by the two phasors. As the (x_1 , x_2)-ellipse changes so do the amplitude and phases of the x_1 and x_2 phasors.

This complicated motion is called *beating* after the effect by the same name that we hear all the time in music and acoustics. The rate ω_{Beat} of beating is simply the *relative phase velocity* $\frac{d\rho}{dt}$, that is, the difference between the FAST and SLOW angular rates $\omega_- = \frac{d\theta_-}{dt}$ and $\omega_+ = \frac{d\theta_+}{dt}$.

$$\omega_{Beat} = \omega_- - \omega_+ = \frac{d\rho}{dt} = \frac{d\theta_-}{dt} - \frac{d\theta_+}{dt} \tag{3.9}$$

From the results of (3.8) we obtain the *angular beat frequency*.

$$\omega_{Beat} = \omega_- - \omega_+ = \sqrt{\frac{k + 2k_{12}}{m}} - \sqrt{\frac{k}{m}} \tag{3.10a}$$

Its binomial approximation $\left((a+b)^{\frac{1}{2}} = a^{\frac{1}{2}} + \frac{1}{2} a^{-\frac{1}{2}} b + \ldots \right)$, at first, grows linearly with coupling constant k_{12}.

$$\omega_{Beat} \cong \frac{1}{2} \frac{2k_{12}}{\sqrt{k\,m}} = \frac{k_{12}}{k} \sqrt{\frac{k}{m}} \quad \text{for: } k_{12} << k \tag{3.10b}$$

At the moment shown in Fig. 3.3(a) the *SLOW* U_+-mode phase is about ρ=60° behind the *FAST* U_--mode phase. At a slightly later time in Fig. 3.3(b) the phase lag increases to ρ=90° and continues increasing at beat rate ω_{Beat} (3.10). As ρ rolls through 2π the (x_1,x_2)-phasors and their (x_1,x_2)-ellipse beat or pulse in and out. The (x_1,x_2)-beat goes on while the U_+-U_--phasors each turn constantly.

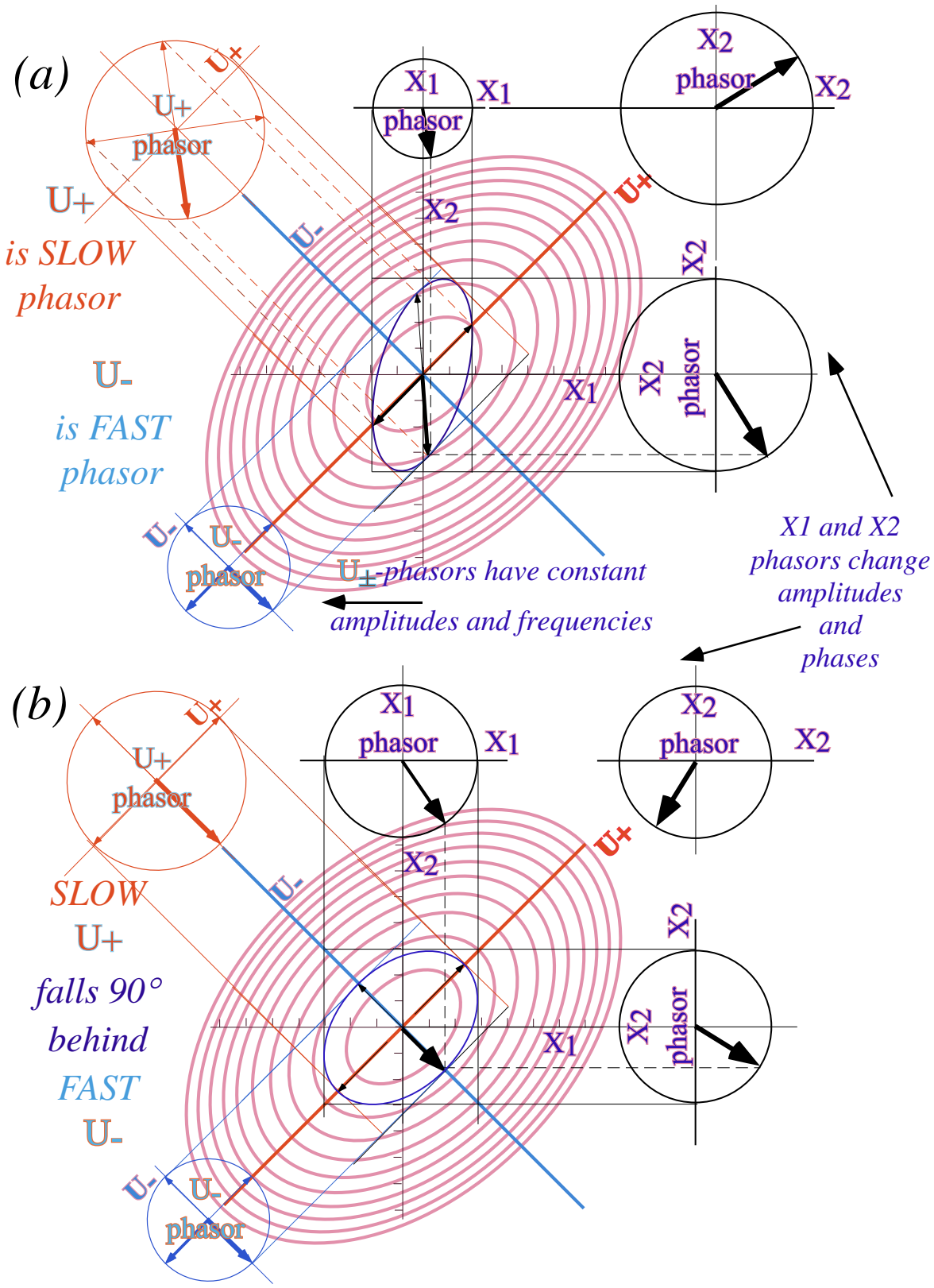

Fig. 3.3 Superposition of the U+ and U- modes from Fig. 3.2 (a-b). (a)One time (b)Later time

Chapter 4 Complex phasor analysis of oscillation, beats, and modes

The simplest oscillation is *harmonic oscillation*, for which *anguolar frequency* ω (wiggles per 2π second) is constant regardless of *amplitude* A as in an ideal pendulum or mass on a spring. To track oscillation we use time plots of x *versus* t, that is, $x(t)$, as well as phase plots of oscillating mass position $x=A\cos\omega t$ versus its velocity $v= -A\omega\sin\omega t$. On a graph of x *versus* v/ω in Fig. 4.1, the point moves on a circle like a clock hand as in previous examples in Fig. 3.3 and first introduced in Fig. 10.5b of Unit 1. Here we treat the phase plot in Fig. 4.1 as an actual 12-hour clock starting at 3 AM.

A day in the life of this oscillator begins at 3AM with it standing still at $x=1$. By 4AM it is at $x=0.866$ (x is $\cos(-1\cdot 2\pi/12)$) going with a negative velocity toward the origin. By 5AM it is half way to origin at $x=0.5$ (x is $\cos(-2\cdot 2\pi/12)$) going with even faster negative velocity given by $\sin(-2\cdot 2\pi/12)$ in units of frequency ω. Here the clock *angular frequency* ω is -2π radians per 12-hour day or a *Hertz frequency* ν of 1-per-day, and a *period* $\tau=1/\nu$ of $\tau=1$ *day=12 hours =12(60) minutes =12(3600) seconds*.

At 6AM it passes origin at $x=0$ (x is $\cos(-3\cdot 2\pi/12)$) going with maximum negative velocity (v is $\sin(-3\cdot 2\pi/12)=-1$ in units of frequency ω. 6AM is halfway through the "compression" phase.

At 9AM it arrives on the other side of origin at $x=-1$ (x is $\cos(-6\cdot 2\pi/12)$) and comes to a stop at zero velocity (v is $\sin(-6\cdot 2\pi/12)$ in units of ω. This ends the "compression" phase in the Fig. 4.1(b).

The rest of the day from 9AM to 3PM (as the oscillator returns home) is its "expansion" phase in which its velocity is positive. Then its phasor clock is in the upper half of the clock dial at the top of Fig. 4.1(b) that represents positive velocity. The lower half indicates negative velocity.

(a) Introducing complex phasors and wavefunctions: Real and imaginary axes

The phase-plot velocity-axis is called the *imaginary axis* by engineers and physicists who prefer to use *complex phasor* clocks like the one shown in Fig. 4.1(c). It's the same as the clock drawn in the upper part of the figure, except it is based on what may be one of the most important mathematical results of all time, the so called *Euler identity*. (The French call it the *Theorem of DeMoivre*.)

$$e^{-i\Theta} = \cos\Theta - i\sin\Theta \qquad (i=\sqrt{-1}) \qquad (4.1a)$$

A wave function or oscillation function Ψ of a given *angular frequency* ω is written using Euler's form.

$$\Psi = A\,e^{-i\omega t} = A\cos\omega t - i\,A\sin\omega t \quad (i=\sqrt{-1}) \qquad (4.1b)$$

The *real part* $\mathrm{Re}\ \Psi = A\cos\omega t$ and the *imaginary part* $\mathrm{Im}\ \Psi = -A\sin\omega t$ are the Cartesian coordinates of the phasor clock in Fig. 4.1.(c). The *absolute value* $|\Psi|= A$ and *argument* $ARG\,\Psi=-\omega t$ or *phase angle* are the phasor polar coordinates. This is the main reason your calculator has Polar-Rect and Rect-Polar buttons!

Chapter 10 of Unit 1 introduced the complex phasor, *Euler's number e=2.7182818…*, and exponential functions in general. Here we give a quick description of applications of complex $e^{-i\omega t}$ numbers to the beats described in the preceding Chapter 3 and relate them to ellipse geometry.

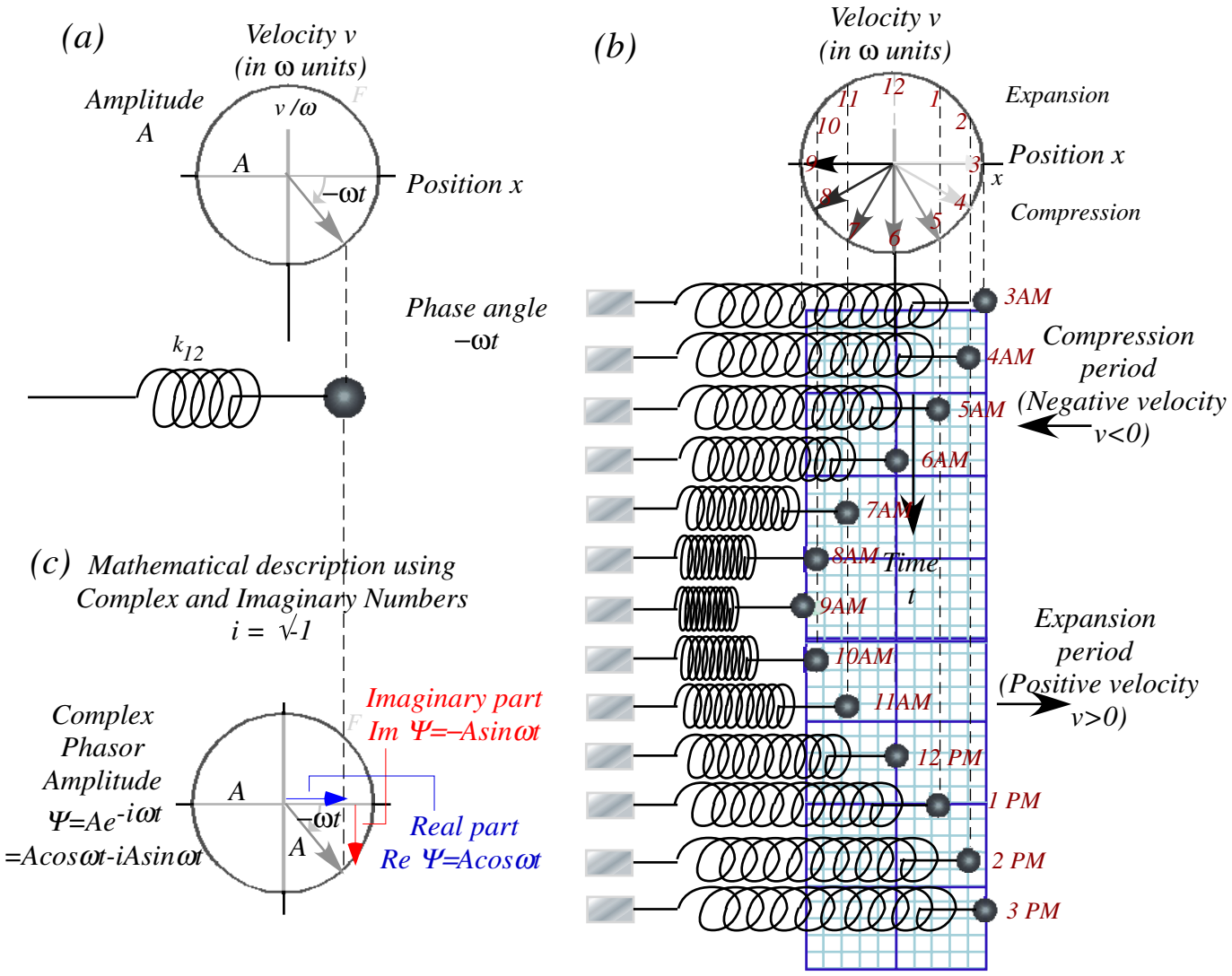

Fig. 4.1 Single pendulum oscillation. (a) phasor plots. (b) Spacetime plot. (c) Complex phasor "clock."

(b) Coupled oscillation between identical pendulums

The resonance process, by which two identical oscillators trade energy and momentum, may be analyzed by first looking at the very simplest motions that the two can undergo. The two modes of the oscillators are shown in Fig. 4.2. This is another and simpler way to look at the ones in Fig. 3.2

The *slow mode* in Fig. 4.2(a) is simply the two pendulums swinging together as though they were one. The spring connecting them might as well not even exist. It does nothing since it is neither stretched nor compressed by this motion. This is the same as Fig. 3.2(b).

The opposite situation holds in Fig. 4.2(b) or Fig. 3.2(c) where pendulums swing oppositely as though each was connected to an immovable wall between them. Because both stretch and compress their connecting spring at once, this *fast mode* motion will have a higher frequency than the *slow mode* in Fig. 4.2(a) effectively doubling the force of spring k_{12}. This explains the $2k_{12}$ in the ω_- frequency formula (3.8b) for the (-)-mode and no k_{12} in the ω_+ frequency formula (3.8a) for the (+)-mode

For the sake of argument we will take the frequency of the fast mode to be twice that of the slow mode. (That is $k_{12}=3k$ in (3.8).) This means that while the slow mode swings both masses on a one-way trip to the other side between 3AM and 9AM, the fast mode brings them together *and* sends them back home in that time and then repeats that whole two-way trip by 3PM in the afternoon.

(c) Summing phasors using Euler's identity: Beats

The frequency ω of a single harmonic oscillator is unaffected by changing amplitude A of oscillation. This is because a harmonic spring is *linear*, that is, the force it exerts is *proportional* to the distance x from origin or equilibrium. So acceleration is a constant ω^2 times the amplitude A , and this is true no matter how big A is. (Recall the $\mathbf{a}(t)$ equation in the middle of (2.1).)

Similarly, the mode frequencies ω_{slow} and ω_{fast} of a double harmonic oscillator are not affected by their amplitudes, either. That means neither A_{fast} nor A_{slow} affect either ω_{slow} or ω_{fast} even if they are *both turned on at once*! The system can swing at ω_{slow} while vibrating at ω_{fast} and neither frequency changes. It's a little like walking back and forth while chewing gum at the same time and not missing a beat!

This is no surprise if you followed the superposition (10.51) in Unit 1 or the analogy between two 1-dimensional pendulums and one 2-dimensional "starlet" oscillator-orbiter first introduced in Unit 1 Chapter 9. The two-1D to one-2D connection is a deep one that we use often. It's appearance in quantum theory is particularly interesting where one relates an m-particle n-dimensional system to an n-particle m-dimensional system or to an 1-particle mn-dimensional one!

Suppose we turn on both modes with equal amplitude, that is let $A_{fast}=1=A_{slow}$. Then we get a sum of two mode phasors describing mass-1 and difference of two mode phasors describing mass-2.

$$\Psi_{\text{mass-1}} = A_{fast}\, exp(-i\omega_{fast}t) + A_{slow}\, exp(-i\omega_{slow}t) = exp(-i\omega_{fast}t) + exp(-i\omega_{slow}t) \quad (4.2a)$$

$$\Psi_{\text{mass-2}} = A_{fast}\, exp(-i\omega_{fast}t) - A_{slow}\, exp(-i\omega_{slow}t) = exp(-i\omega_{fast}t) - exp(-i\omega_{slow}t) \quad (4.2b)$$

These sum and differences are done by geometry in the next several figures. However, for this case it is quite easy to analyze them using Euler's forms with $a=\omega_{fast}t=2.0t$ and $b=\omega_{slow}t=1.0t$.

$$e^{ia} + e^{ib} = e^{i(a+b)/2}\,(e^{i(a-b)/2} + e^{-i(a-b)/2}) \quad (4.3a)$$

$$e^{ia} - e^{ib} = e^{i(a+b)/2}\,(e^{i(a-b)/2} - e^{-i(a-b)/2}) \quad (4.3b)$$

Now we use the cosine $cos\ x = (e^{ix} + e^{-ix})/2$ and sine $sin\ x = (e^{ix} - e^{-ix})/2i$ in Euler form.

$$\Psi_{\text{mass-1}} = e^{ia} + e^{ib} = 2\, e^{i(a+b)/2}\, cos\ (a-b)/2 = 2\, e^{i3t/2}\, cos\ t/2 \quad (4.4a)$$

$$\Psi_{\text{mass-2}} = e^{ia} - e^{ib} = 2i\, e^{i(a+b)/2}\, sin\ (a-b)/2 = 2i\, e^{i3t/2}\, sin\ t/2 \quad (4.4b)$$

In Fig. 4.3 the mass-1 and mass-2 phasors are summed starting at 12PM *(t=0)* and then at 1 PM *(t=1)*.

Transverse or Longitudinal?

This analysis applies equally to two pendulums that swing side-by-side like the ones in Fig. 4.3 (and demonstrated in class). These are called *transverse* oscillators as opposed to *longitudinal* oscillators pictured in Fig. 4.2. The motions in Fig. 4.3 are transverse to their connection or coupling while the masses in Fig. 4.2 move along a line connecting them.

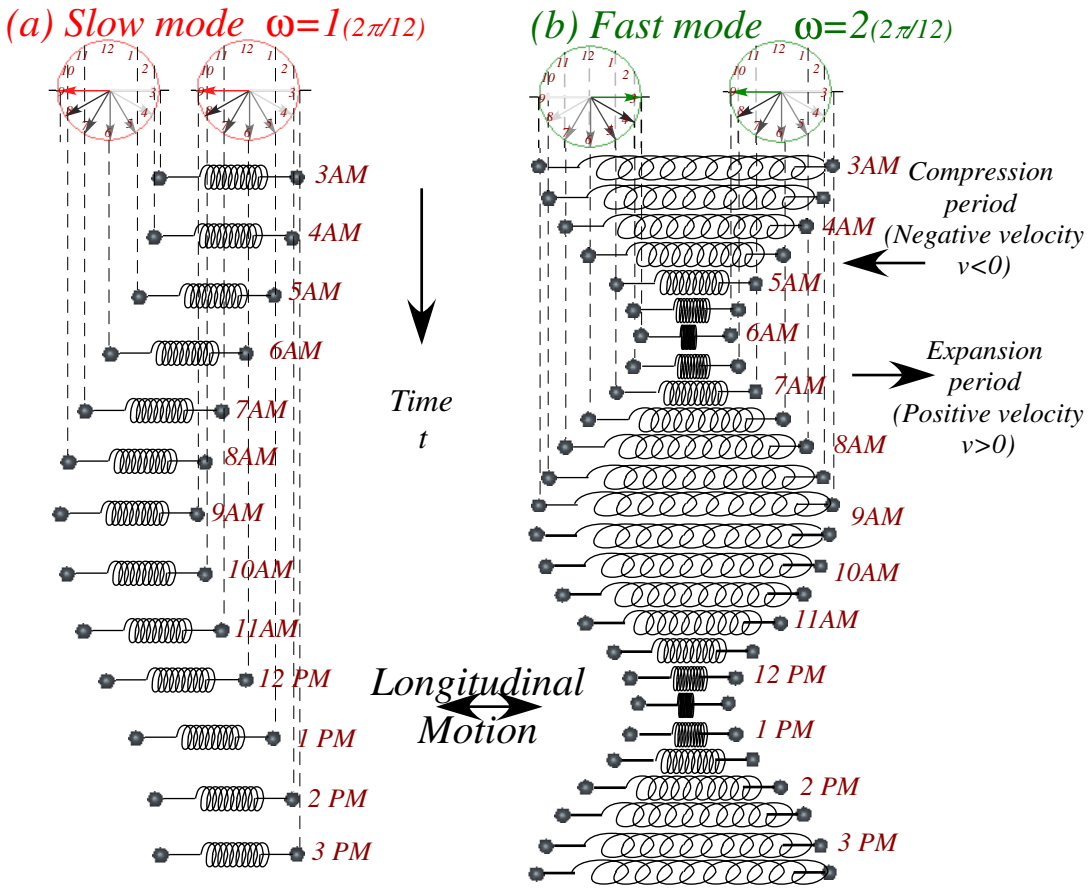

Fig. 4.2 Coupled oscillators. (a)Slow-ω=1 mode swings in phase and does not stretch connector.
(b) Fast-ω=2 mode swings π out of phase and stretches connector by twice.

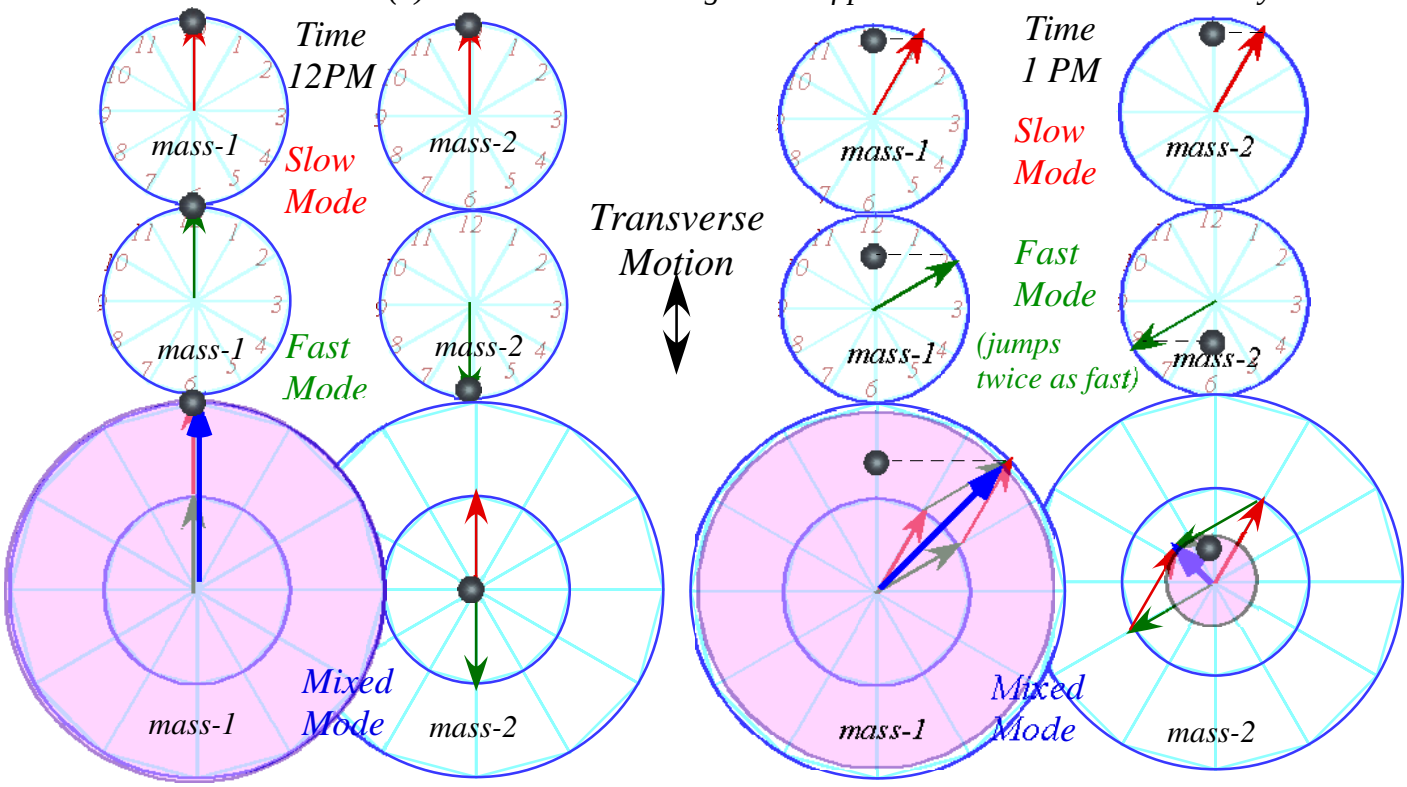

Fig. 4.3 Coupled pendulum with mixed mode (sum of fast and slow modes) (a) 12 PM. (b) 1 PM

Here in Fig. 4.3 the pendulums swing transverse to their connectors so the real position *x*-axis is vertical and the (imaginary) velocity *v*-axis points horizontally off to the left.

In Fig. 4.3 at 12PM mass-1 is standing still with double amplitude and mass-2 is stuck at origin with no energy at all. But, by 1PM mass-1 is moving in a negative direction and about three quarters of the way to origin. Its amplitude is slightly reduced to $2\cos(0.5\cdot 2\pi/12)$ by eq. (3.4a) (See big lavender circle in Fig. 4.3(right)) while mass-2 has acquired an amplitude of $(2\sin(0.5\cdot 2\pi/12)$ (See small lavender circle in Fig. 4.3(extreme right)). Throughout this process the sum of the areas of the lavender circles will remain constant. Each lavender area is proportional to the total energy of each oscillator. Recall why total phasor area is constant in Fig. 1.11.

Note that the phasor arrow for mass-2 lags $90°$ or $\pi/2$ radians behind that of mass-1. This checks with the (i)-factor in equation (4.4b). An $(i=e^{i\pi/2})$-factor represents a $90°$ rotation the is *counter*-clockwise. So. it sets mass-2's clock *back* a quarter turn or 3 hours.

A $90°$ phase lag is a very important thing to physics and engineering. It is the phase lag that is most efficient at transferring energy from one oscillator to another. Then force and velocity are in phase so that power, which is force times velocity, is as big as it can be.

In Fig. 4.4 the time sequence continues as the phasors rotate according to the phase factor $e^{i3t/2}$ in equations (3.4) but the $(i=e^{i\pi/2})$-factor on mass-2 keeps it $90°$ or $\pi/2$ radians behind that of mass-1 until mass-1 runs out of energy and at 6PM mass-2 has it all. That marks the halfway point of the first *beat*.

At 7 PM the phasor for mass-1 comes out $90°$ or $\pi/2$ radians behind that of mass-2, and the tables are turned with mass-2 the energy donor and mass-1 soaking it up as fast as it can from 7PM to 12PM. Finally, at 12 PM (not shown) the first beat completes itself and the whole sequence occurs again.

(c) Slow(er) Beats

The beat frequency in (4.4) is half the difference between the two mode frequencies in (4.1), in this case that is $(\omega_{fast}-\omega_{slow})/2=0.5$, which means it will take 24 hours or two full slow-clock rotations. In that time the fast clock laps the slow clock *twice*.

But, if you could only see the lavender circles and not the phase vectors inside, one beat appears to go from mass-1 to mass-2 by 6 PM in Fig. 4.4 and will be back by 12 PM. All that is needed is for the fast clock to lap the slow clock just *once*. The lavender-circle beat frequency is the relative angular velocity of the fast versus slow clocks around the phasor track. Here $(\omega_{fast}-\omega_{slow})=1.0$ per 12-hr day.

$$\omega_{beat}=\omega_{fast}-\omega_{slow} \qquad (4.5)$$

If two modes have very nearly the same frequency, then a beat takes a longer time because the faster phasor takes longer to lap the slower one. In Fig. 4.5 it takes a little over 4 phase oscillations to complete one beat "lump" or group wave. In atomic laser optics this number is often more like 40 or 50 *million*. In nuclear physics it can be way over a *million-million*. That's a lot of very patient persuasion! To understand some of the subtler aspects of modern physics we must find ways to begin comprehending the consequences of such an enormous amount of persuasion.

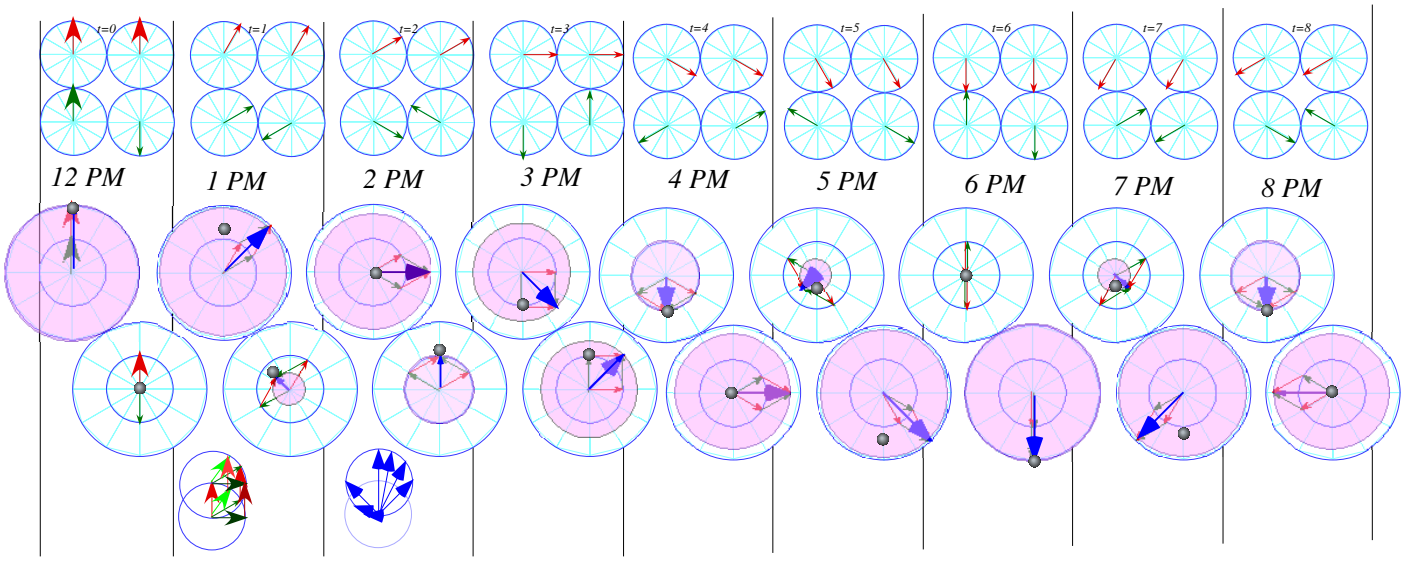

Fig. 4.4 Coupled pendulum with mixed mode (sum of fast and slow modes) from 12 PM to 8 PM

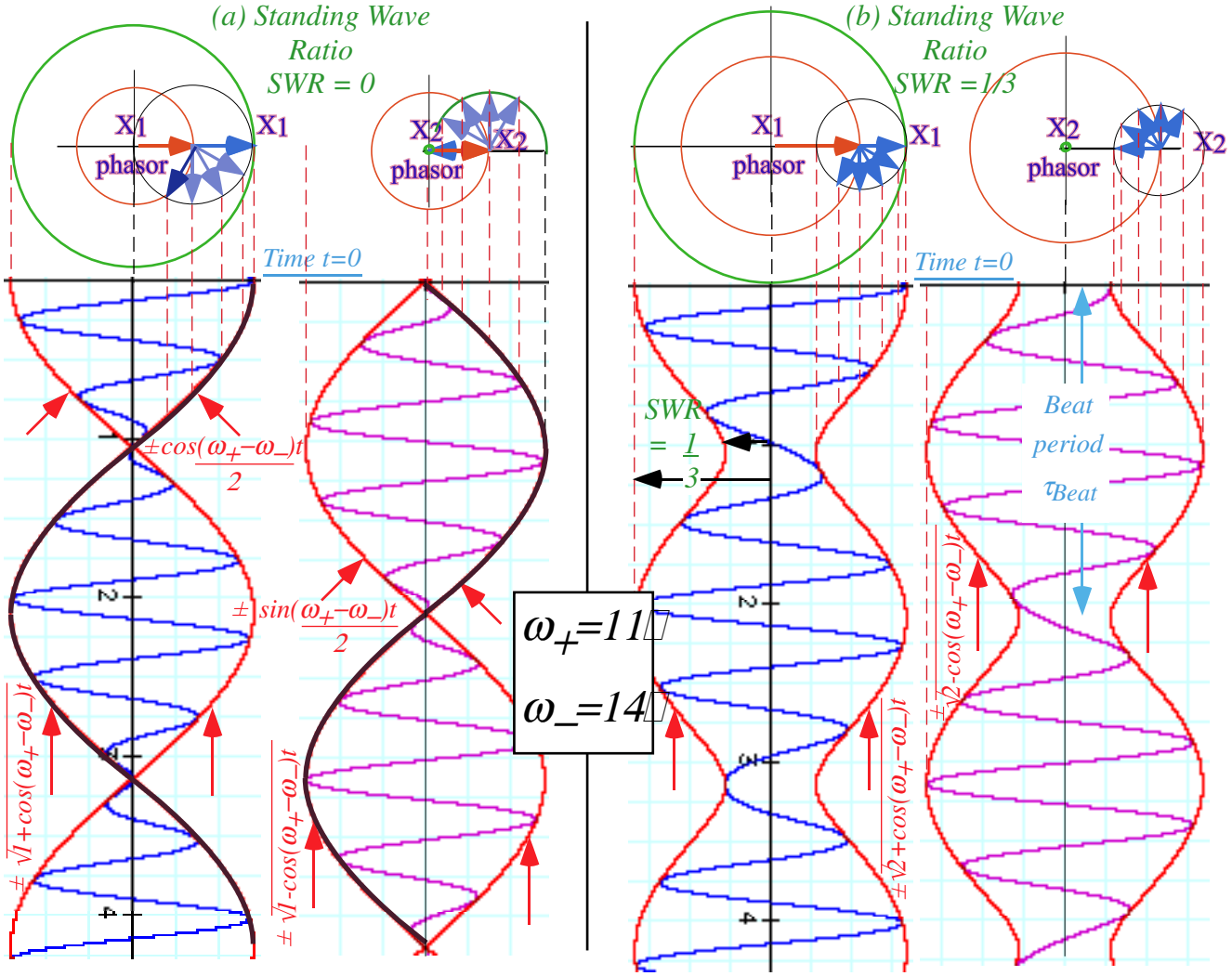

Fig. 4.5 Coupled pendulum with mixed mode and more nearly equal mode frequencies.

(d) Geometry of resonance and phasor beats

Fig. 4.4 and Fig. 4.5 show some ways to plot the complex wave sums $\Psi = A\,e^{-i\omega_A t} + B\,e^{-i\omega_B t}$ of mode phasors in (4.2) over time. Now we consider the geometry of phasor vector sums and differences.

Head-to-tail addition of phasors in Fig. 4.5 gives nodes in Fig. 4.5(a) for equal amplitudes *(A_1=A_2)* but not for unequal amplitudes in Fig. 4.5(b). The ratio of the nodal minimum amplitude ($|A|$-$|B|$ at points of *destructive interference*) to the maximum possible amplitude ($|A|+|B|$ at points of *constructive interference*) is a *standing wave ratio (SWR)* . Its inverse is the *standing wave quotient (SWQ)*.

$$SWR=(|A|-|B|)/(|A|+|B|) \quad (4.6a) \qquad SWQ=(|A|+|B|)/(|A|-|B|) \quad (4.6b)$$

Zero *SWR* or infinite *SWQ* means equal "50-50" amplitudes as sketched in Fig. 4.5(a).

How a phasor is plotted depends upon what one chooses for the overall phase that is factored out. This corresponds to choosing a reference plotting frame in phasor space. Fig. 4.6 displays three main choices corresponding to the three factorizations below.

$$\Psi = Ae^{-i\omega_A t} + Be^{-i\omega_B t} \qquad (4.7)$$

$$= e^{-i\omega_A t}\left(A + Be^{-i(\omega_B-\omega_A)t}\right) = e^{-i\omega_B t}\left(Ae^{+i(\omega_B-\omega_A)t} + B\right) = e^{-i(\omega_B+\omega_A)t/2}\left(Ae^{+i(\omega_B-\omega_A)t/2} + Be^{-i(\omega_B-\omega_A)t/2}\right)$$

A - phasor view *B - phasor view* *A + B average - phasor view*

The *A*-frame view rides with the *A*-phasor by ignoring its $e^{-i\omega_A t}$ rotation as shown in Fig. 4.5(a) for three different SWR values. In each case, a circle of radius *B* is traced around a fixed *A*-vector.

The *B*-frame view rides with the *B*-phasor by ignoring its $e^{-i\omega_B t}$ rotation as shown in Fig. 4.5(b) for three different SWR values. In each case, a circle of radius *A* is traced around the *B*-vector.

In each of these the angle between the sum *(A+B)* and difference *(A-B)* phasors should be noted particularly for the *(SWR=0)*-case where that angle is either $+90°$ or else $-90°$. We have noted the $\pm 90°$ phase between mass-1 and mass-2 in Fig. 4.4 and how it switches each time one of the phases loses all its energy. Now we see that behavior has a simple geometric explanation based upon right triangles inscribed in a circle with diameter on the hypotenuse.

The figures (a2) and particularly (b2) show a quite violent motion that the sum or difference phasor must undergo each time it passes close to the origin and switches from nearly $+90°$ to nearly $-90°$ or *vice-versa*. This galloping behavior is responsible for faster-than-light laser waves later.

The *AB average*-frame view factors out the average phase $e^{-i(\omega_B+\omega_A)t/2}$ so that *A* and *B* rotate with opposite but opposite angles, one centered on the other as shown in Fig. 4.5(c). The resultants generate elliptical orbits of major radius $a=A+B$ and minor radius $b=A-B$. The construction is quite the same as the one in Fig. 2.2 and gives both the ellipse, by phasor sum $A+B$, and the inverse ellipse, by the difference phasor $A-B$, whose vectors are the diagonal of the rectangle connecting the two ellipses.

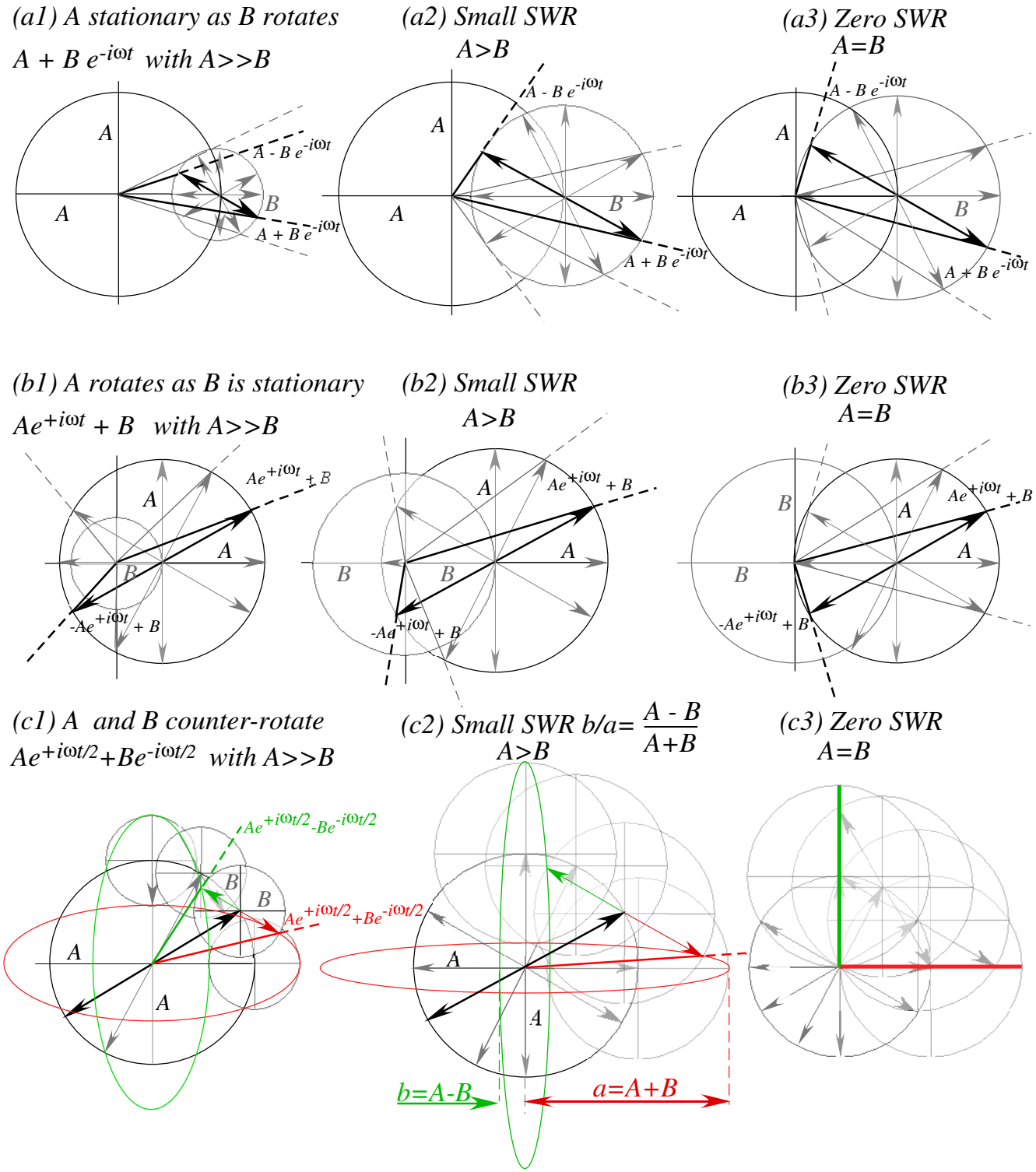

Fig. 4.6 Three views of phasor sums A±B having three different SWR values.

Views (a1-a3) Phasor A fixed. Views (b1-b3) Phasor B fixed. Views (c1-c3) A and B counter rotate.

(e) Adding complex phasors

The best way known for adding up our phasors uses *complex* numbers, that is, numbers like $2+i$ containing the *imaginary* square root $i=\sqrt{-1}$ of minus one. Every physicist should be able to add (and multiply) $2+i$ and $2+i$ quickly as well as find $\sin(2+i)$ and $(2+i)^{2+i}$. Do complex numbers make you queasy? Then you'll be like a doctor that faints at the sight of blood. Let's see how they work here.

The basic description of the 2-identical-oscillator is a complex 2D vector $|X\rangle$ having complex components $z_1=x_1+iv_1$ and $z_2=x_2+iv_2$ represented by X_1 and X_2 phasors in Fig. 4.7. Here we use (3.7b).

$$|X\rangle=\begin{pmatrix} z_1(t) \\ z_2(t) \end{pmatrix}=\begin{pmatrix} \dfrac{u_+(t)-u_-(t)}{\sqrt{2}} \\ \dfrac{u_+(t)+u_-(t)}{\sqrt{2}} \end{pmatrix}=u_+(t)\begin{pmatrix} \dfrac{1}{\sqrt{2}} \\ \dfrac{1}{\sqrt{2}} \end{pmatrix}+u_-(t)\begin{pmatrix} \dfrac{-1}{\sqrt{2}} \\ \dfrac{1}{\sqrt{2}} \end{pmatrix}=u_+(t)|U_+\rangle+u_-(t)|U_-\rangle \qquad (4.8)$$

The driving phasors are the *SLOW* U_+-mode and *FAST* U_--mode phasors whose complex components u_+ and u_- do nothing more than oscillate at their initially assigned amplitudes $u_\pm(0)$ and frequencies $\omega_\pm$.

$$u_+(t)=u_+(0)e^{-i\omega_+t} \qquad (4.9a) \qquad\qquad u_-(t)=u_-(0)e^{-i\omega_-t} \qquad (4.9b)$$

The object of Fig. 4.7 is to construct the pulsing X_1 and X_2 -phasors for a single beat.

$$|X\rangle=\begin{pmatrix} z_1(t) \\ z_2(t) \end{pmatrix}=\frac{u_+(t)}{\sqrt{2}}\begin{pmatrix} 1 \\ 1 \end{pmatrix}+\frac{u_-(t)}{\sqrt{2}}\begin{pmatrix} -1 \\ 1 \end{pmatrix}=\frac{u_+(0)}{\sqrt{2}}\begin{pmatrix} e^{-i\omega_+t} \\ e^{-i\omega_+t} \end{pmatrix}+\frac{u_-(0)}{\sqrt{2}}\begin{pmatrix} -e^{-i\omega_-t} \\ e^{-i\omega_-t} \end{pmatrix} \qquad (4.10a)$$

Fig. 4.7 has equal-but-opposite mode components $u_+(0)=1/\sqrt{2}=-u_-(0)$. To simplify the construction let *SLOW* U_+ be *really* slow ($\omega_+=0$) and only vary *FAST* U_--phasor (or phase lag ρ of U_- behind U_+). With equal but opposite amplitudes ($u_+(0)=1/\sqrt{2}=-u_-(0)$) the complex algebra simplifies a lot.

$$|X\rangle=\begin{pmatrix} z_1(t) \\ z_2(t) \end{pmatrix}=\frac{1}{\sqrt{2}}\begin{pmatrix} u_+(0)e^{-i\omega_+t}-u_-(0)e^{-i\omega_-t} \\ u_+(0)e^{-i\omega_+t}+u_-(0)e^{-i\omega_-t} \end{pmatrix}=\frac{1}{2}\begin{pmatrix} e^{-i\omega_+t}+e^{-i\omega_-t} \\ e^{-i\omega_+t}-e^{-i\omega_-t} \end{pmatrix} \qquad (4.10b)$$

We separate *average* or *overall phase* $(\omega_-+\omega_+)t/2$ from more easily observable *relative phase* $(\omega_--\omega_+)t/2$.

$$|X\rangle=\begin{pmatrix} z_1(t) \\ z_2(t) \end{pmatrix}=e^{\frac{-i(\omega_++\omega_-)t}{2}}\begin{pmatrix} \cos\dfrac{(\omega_--\omega_+)t}{2} \\ i\sin\dfrac{(\omega_--\omega_+)t}{2} \end{pmatrix} \qquad (4.10c)$$

This is an example the *sine-expo* and *cosine-expo identities* introduced in (4.3).

$$e^{ia}-e^{ib}=e^{i\frac{a+b}{2}}\left(e^{i\frac{a-b}{2}}-e^{-i\frac{a-b}{2}}\right) \qquad (4.10d)$$
$$=2ie^{i\frac{a+b}{2}}\sin\frac{a-b}{2}$$

$$e^{ia}+e^{ib}=e^{i\frac{a+b}{2}}\left(e^{i\frac{a-b}{2}}+e^{-i\frac{a-b}{2}}\right) \qquad (4.10e)$$
$$=2e^{i\frac{a+b}{2}}\cos\frac{a-b}{2}$$

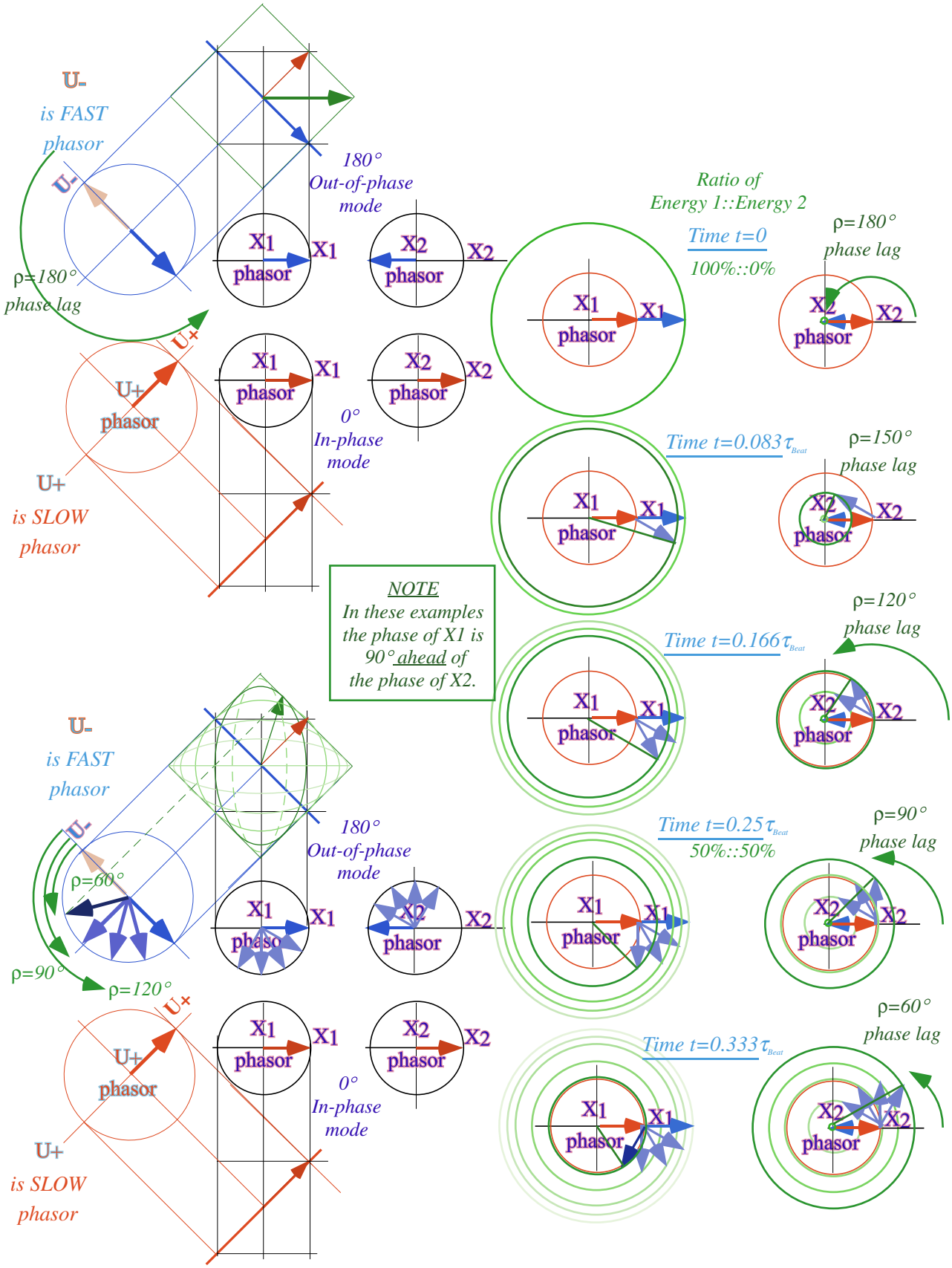

Fig. 4.7 Oscillator phases for a symmetric beat. (Initial amplitudes $u_+(0)=1/\sqrt{2}= -u_-(0)$.)

Wave *phasor-area* $|z^*z|$ or *envelope* $|z|=\sqrt{|z^*z|}$ oscillates at a slower *relative frequency* $\omega_-\text{-}\omega_+$.

$$|z_1(t)|^2 = z_1(t)^* z_1(t) = \cos^2\frac{(\omega_- - \omega_+)t}{2} \qquad (4.11a) \qquad |z_1(t)| = \sqrt{\frac{1+\cos(\omega_- - \omega_+)t}{2}} \qquad (4.11b)$$

$$|z_2(t)|^2 = z_2(t)^* z_2(t) = \sin^2\frac{(\omega_- - \omega_+)t}{2} \qquad (4.11a) \qquad |z_2(t)| = \sqrt{\frac{1-\cos(\omega_- - \omega_+)t}{2}} \qquad (4.11b)$$

Fig. 4.7 and Fig. 4.8(a) shows the time evolution of the amplitudes (4.10). It is easier to measure the envelope beats that have a slower frequency $\omega_{Beat} = \omega_- - \omega_+$ than the faster oscillation inside the envelope that has the *average* or *carrier frequency* $\omega_{Average} = (\omega_- + \omega_+)/2 = \omega_{Carrier}$.

The same frequencies apply for more general initial amplitudes. Fig. 4.8(b) shows the result of initial amplitudes ($u_+(0)= \sqrt{2}$, $u_-(0)=-\sqrt{2}/2$) that give initial ($x_1(0)=1.5, x_2(0)=0.5$).

$$|X\rangle = \begin{pmatrix} z_1(t) \\ z_2(t) \end{pmatrix} = \frac{1}{\sqrt{2}}\begin{pmatrix} u_+(0)e^{-i\omega_+ t} - u_-(0)e^{-i\omega_- t} \\ u_+(0)e^{-i\omega_+ t} + u_-(0)e^{-i\omega_- t} \end{pmatrix} = \frac{1}{2}\begin{pmatrix} 2e^{-i\omega_+ t} + e^{-i\omega_- t} \\ 2e^{-i\omega_+ t} - e^{-i\omega_- t} \end{pmatrix} \qquad (4.10b)$$

Envelope functions now need the complex sum or difference and complex square from (5.20).

$$|z_1(t)| = \sqrt{\frac{1}{2}\left(|u_+(0)|^2 + |u_-(0)|^2 - 2u_+(0)u_-(0)\cos(\omega_- - \omega_+)t\right)} = \sqrt{\frac{5}{4} + \cos\omega_{Beat}t} = \begin{cases} 1.5 & (t=0) \\ 0.5 & (\omega_{Beat}t = \pi) \end{cases} \qquad (4.12a)$$

$$|z_2(t)| = \sqrt{\frac{1}{2}\left(|u_+(0)|^2 + |u_-(0)|^2 + 2u_+(0)u_-(0)\cos(\omega_- - \omega_+)t\right)} = \sqrt{\frac{5}{4} - \cos\omega_{Beat}t} = \begin{cases} 0.5 & (t=0) \\ 1.5 & (\omega_{Beat}t = \pi) \end{cases} \qquad (4.12b)$$

The minimum-to-maximum amplitude ratio is the *Standing Wave Ratio SWR* introduced in (4.6).

$$\frac{z_{MIN}}{z_{MAX}} = \frac{|u_+(0)| - |u_-(0)|}{|u_+(0)| + |u_-(0)|} \quad \left(= \frac{|1.5| - |-0.5|}{|1.5| + |-0.5|} = \frac{1}{3} \text{ for: } u_+(0) = \sqrt{2}, u_-(0) = \frac{-\sqrt{2}}{2}\right) \qquad (4.13)$$

For the ($u_+(0)=1/\sqrt{2}=-u_-(0)$) case in Fig. 4.8(a) *SWR* is zero. For Fig. 4.8(b) *SWR*=1/3.

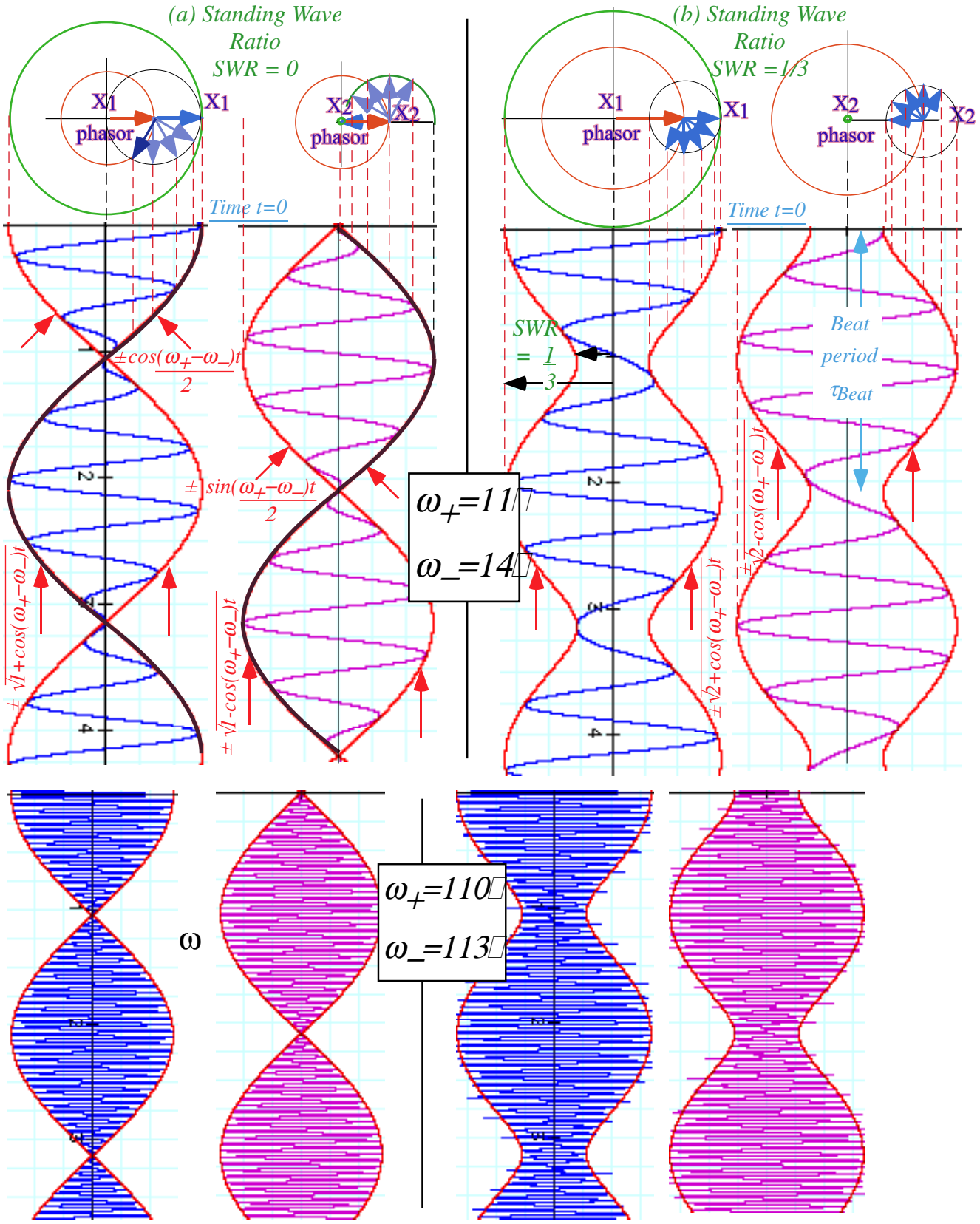

Fig. 4.8 Time evolution of symmetric oscillator beats. (a) Standing Wave Ratio SWR=0. (b) SWR=1/3.

Chapter 5 Quaternion-Spinor Analysis of Oscillators and Beats

A fundamental equation of quantum evolution, namely *Schrodinger's equation,* is related to that of classical coupled oscillators. Consider, the simplest quantum systems: a *spin-1/2* particle (NMR) or a *two-level atom*. The equation has abstract form (5.1a) that for 2-levels uses 2-D arrays (5.1b-c).

$$i\hbar\frac{\partial}{\partial t}\left|\Psi(t)\right\rangle = \mathbf{H}\left|\Psi(t)\right\rangle \tag{5.1a}$$

$\mathbf{H}$ is a 2-by-2 Hermitian $\left(\mathbf{H}^\dagger = \mathbf{H}\right)$ matrix operator and Dirac ket $\left|\Psi\right\rangle$ is a 2-D complex vector.

$$\mathbf{H} = \begin{pmatrix} A & B-iC \\ B+iC & D \end{pmatrix} \tag{5.1b}$$

$$\left|\Psi\right\rangle = \begin{pmatrix} \Psi_1 \\ \Psi_2 \end{pmatrix} = \begin{pmatrix} x_1+ip_1 \\ x_2+ip_2 \end{pmatrix} = \begin{pmatrix} a_1 \\ a_2 \end{pmatrix} \tag{5.1c}$$

Separating real and imaginary parts of amplitudes (5.1c) lets us convert the complex 2D equation (5.1a) into twice as many real differential equations. The results are as follows.

$$\begin{aligned} \dot{x}_1 &= Ap_1 + Bp_2 - Cx_2 \\ \dot{x}_2 &= Bp_1 + Dp_2 + Cx_1 \end{aligned} \tag{5.2a}$$

$$\begin{aligned} \dot{p}_1 &= -Ax_1 - Bx_2 - Cp_2 \\ \dot{p}_2 &= -Bx_1 - Dx_2 + Cp_1 \end{aligned} \tag{5.2b}$$

A classical analog of Schrodinger dynamics

The same equations arise from a *classical oscillator Hamiltonian* with coordinate and canonical momentum pairs x_j and p_j, respectively. (Note: Canonical momentum $p_j = \frac{\partial H}{\partial \dot{x}_j}$ is <u>not</u> the usual $m\dot{x}_j$.)

$$H_c = \frac{A}{2}\left(p_1^2 + x_1^2\right) + B\left(x_1x_2 + p_1p_2\right) + C\left(x_1p_2 - x_2p_1\right) + \frac{D}{2}\left(p_2^2 + x_2^2\right) \tag{5.3a}$$

Hamilton's equations of motion are identical to Schrodinger's real equations (5.2).

$$\begin{aligned} \dot{x}_1 &= \frac{\partial H_c}{\partial p_1} = Ap_1 + Bp_1 - Cx_2 \\ \dot{x}_2 &= \frac{\partial H_c}{\partial p_1} = Bp_1 + Dp_2 + Cx_1 \end{aligned} \tag{5.3b}$$

$$\begin{aligned} \dot{p}_1 &= -\frac{\partial H_c}{\partial x_1} = -\left(Ax_1 + Bx_1 + Cp_2\right) \\ \dot{p}_2 &= -\frac{\partial H_c}{\partial x_2} = -\left(Ax_1 + Dx_2 - Cp_1\right) \end{aligned} \tag{5.3c}$$

Derivatives of $\dot{x}_j$ in (5.3b) go in $\dot{p}_j$ of (5.3c) to give 2nd order oscillator equations like (3.4).

$$\begin{aligned} \ddot{x}_1 &= A\dot{p}_1 + B\dot{p}_2 - C\dot{x}_2 \\ &= -A\left(Ax_1 + Bx_2 + Cp_2\right) - B\left(Bx_1 + Dx_2 - Cp_1\right) - C\left(Bp_1 + Dp_2 + Cx_1\right) \\ &= -\left(A^2 + B^2 - C^2\right)x_1 - (AB + BD)x_2 - C(A + D)p_2 \end{aligned} \tag{5.4a}$$

$$\begin{aligned} \ddot{x}_2 &= B\dot{p}_1 + D\dot{p}_2 + C\dot{x}_2 \\ &= -B\left(Ax_1 + Bx_2 + Cp_2\right) - D\left(Bx_1 + Dx_2 - Cp_1\right) + C\left(Ap_1 + Bp_2 - Cx_2\right) \\ &= -(AB + BD)x_1 - \left(B^2 + D^2 - C^2\right)x_2 + C(A + D)p_1 \end{aligned} \tag{5.4b}$$

Setting Schrodinger parameter *C* to zero reduces (5.4) to coupled oscillator equations (3.4).

$$-\ddot{x}_1 = K_{11}x_1 + K_{12}x_2 \tag{5.5a}$$

$$-\ddot{x}_2 = K_{21}x_1 + K_{22}x_2 \tag{5.5b}$$

Spring force matrix components K_{mn} are related below to $\mathbf{H}$-matrix parameters *A*, *B*, and *D*.

$$\begin{aligned} K_{11} &= A^2 + B^2, & K_{12} &= AB + BD, \\ K_{21} &= AB + BD, & K_{22} &= B^2 + D^2. \end{aligned} \tag{5.6}$$

The eigenfrequencies for the Schrodinger equation (5.1) with $(C \equiv 0)$ are squares of the eigenvalues of the **K**-matrix in (5.5). This is quickly seen in the case $A = D$ and *C=0* where the quantum Hamiltonian matrix (5.1b) has a super-symmetric form.

$$\mathbf{H} = \begin{pmatrix} A & B \\ B & A \end{pmatrix} \tag{5.7a}$$

This Hamiltonian matrix has the following eigenvalues.

$$\varepsilon_1 = A + B, \qquad \varepsilon_2 = A - B. \tag{5.7b}$$

For the parameters $A = D$, *B*, and *C=0*, the classical **K**-matrix is super-symmetric, just like (3.4).

$$\mathbf{K} = \begin{pmatrix} k + k_{12} & -k_{12} \\ -k_{12} & k + k_{12} \end{pmatrix} = \begin{pmatrix} A^2 + B^2 & 2AB \\ 2AB & A^2 + B^2 \end{pmatrix} = \begin{pmatrix} A & B \\ B & A \end{pmatrix}\begin{pmatrix} A & B \\ B & A \end{pmatrix} = \mathbf{H}^2 \tag{5.8a}$$

A is the matrix square of **H** so the classical acceleration eigenvalues are squares of quantum eigenvalues.

$$K_1 = (A + B)^2 = k + 2k_{12}, \qquad K_2 = (A - B)^2 = k\,. \tag{5.8b}$$

Quantum dynamics differs from classical dynamics in important ways. First, classical equations are *second* order differential equations so eigenvalues involve *squared* frequencies as in (5.8b) rather than frequencies as in (5.7a). Also, quantum stimuli enter *multiplicatively* by varying components *A*, *B*, *C*, or *D* of **H**. Exact quantum equation $i|\dot{\Psi}\rangle = \mathbf{H}|\Psi\rangle$ is *always homogeneous, i.e.* $i|\dot{\Psi}\rangle - \mathbf{H}|\Psi\rangle = 0$ is *always zero* unlike classical $|\ddot{x}\rangle + \mathbf{K}|x\rangle = |a\rangle$. Finally, parameter C corresponds to classical cyclotron or Coriolis effects. It gives circular cyclotron orbits if *B* and *A-D* are zero.

ABCD Symmetry operator analysis and U(2) spinors

Let us decompose the Hamiltonian operator **H** in (5.1) into four *ABCD symmetry operators* that are so labeled to provide helpful dynamic mnemonics and symmetry names (as well as colorful analogies).

$$\begin{pmatrix} A & B - iC \\ B + iC & D \end{pmatrix} = A\begin{pmatrix} 1 & 0 \\ 0 & 0 \end{pmatrix} + B\begin{pmatrix} 0 & 1 \\ 1 & 0 \end{pmatrix} + C\begin{pmatrix} 0 & -i \\ i & 0 \end{pmatrix} + D\begin{pmatrix} 0 & 0 \\ 0 & 1 \end{pmatrix} = A\mathbf{e}_{11} + B\boldsymbol{\sigma}_B + C\boldsymbol{\sigma}_C + D\mathbf{e}_{22}$$

$$= \frac{A - D}{2}\begin{pmatrix} 1 & 0 \\ 0 & -1 \end{pmatrix} + B\begin{pmatrix} 0 & 1 \\ 1 & 0 \end{pmatrix} + C\begin{pmatrix} 0 & -i \\ i & 0 \end{pmatrix} + \frac{A + D}{2}\begin{pmatrix} 1 & 0 \\ 0 & 1 \end{pmatrix}$$

$$\mathbf{H} = \frac{A - D}{2}\,\boldsymbol{\sigma}_A + B\,\boldsymbol{\sigma}_B + C\,\boldsymbol{\sigma}_C + \frac{A + D}{2}\,\boldsymbol{\sigma}_0 \tag{5.9a}$$

The $\{\boldsymbol{\sigma}_1, \boldsymbol{\sigma}_A, \boldsymbol{\sigma}_B, \boldsymbol{\sigma}_C\}$ are best known as *Pauli-spin operators* $\{\boldsymbol{\sigma}_1 = \boldsymbol{\sigma}_0, \boldsymbol{\sigma}_B = \boldsymbol{\sigma}_X, \boldsymbol{\sigma}_C = \boldsymbol{\sigma}_Y, \boldsymbol{\sigma}_A = \boldsymbol{\sigma}_Z\}$ but ones quite like them were discovered a century earlier by Hamilton who was looking to generalize complex numbers to 3-dimensional space. Hamilton's *quaternions* **{1, i, j, k}** are related as follows to the *ABCD* or *ZXY0* operators. (He carved them into a bridge in Dublin in 1843, though, not in technicolor.)

$$\{\boldsymbol{\sigma}_1 = \mathbf{1} = \boldsymbol{\sigma}_0,\ i\boldsymbol{\sigma}_B = \mathbf{i} = i\boldsymbol{\sigma}_X,\ i\boldsymbol{\sigma}_C = \mathbf{j} = i\boldsymbol{\sigma}_Y,\ i\boldsymbol{\sigma}_A = \mathbf{k} = i\boldsymbol{\sigma}_Z\} \tag{5.9b}$$

Note: $\mathbf{i}^2 = \mathbf{j}^2 = \mathbf{k}^2 = -\mathbf{1}$. Each squares to *negative*-**1** like imaginary $i = \sqrt{-1}$ $(i^2 = -1)$. Pauli's $\boldsymbol{\sigma}$'s drop the *i* factor so each σ_μ squares to *positive* **1** $(\boldsymbol{\sigma}_X^2 = \boldsymbol{\sigma}_Y^2 = \boldsymbol{\sigma}_Z^2 = +\mathbf{1})$ and each belongs to a cyclic C_2 group.

We'll consider each C_2 symmetry $C_2{}^A=\{\mathbf{1},\boldsymbol{\sigma}_A\}$, $C_2{}^B=\{\mathbf{1},\boldsymbol{\sigma}_B\}$, and $C_2{}^C=\{\mathbf{1},\boldsymbol{\sigma}_C\}$ in turn. They are labeled as *A (Asymmetric-diagonal)*, *B (Bilateral-balanced)*, or *C (Chiral-circular)* symmetry. Each is an archetype of dynamics and symmetry. The systems in Sec. 4.3 belong to *A-to-B* cases in Fig. 5.1 below.

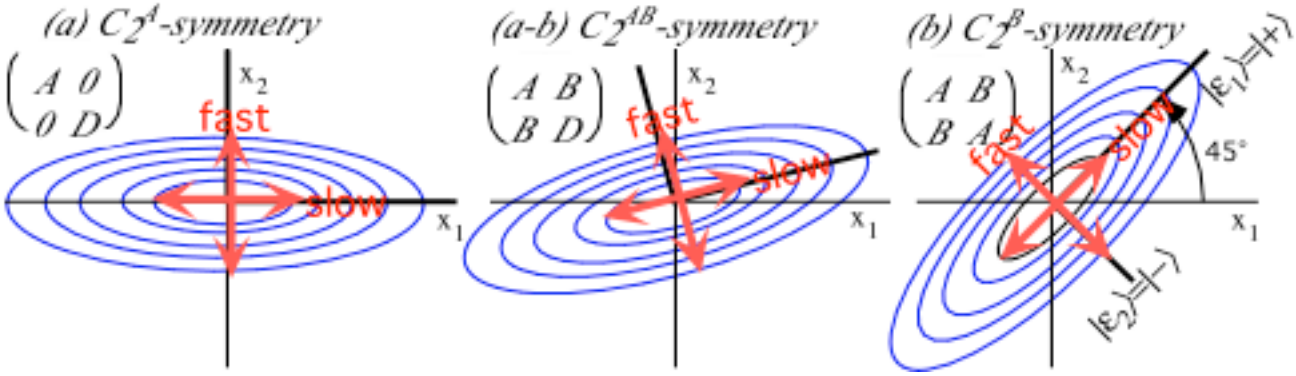

Fig. 5.1 Potentials for (a) $C_2{}^A$-asymmetric-diagonal, (ab) $C_2{}^{AB}$-mixed , (b) $C_2{}^B$-bilateral U(2)system.

A secret to Hamilton's Hamiltonian decomposition (5.9) lies in how it can solve the fundamental 1st order $i|\dot{\Psi}\rangle-\mathbf{H}|\Psi\rangle=0$ equation (5.1) by evaluating and (*most* important!) *visualizing* matrix-exponent solutions.

$$|\Psi(t)\rangle=e^{-i\mathbf{H}\cdot t}|\Psi(0)\rangle \tag{5.10a}$$

Hamilton generalized Euler's expansion $e^{-i\Omega t}=\cos\Omega t-i\sin\Omega t$ so a matrix exponential becomes powerful.

$$e^{-i\mathbf{H}\cdot t}=e^{-i\begin{pmatrix} A & B-iC \\ B+iC & D \end{pmatrix}\cdot t}=e^{-i\frac{A-D}{2}\begin{pmatrix}1&0\\0&-1\end{pmatrix}\cdot t-iB\begin{pmatrix}0&1\\1&0\end{pmatrix}\cdot t-iC\begin{pmatrix}0&-i\\i&0\end{pmatrix}\cdot t-i\frac{A+D}{2}\begin{pmatrix}1&0\\0&1\end{pmatrix}\cdot t}$$

$$=e^{-i\boldsymbol{\sigma}\bullet\boldsymbol{\Omega}\cdot t/2}e^{-i\Omega_0\cdot t}\ \text{where:}\ \boldsymbol{\Theta}=\boldsymbol{\Omega}\cdot t=\begin{pmatrix}\Omega_A\\ \Omega_B\\ \Omega_C\end{pmatrix}\cdot t=\begin{pmatrix}A-D\\ 2B\\ 2C\end{pmatrix}\cdot t\ \text{and:}\ \Omega_0=\frac{A+D}{2} \tag{5.10b}$$

Each matrix $\mathbf{H}$ has a rotation *crank vector* $\boldsymbol{\Theta}=\boldsymbol{\Omega}\cdot t$ that dots with quaternions to solve (5.1). $\boldsymbol{\Omega}$ is a 3D *ABC*- or *XYZ* -space whirl rate like phasor ω described in Ch. 10. Hamilton generalized a *2D* phasor rotation $e^{-i\Omega t}=\cos\Omega t-i\sin\Omega t$ and he did this by first generalizing the imaginary number $i=\sqrt{-1}$ as described below.

(a) How spinors and quaternions *work*

Symmetry relations make spinors σ_X, σ_Y, and σ_Z or quaternions $\mathbf{i}=-i\sigma_X$, $\mathbf{j}=-i\sigma_Y$, and $\mathbf{k}=-i\sigma_Z$ powerful. Each σ_X squares to one (unit matrix $\mathbf{1}=\sigma_X\cdot\sigma_X$) and each quaternion squares to minus-one (**–1=i·i=j·j**, *etc.*) just like $i=\sqrt{-1}$. This is true even for spinor components based on *any* unit vector $\hat{\mathbf{a}}=(a_X,a_Y,a_Z)$ for which $\hat{\mathbf{a}}\bullet\hat{\mathbf{a}}=1=a_X{}^2+a_Y{}^2+a_Z{}^2$. To see this just try it out on any $\hat{\mathbf{a}}$-component: $\sigma_a=\sigma\bullet\hat{\mathbf{a}}=a_X\sigma_X+a_Y\sigma_Y+a_Z\sigma_Z$.

$$\sigma_a{}^2=(\sigma\bullet\hat{\mathbf{a}})(\sigma\bullet\hat{\mathbf{a}})=(a_X\sigma_X+a_Y\sigma_Y+a_Z\sigma_Z)(a_X\sigma_X+a_Y\sigma_Y+a_Z\sigma_Z)$$

$$\begin{matrix} a_X\sigma_Xa_X\sigma_X & +a_X\sigma_Xa_Y\sigma_Y & +a_X\sigma_Xa_Z\sigma_Z & a_Xa_X\sigma_X\sigma_X & +a_Xa_Y\sigma_X\sigma_Y & +a_Xa_Z\sigma_X\sigma_Z \\ =+a_Y\sigma_Ya_X\sigma_X & +a_Y\sigma_Ya_Y\sigma_Y & +a_Y\sigma_Ya_Z\sigma_Z & =+a_Ya_X\sigma_Y\sigma_X & +a_Ya_Y\sigma_Y\sigma_Y & +a_Ya_Z\sigma_Y\sigma_Z \\ +a_Z\sigma_Za_X\sigma_X & +a_Z\sigma_Za_Y\sigma_Y & +a_Z\sigma_Za_Z\sigma_Z & +a_Za_X\sigma_Z\sigma_X & +a_Za_Y\sigma_Z\sigma_Y & +a_Za_Z\sigma_Z\sigma_Z \end{matrix}$$

To finish we need another symmetry property called *anti-commutation*: $\sigma_X\sigma_Y = -\sigma_Y\sigma_X$, *etc.* (Check this!) Put this together with unit squares $\mathbf{1} = \sigma_X{}^2$, *etc.* Then all off-diagonal terms cancel so that $\mathbf{1} = \sigma_a{}^2$, too.

$$\begin{aligned}\sigma_a{}^2 = (\sigma\bullet\hat{\mathbf{a}})(\sigma\bullet\hat{\mathbf{a}}) &= (a_X\sigma_X + a_Y\sigma_Y + a_Z\sigma_Z)(a_X\sigma_X + a_Y\sigma_Y + a_Z\sigma_Z)\\ a_X{}^2\mathbf{1} \quad &+a_Xa_Y\sigma_X\sigma_Y \quad +a_Xa_Z\sigma_X\sigma_Z\\ = -a_Xa_Y\sigma_X\sigma_Y \quad &+a_Y{}^2\mathbf{1} \quad +a_Ya_Z\sigma_Y\sigma_Z \quad = (a_X{}^2 + a_Y{}^2 + a_Z{}^2)\mathbf{1} = \mathbf{1}\\ -a_Xa_Z\sigma_X\sigma_Z \quad &-a_Ya_Z\sigma_Y\sigma_Z \quad +a_Z{}^2\mathbf{1}\end{aligned} \tag{5.11}$$

Finally, that anti-commutation relation is cyclic: $\sigma_X\sigma_Y = i\sigma_Z = -\sigma_Y\sigma_X$, $\sigma_Z\sigma_X = i\sigma_Y = -\sigma_X\sigma_Z$, and $\sigma_Y\sigma_Z = i\sigma_X = -\sigma_Z\sigma_Y$. So, **σ**-products do dot • *and* cross × products.

$$\begin{aligned}\sigma_a\sigma_b = (\sigma\bullet\mathbf{a})(\sigma\bullet\mathbf{b}) &= (a_X\sigma_X + a_Y\sigma_Y + a_Z\sigma_Z)(b_X\sigma_X + b_Y\sigma_Y + b_Z\sigma_Z)\\ a_Xb_X\mathbf{1} \quad &+a_Xb_Y\sigma_X\sigma_Y \quad -a_Xb_Z\sigma_Z\sigma_X \quad +i(a_Yb_Z - a_Zb_Y)\sigma_X\\ = -a_Yb_X\sigma_X\sigma_Y \quad &+a_Yb_Y\mathbf{1} \quad +a_Yb_Z\sigma_Y\sigma_Z \quad = (a_Xb_X + a_Yb_Y + a_Zb_Z)\mathbf{1} \quad +i(a_Zb_X - a_Xb_Z)\sigma_Y\\ +a_Zb_X\sigma_Z\sigma_X \quad &-a_Zb_X\sigma_Y\sigma_Z \quad +a_Zb_Z\mathbf{1} \quad +i(a_Xb_Y - a_Yb_X)\sigma_Z\end{aligned} \tag{5.12a}$$

To see this we write the product in Gibbs notation. (Where do you think Gibbs *got* his **{i,j,k}** notation!)

$$\sigma_a\sigma_b = (\sigma\bullet\mathbf{a})(\sigma\bullet\mathbf{b}) = \quad (\mathbf{a}\bullet\mathbf{b})\mathbf{1} \quad + \quad i(\mathbf{a}\times\mathbf{b})\bullet\sigma \tag{5.12b}$$

Complex numbers $A=A_X+iA_Y$ do a similar thing if you *-multiply them as follows.

$$A^*B=(A_X+iA_Y)^*(B_X+iB_Y)=(A_X-iA_Y)(B_X+iB_Y)=(A_XB_X+A_YB_Y)+i(A_XB_Y-A_YB_X)=(\mathbf{A}\bullet\mathbf{B})+i(\mathbf{A}\times\mathbf{B}) \tag{5.13}$$

Of course, the results are just the *2D* versions of dot and cross products. Hamilton's idea was to generalize to three dimensions and even four dimensions. (Lorentz relativity transformations are done by spinors, too!) So finally Hamilton is able to generalize Euler's complex rotation operators $e^{+i\varphi}$ and $e^{-i\varphi}$.

$$\begin{aligned}e^{-i\varphi} = 1 + (-i\varphi) + \frac{1}{2!}(-i\varphi)^2 + \frac{1}{3!}(-i\varphi)^3 + \frac{1}{4!}(-i\varphi)^4\cdots = \ &[1 \quad -\frac{1}{2!}\varphi^2 \quad +\frac{1}{4!}\varphi^4\cdots] = \quad [\cos\varphi]\\ &-i(\varphi \quad +\frac{1}{3!}\varphi^3 \quad \cdots) \quad -i(\sin\varphi)\end{aligned}$$

Euler's series is the result of the binomial series definition of the exponential growth function e^{rt}.

$$e^{rt} = \lim_{N\to\infty}(1+\frac{rt}{N})^N = \lim_{N\to\infty}(1 + N\frac{rt}{N} + \frac{N(N-1)}{2!}\left(\frac{rt}{N}\right)^2 + \frac{N(N-1)(N-2)}{3!}\left(\frac{rt}{N}\right)^3 + \ldots)$$

Euler's identity works because even powers of *(-i)* are *±1* and odd powers of *(-i)* are *±i*. That is how $-i\sigma_a$ works, too. Hamilton replaces *(-i)* with $-i\sigma_a$ in an $e^{-i\varphi}$ power series to get a sequence of terms

$$(-i\sigma_a)^0 = +\mathbf{1},\ (-i\sigma_a)^1 = -i\sigma_a,\ (-i\sigma_a)^2 = -\mathbf{1},\ (-i\sigma_a)^3 = +i\sigma_a,\ (-i\sigma_a)^4 = +\mathbf{1},\ (-i\sigma_a)^5 = -i\sigma_a, \textit{etc.}$$

This allows Hamilton to generalize Euler's $e^{-i\varphi}$ rotation to $e^{-i\boldsymbol{\sigma}_a\varphi}$ for any $\sigma_a = (\sigma\bullet\mathbf{a}) = a_X\sigma_X + a_Y\sigma_Y + a_Z\sigma_Z$.

$$e^{-i\varphi} = 1\cos\varphi \quad - \quad i\sin\varphi \qquad \textit{generalizes to:} \quad e^{-i\boldsymbol{\sigma}_a\varphi} = \mathbf{1}\cos\varphi \quad - \quad i\,\boldsymbol{\sigma}_a\sin\varphi$$

Below are $\sigma_A = \sigma_Z$ and $\sigma_C = \sigma_Y$ rotations and a σ_a-rotation around a general *3D* whirl axis $\hat{\boldsymbol{\omega}} = \hat{\boldsymbol{\Theta}}_a = \hat{\mathbf{a}}$.

$$e^{-i(\sigma_A)\varphi_A} = \quad \mathbf{1} \quad \cos\varphi_A \quad - \quad i\ (\sigma_A)\ \sin\varphi_A = \mathbf{R}(\varphi_A)$$

$$e^{-i\begin{pmatrix}1 & 0\\ 0 & -1\end{pmatrix}\varphi_A} = \begin{pmatrix}1 & 0\\ 0 & 1\end{pmatrix}\cos\varphi_A - i\begin{pmatrix}1 & 0\\ 0 & -1\end{pmatrix}\sin\varphi_A$$

$$= \begin{pmatrix}\cos\varphi_A - i\sin\varphi_A & 0\\ 0 & \cos\varphi_A - i\sin\varphi_A\end{pmatrix} = \begin{pmatrix}e^{-i\varphi_A} & 0\\ 0 & e^{i\varphi_A}\end{pmatrix} \tag{5.14a}$$

$$e^{-i(\sigma_C)\varphi_C} = \quad \mathbf{1}\ \cos\varphi_C - i\ (\sigma_C)\ \sin\varphi_C = \mathbf{R}(\varphi_C)$$

$$e^{-i\begin{pmatrix}0 & -i\\ i & 0\end{pmatrix}\varphi_C} = \begin{pmatrix}1 & 0\\ 0 & 1\end{pmatrix}\cos\varphi_C - i\begin{pmatrix}0 & -i\\ i & 0\end{pmatrix}\sin\varphi_C$$

$$= \begin{pmatrix}\cos\varphi_C & -\sin\varphi_C\\ \sin\varphi_C & \cos\varphi_C\end{pmatrix} \tag{5.14c}$$

$$e^{-i\sigma_a\varphi_a} = e^{-i(\boldsymbol{\sigma}\bullet\hat{\mathbf{a}})\varphi_a} = \mathbf{1}\cos\varphi_a - i\ (\boldsymbol{\sigma}\bullet\hat{\mathbf{a}})\sin\varphi_a \tag{5.14b}$$

We now see that *3D* (*ABC*) rotations are by an angle $\Theta_a=2\varphi_a$ that is *twice* the angle φ_a in *2D* space$\{x_1,x_2\}$.

The "mysterious" factors of 2

A factor of 2 or $\frac{1}{2}$ relates φ_a-rotation of *2D* oscillator variables $\{x_1,x_2\}$ to *3D* vector rotation Θ_a in *ZXY* or *ABC*-space. *3D* vector $\hat{\mathbf{a}}$ defines a combination $\boldsymbol{\sigma}_a=a_A\boldsymbol{\sigma}_A+a_B\boldsymbol{\sigma}_B+a_C\boldsymbol{\sigma}_C$ of *operators* $\boldsymbol{\sigma}_A,\boldsymbol{\sigma}_B,\boldsymbol{\sigma}_C$ to be rotated by 2-by-2 matrices (5.15) acting *twice*, fore and aft^{-1}(as operators do in (4.B.6)) by *twice* the *2D* angle φ_a.

$$\mathbf{R}(\varphi_C)\cdot\boldsymbol{\sigma}_A\cdot\mathbf{R}^{-1}(\varphi_C)$$
$$=\begin{pmatrix}\cos\varphi_C & -\sin\varphi_C\\ \sin\varphi_C & \cos\varphi_C\end{pmatrix}\begin{pmatrix}1 & 0\\ 0 & -1\end{pmatrix}\begin{pmatrix}\cos\varphi_C & \sin\varphi_C\\ -\sin\varphi_C & \cos\varphi_C\end{pmatrix}$$
$$=\begin{pmatrix}\cos^2\varphi_C-\sin^2\varphi_C & 2\sin\varphi_C\cos\varphi_C\\ 2\sin\varphi_C\cos\varphi_C & \sin^2\varphi_C-\cos^2\varphi_C\end{pmatrix}$$
$$=\begin{pmatrix}1 & 0\\ 0 & -1\end{pmatrix}\cos 2\varphi_C+\begin{pmatrix}0 & 1\\ 1 & 0\end{pmatrix}\sin 2\varphi_C$$
$$=\boldsymbol{\sigma}_A\cos 2\varphi_C+\boldsymbol{\sigma}_B\sin 2\varphi_C$$

$$\mathbf{R}(\varphi_C)\cdot\boldsymbol{\sigma}_B\cdot\mathbf{R}^{-1}(\varphi_C)$$
$$=\begin{pmatrix}\cos\varphi_C & -\sin\varphi_C\\ \sin\varphi_C & \cos\varphi_C\end{pmatrix}\begin{pmatrix}0 & 1\\ 1 & 0\end{pmatrix}\begin{pmatrix}\cos\varphi_C & \sin\varphi_C\\ -\sin\varphi_C & \cos\varphi_C\end{pmatrix}$$
$$=\begin{pmatrix}-2\sin\varphi_C\cos\varphi_C & \cos^2\varphi_C-\sin^2\varphi_C\\ \cos^2\varphi_C-\sin^2\varphi_C & 2\sin\varphi_C\cos\varphi_C\end{pmatrix}$$
$$=\begin{pmatrix}-1 & 0\\ 0 & 1\end{pmatrix}\sin 2\varphi_C+\begin{pmatrix}0 & 1\\ 1 & 0\end{pmatrix}\cos 2\varphi_C$$
$$=-\boldsymbol{\sigma}_A\sin 2\varphi_C+\boldsymbol{\sigma}_B\cos 2\varphi_C$$

So the *2D* rotation φ_a angle must be exactly $\frac{1}{2}$ the *3D* angle Θ_a of rotation. When a spin axis goes from *up-A* to *down-A* that is a rotation by $\Theta_C=\pi$ or *180°* in *ZXY* or *ABC*-space, but only by $\varphi_C=\pi/2$ or *90°* in spinor space $\{x_1,x_2\}$. State $|\uparrow\rangle$ of spin *up-Z* and the state $|\downarrow\rangle$ of spin *down-Z* are orthogonal kets *90°* apart. This analogy to a *2D*$\{x_1,x_2\}$-oscillator underlies spin $\frac{1}{2}$. So, *3D crank vector* $\vec{\boldsymbol{\Theta}}$ and *spin operator* $\mathbf{S}$ are defined for *3D ZXY* or *ABC*-space with a ratio $\frac{1}{2}$ or 2 between Θ_a and $\varphi_a=\frac{1}{2}\Theta_a$ or between $\mathbf{S}$ and $\boldsymbol{\sigma}=2\mathbf{S}$.

$$e^{-i\boldsymbol{\sigma}\bullet\vec{\boldsymbol{\varphi}}}=e^{-i\boldsymbol{\sigma}\bullet\vec{\boldsymbol{\Theta}}/2}=e^{-i\mathbf{S}\bullet\vec{\boldsymbol{\Theta}}}=\mathbf{1}\cos\frac{\Theta}{2}-i\,(\boldsymbol{\sigma}\bullet\hat{\boldsymbol{\Theta}})\sin\frac{\Theta}{2}=\begin{pmatrix}\cos\frac{\Theta}{2}-i\hat{\Theta}_A\sin\frac{\Theta}{2} & (-i\hat{\Theta}_B-\hat{\Theta}_C)\sin\frac{\Theta}{2}\\ (-i\hat{\Theta}_B+\hat{\Theta}_C)\sin\frac{\Theta}{2} & \cos\frac{\Theta}{2}+i\hat{\Theta}_A\sin\frac{\Theta}{2}\end{pmatrix}\quad(5.15a)$$

2D angle: $\varphi=\frac{1}{2}\Theta$ (5.15b) *3D Crank vector*: $\vec{\boldsymbol{\Theta}}=\Theta\hat{\boldsymbol{\Theta}}=2\varphi_a\hat{\mathbf{a}}=2\vec{\boldsymbol{\varphi}}$ (5.15c) *2D spin matrix:* $\mathbf{S}=\frac{1}{2}\boldsymbol{\sigma}$ (5.15d)

Eighty years after Hamilton (1924) comes Pauli and Jordan spin $\mathbf{S}=\frac{\hbar}{2}\boldsymbol{\sigma}$ with its *half-quantum* factor $\frac{\hbar}{2}$.

2D polarization and 3D Stokes vector S

In 1862 George Stokes found an application of Hamilton's mathematics to optical polarization that has a *2D* complex oscillator space $\{E_1,E_2\}$ analogous to Ψ-space $\{a_1,a_2\}=\{x_1+ip_1,x_2+ip_2\}$ in (5.1c). He gave 3 *Stokes vector components* S_a that wonderfully define polarization ellipses, *2D* HO orbits, and spin $\frac{1}{2}$ states.

$$\textit{Asymmetry}\quad S_A=\frac{1}{2}\langle a|\sigma_A|a\rangle=\frac{1}{2}\begin{pmatrix}a_1^* & a_2^*\end{pmatrix}\begin{pmatrix}1 & 0\\ 0 & -1\end{pmatrix}\begin{pmatrix}a_1\\ a_2\end{pmatrix}=\frac{1}{2}\left[a_1^*a_1-a_2^*a_2\right]=\frac{1}{2}\left[x_1^2+p_1^2-x_2^2-p_2^2\right]\quad(5.16a)$$

$$\textit{Balance}\quad S_B=\frac{1}{2}\langle a|\sigma_B|a\rangle=\frac{1}{2}\begin{pmatrix}a_1^* & a_2^*\end{pmatrix}\begin{pmatrix}0 & 1\\ 1 & 0\end{pmatrix}\begin{pmatrix}a_1\\ a_2\end{pmatrix}=\frac{1}{2}\left[a_1^*a_2+a_2^*a_1\right]=\left[p_1p_2+x_1x_2\right]\quad(5.16b)$$

$$\textit{Chirality}\quad S_C=\frac{1}{2}\langle a|\sigma_C|a\rangle=\frac{1}{2}\begin{pmatrix}a_1^* & a_2^*\end{pmatrix}\begin{pmatrix}0 & -i\\ i & 0\end{pmatrix}\begin{pmatrix}a_1\\ a_2\end{pmatrix}=\frac{-i}{2}\left[a_1^*a_2-a_2^*a_1\right]=\left[x_1p_2-x_2p_1\right]\quad(5.16c)$$

Components of real *3D* spin-vector S=(S_A, S_B, S_C) label orbit *states* in 4D phase space (x_1,p_1,x_2,p_2) just as real components of *3D* whirl-vector $\boldsymbol{\Omega}$=(Ω_A,Ω_B,Ω_C) label 4D matrix *operators* **H** that whirl these states.

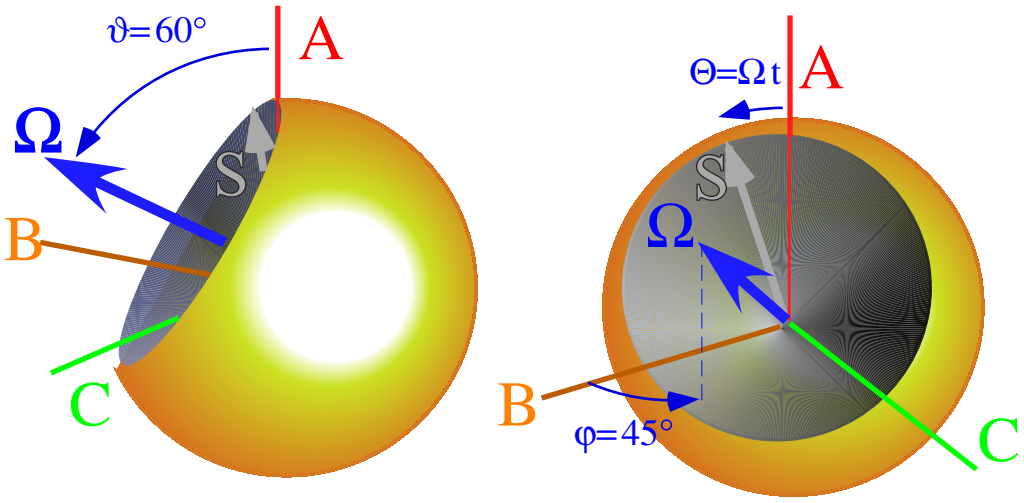

Fig. 5.2 Two views of Hamilton crank vector $\boldsymbol{\Omega}(\varphi,\vartheta)$ *whirling Stokes state vector* S *in ABC-space.*

Matrix **H** cranks S around rotation axis $\boldsymbol{\Theta} = \boldsymbol{\Omega}\cdot t$ according to (5.15) at whirl rate Ω as Fig. 5.2 depicts.

$$\Omega = |\boldsymbol{\Omega}| = \sqrt{\Omega_A^{\,2} + \Omega_B^{\,2} + \Omega_C^{\,2}} \qquad (5.17)$$

Length of $\boldsymbol{\Theta}$=(Θ_A,Θ_B,Θ_C)= $\boldsymbol{\Omega}\cdot t$ =($\Omega_A\cdot t$,$\Omega_B\cdot t$,$\Omega_C\cdot t$) grows at a constant rate Ω but its direction is fixed if the constants (A,B,C,D) or ($\Omega_A = A - D$, $\Omega_B = 2B$, $\Omega_C = 2C$) in **H** are held constant. The $\boldsymbol{\Omega}$-whirl direction is given by polar coordinates (φ,ϑ) that we call *Darboux angles* after the inventor of $\boldsymbol{\omega}$-whirl vectors. The spin S-vector has polar coordinates, too, so designated in the next section by *Euler angles* (α,β).

Fixed points: A port in the storm of action

It helps to look at Fig. 5.2 as analogous to phasor space Fig. 2.15.1. A point on **H** whirl vector $\boldsymbol{\Omega}$ is a stable fixed point for state spin-S where it can rest and not be whirled. It still twists if S could do so. Such a twist is in the 0^{th}-overall average angular phase rate Ω_0=(A+D)/2 in (5.10). S-states with S aligned (α,β)=(φ,ϑ) or anti-aligned $(\alpha,\pi-\beta)$=(φ,ϑ) to $\boldsymbol{\Omega}$ are called own-states or *eigenstates* of **H**. This lets us compute them.

The S_a-terms in (5.16) are the same as the parts of the classical Hamiltonian H_c in (5.3a).

$$H_c = \frac{A}{2}\left(p_1^2 + x_1^2\right) + B\left(x_1x_2 + p_1p_2\right) + C\left(x_1p_2 - x_2p_1\right) + \frac{D}{2}\left(p_2^2 + x_2^2\right) \qquad (5.3a)_{repeated}$$

Rearranging the A and D terms lends a classical action form $\dot{q}^m p_m = \boldsymbol{\omega}\cdot\mathbf{J} = \boldsymbol{\Omega}\cdot\mathbf{S}$ to the expression of H_c.

$$H_c = \frac{A-D}{2}\left[\frac{x_1^2 + p_1^2 - x_2^2 - p_2^2}{2}\right] + B\left[p_1p_2 + x_1x_2\right] + C\left[x_1p_2 - x_2p_1\right] + \frac{1}{2}\frac{A+D}{2}\left[p_1^2 + x_1^2 + p_2^2 + x_2^2\right]$$

$$= \frac{1}{2}\Omega_A\left[S_A\right] + \frac{1}{2}\Omega_B\left[S_B\right] + \frac{1}{2}\Omega_C\left[S_C\right] + \frac{1}{2}\Omega_0\left[I\right] \qquad (5.18a)$$

Contrast this with the quantum spin matrix operator form for $\mathbf{H}=\boldsymbol{\Omega}\cdot\mathbf{S}+\Omega_0\mathbf{1}$ given by (5.9) thru (5.15).

$$\begin{pmatrix} A & B-iC \\ B+iC & D \end{pmatrix} = [A-D]\begin{pmatrix} \frac{1}{2} & 0 \\ 0 & -\frac{1}{2} \end{pmatrix} + 2B\begin{pmatrix} 0 & \frac{1}{2} \\ \frac{1}{2} & 0 \end{pmatrix} + 2C\begin{pmatrix} 0 & -\frac{i}{2} \\ \frac{i}{2} & 0 \end{pmatrix} + \frac{A+D}{2}\begin{pmatrix} 1 & 0 \\ 0 & 1 \end{pmatrix} \qquad (5.18b)$$

$$\mathbf{H} = \Omega_A \mathbf{S}_A + \Omega_B \mathbf{S}_B + \Omega_C \mathbf{S}_C + \Omega_0 \mathbf{1}$$

Classical S_a-magnitude is $I/2 = \sqrt{S_A^2 + S_B^2 + S_C^2}$ but the matrix forms give: $\mathbf{S}_A^2 + \mathbf{S}_B^2 + \mathbf{S}_C^2 = \frac{3}{4}\mathbf{1}$.

(b) Oscillator states by spinor rotation

Sophus Lie sought to define classical dynamics in terms of transformation operators. The preceding (5.10) and (5.15) let us do this for a *2D* oscillator by relating it to a *3D* spinning body. All states $|a\rangle = \binom{a_1}{a_2}$ of a *2D* oscillator or *3D* body are defined by rotation **R** of an initial *2D* state $|1\rangle = \binom{1}{0}$ or *3D* vector $\mathbf{S}(1) = (0,0,1)$.

$$|a\rangle = \begin{pmatrix} a_1 \\ a_2 \end{pmatrix} = \mathbf{R}(a)|1\rangle = \left\langle e^{-i\boldsymbol{\sigma}\bullet\vec{\boldsymbol{\varphi}}_a} \right\rangle_{2\times 2}\begin{pmatrix} 1 \\ 0 \end{pmatrix} \quad (5.19a) \qquad \mathbf{S}(a) = \begin{pmatrix} S_A(a) \\ S_B(a) \\ S_C(a) \end{pmatrix} = \mathbf{R}(a)\bullet\mathbf{S}(1) = \left\langle e^{-i\mathbf{S}\bullet\vec{\boldsymbol{\Theta}}} \right\rangle_{3\times 3}\begin{pmatrix} 0 \\ 0 \\ 1 \end{pmatrix} \quad (5.19b)$$

3D rotation **R** has 3 parameters $(\Theta_A,\Theta_B,\Theta_C)$ or else 3 *Euler angles* (α,β,γ) as shown in Fig. 5.3. That can define a *2D* oscillator's 4 phase variables (x_1,p_1,x_2,p_2) if energy is conserved. Else, we need to include an *intensity amplitude* $I^{1/2} = A$ with the 3 rotation angles. Euler's *ZYZ* or *ACA* rotation of 1st-state $|1\rangle$ gives state $|a\rangle = \mathbf{R}_a|1\rangle$ of spin *S* with 2 polar angles (α,β) and a *phase factor* $e^{-i\frac{\gamma}{2}}$ with phase $-\gamma/2$.

$$|a\rangle = \mathbf{R}(\alpha\beta\gamma)|1\rangle \qquad \textit{(Euler's definition of any state } |a\rangle\textit{)} \qquad (5.20a)$$

$$= \mathbf{R}[\alpha \text{ about } Z]\cdot\mathbf{R}[\beta \text{ about } Y]\cdot\mathbf{R}[\gamma \text{ about } Z]|\uparrow\rangle \qquad \textit{(Using matrix } \mathbf{R}(\alpha/2) \textit{ of (5.14a) and } \mathbf{R}(\beta/2) \textit{ of (5.14c))}$$

$$= \begin{pmatrix} e^{-i\frac{\alpha}{2}} & 0 \\ 0 & e^{i\frac{\alpha}{2}} \end{pmatrix}\begin{pmatrix} \cos\frac{\beta}{2} & -\sin\frac{\beta}{2} \\ \sin\frac{\beta}{2} & \cos\frac{\beta}{2} \end{pmatrix}\begin{pmatrix} e^{-i\frac{\gamma}{2}} & 0 \\ 0 & e^{i\frac{\gamma}{2}} \end{pmatrix}\begin{pmatrix} A \\ 0 \end{pmatrix} = \begin{pmatrix} e^{-i\frac{\alpha+\gamma}{2}}\cos\frac{\beta}{2} & -e^{-i\frac{\alpha-\gamma}{2}}\sin\frac{\beta}{2} \\ e^{i\frac{\alpha-\gamma}{2}}\sin\frac{\beta}{2} & e^{i\frac{\alpha+\gamma}{2}}\cos\frac{\beta}{2} \end{pmatrix}\begin{pmatrix} A \\ 0 \end{pmatrix} = A\begin{pmatrix} e^{-i\frac{\alpha}{2}}\cos\frac{\beta}{2} \\ e^{i\frac{\alpha}{2}}\sin\frac{\beta}{2} \end{pmatrix}e^{-i\frac{\gamma}{2}} = \begin{pmatrix} x_1 + ip_1 \\ x_2 + ip_2 \end{pmatrix}$$

Real x_k and imaginary p_k parts of phasor variables $a_k = x_k + ip_k$ are functions of 3 Euler angles (α,β,γ) and A.

$$x_1 = A\cos(\alpha+\gamma)/2\cdot\cos\beta/2 \qquad x_2 = A\cos(\alpha-\gamma)/2\cdot\sin\beta/2 \qquad (5.20b)$$

$$p_1 = -A\sin(\alpha+\gamma)/2\cdot\cos\beta/2 \qquad p_2 = A\sin(\alpha-\gamma)/2\cdot\sin\beta/2 \qquad (5.20c)$$

But, the 3 components (5.16) of spin vector *S* depend on only 2 polar angles (α,β) and I as in Fig. 5.3.

$$S_A = \frac{1}{2}\left[x_1^2 + p_1^2 - x_2^2 - p_2^2\right] = \frac{I}{2}[\cos^2\frac{\beta}{2} - \sin^2\frac{\beta}{2}] = \frac{I}{2}\cos\beta \qquad (5.21a)$$

$$S_B = \left[p_1 p_2 + x_1 x_2\right] = I\left[-\sin\frac{\alpha+\gamma}{2}\sin\frac{\alpha-\gamma}{2} + \cos\frac{\alpha+\gamma}{2}\cos\frac{\alpha-\gamma}{2}\right]\cos\frac{\beta}{2}\sin\frac{\beta}{2} = \frac{I}{2}\cos\alpha\sin\beta \qquad (5.21b)$$

$$S_C = \left[x_1 p_2 - x_2 p_1\right] = I\left[\cos\frac{\alpha+\gamma}{2}\sin\frac{\alpha-\gamma}{2} - \cos\frac{\alpha-\gamma}{2}\cdot-\sin\frac{\alpha+\gamma}{2}\right]\cos\frac{\beta}{2}\sin\frac{\beta}{2} = \frac{I}{2}\sin\alpha\sin\beta \qquad (5.21c)$$

Intensity factor $I = A^2$ is called a *norm* and is unity $(I = 1 = A)$ for quantum states. Here it is the total *action* of classical oscillators. Spin (S_A,S_B,S_C) is independent of phase $-\gamma/2$. Action I is independent of γ, β, and α.

$$\textit{Action} = 2S_0 = \left(a\left|\mathbf{1}\right|a\right) = \left[x_1^2 + p_1^2 + x_2^2 + p_2^2\right] = I[\cos^2\frac{\beta}{2} + \sin^2\frac{\beta}{2}] = I = \textit{Intensity} \qquad (5.21d)$$

According to (5.18 a,b,c) action is twice the spin magnitude: $I/2 = \sqrt{S_A^2 + S_B^2 + S_C^2}$.

Let a *2D* elliptic orbit of frequency ω have amplitudes A_1 and A_2, and phase shifts ρ_1 and $\rho_2 = -\rho_1$.

$$x_1 = A_1\cos(\omega t+\rho_1) \qquad x_2 = A_2\cos(\omega t-\rho_1) \tag{5.22a}$$

$$p_1 = -A_1\sin(\omega t+\rho_1) \qquad p_2 = -A_2\sin(\omega t-\rho_1) \tag{5.22b}$$

This is a case of (5.20). Euler angles (α,β,γ) and action amplitude A are set to match (5.22) as follows.

$$\alpha = 2\rho_1 \qquad \tan\beta/2 = A_2/A_1 \qquad \gamma = 2\omega\cdot t \qquad A^2 = A_1^2+A_2^2 \tag{5.22c}$$

This example is used to show how the Stokes-Hamilton formulas expose orbital geometry and dynamics.

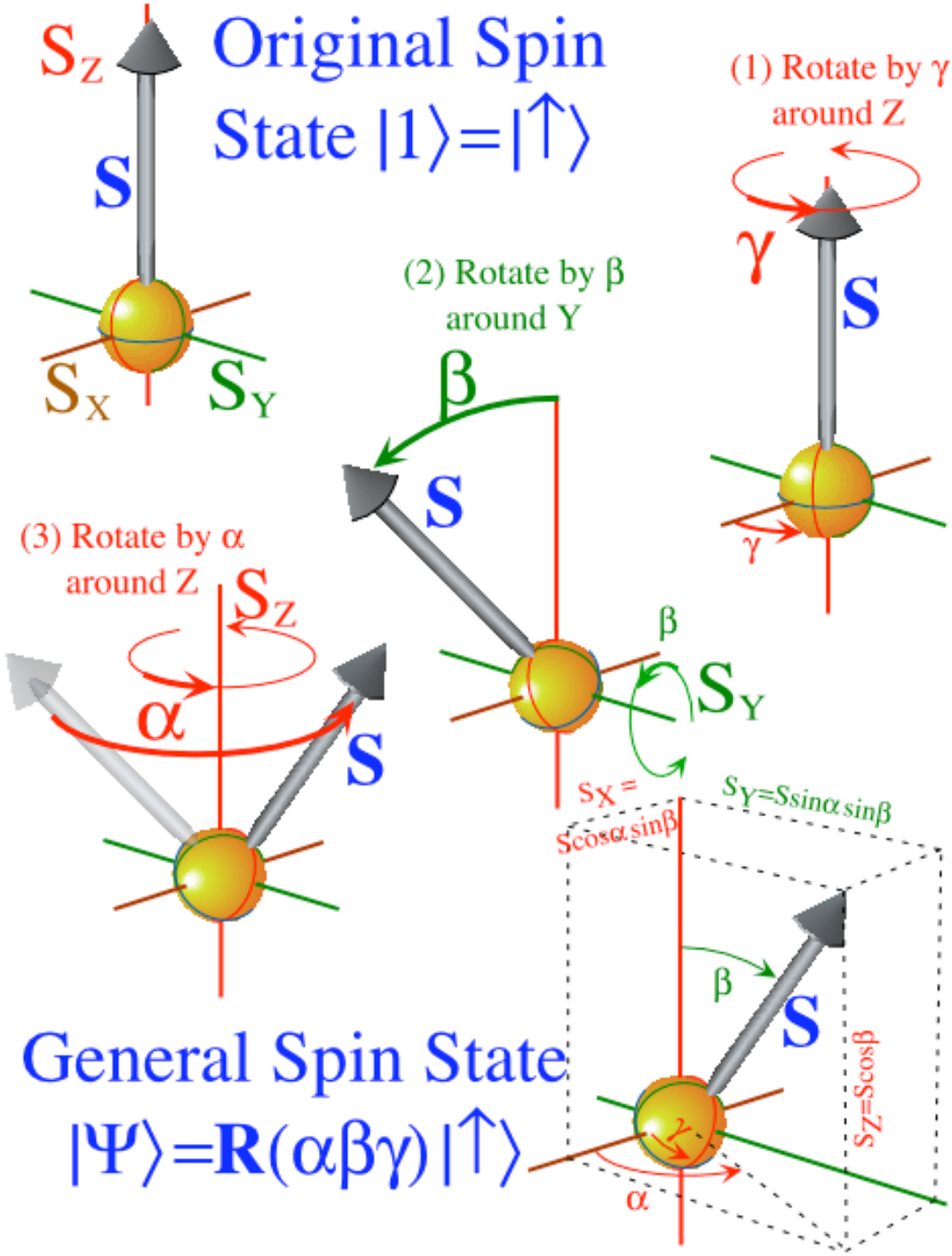

Fig. 5.3 The operational definition of Euler $(\alpha\beta\gamma)$-angle coordinates is applied to a unit spin-state.

The A-view in {x₁,x₂}-basis

The orbit (5.22) has angles $\alpha_A=\rho_1-\rho_2=2\rho_1$, $\beta_A=2\tan^{-1}A_2/A_1$, and $\gamma_A=\omega t/2$ with intensity $I=A^2=A_1^2+A_2^2$.

$$\begin{pmatrix} a_1 \\ a_2 \end{pmatrix} = A\begin{pmatrix} e^{-i\alpha_A/2}\cos\frac{\beta_A}{2} \\ e^{+i\alpha_A/2}\sin\frac{\beta_A}{2} \end{pmatrix} e^{-i\omega t} = A\begin{pmatrix} \left(\cos(\omega t+\frac{\alpha_A}{2})-i\sin(\omega t+\frac{\alpha_A}{2})\right)\cos\frac{\beta_A}{2} \\ \left(\cos(\omega t-\frac{\alpha_A}{2})-i\sin(\omega t-\frac{\alpha_A}{2})\right)\sin\frac{\beta_A}{2} \end{pmatrix} = \begin{pmatrix} x_1+ip_1 \\ x_2+ip_2 \end{pmatrix} \qquad (5.23)$$

Fig. 5.3 shows an ellipse (5.22) next to its *ABC* space S-vector (5.21) for *A* or *Z*-axis Euler angles

$\alpha=\alpha_A=\rho_1-\rho_2=2\rho_1=60°$ (5.24a) $\beta=\beta_A=2\tan^{-1}A_2/A_1=60°$ (5.24b) $\gamma_A=\omega t/2$. (5.24c)

Cartesian-x_1x_2 axes in Fig. 5.3a map onto ± *A* or *Z* -axis in Fig. 5.3b. Azimuth angle-α_A off the *B*-axis is the phase lag between $a_1=e^{-i\alpha/2}|a_1|$ and $a_2=e^{+i\alpha/2}|a_2|$ in (5.23). Note projected A_1 or A_2 box contact points in Fig. 5.2a. Contact points go to the box diagonal for $\alpha_A=0°$ or the other diagonal for $\alpha_A=180°$, or the box x_k-axes for $\alpha_A=\pm 90°$. Polar β_A angle of S from *A*-or-*z*-axis is the angle between ellipse box diagonals in Fig. 5.2a. An orbit with $\beta_A=0°(180°)$ is $x_1(x_2)$-polarized. Circular orbits have $\beta_A=\pm 90°=\alpha_A$.

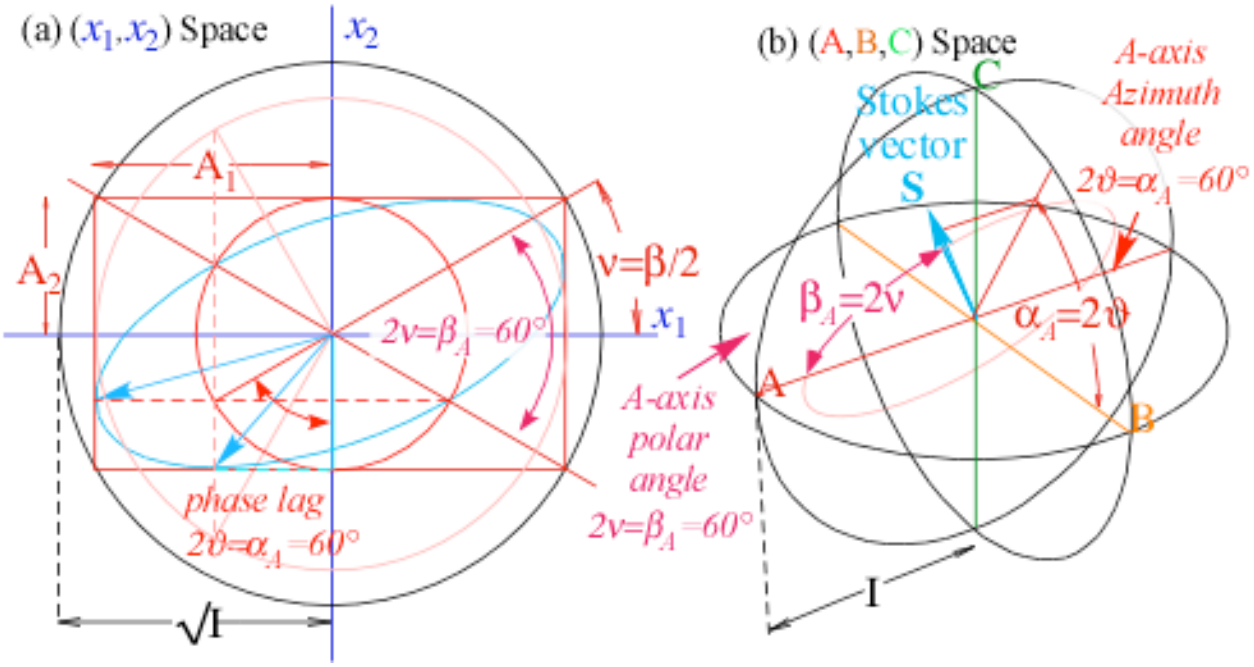

Fig. 5.3 Polarization described by (a) plane-x_1x_2 bases and (b) A-axis polar angles of Stokes vector.

Converting an *A*-based set (5.20) of Stokes parameters into a *C*-based one or into a *B*-based one is simply a matter of cyclic permutation of *A*, *B*, and *C* polar formulas as follows.

$$\text{Asymmetry } S_A=\frac{I}{2}\cos\beta_A \quad =\frac{I}{2}\sin\alpha_B\sin\beta_B=\frac{I}{2}\cos\alpha_C\sin\beta_C \qquad (5.25a)$$

$$\text{Balance } \quad S_B=\frac{I}{2}\cos\alpha_A\sin\beta_A=\frac{I}{2}\cos\beta_B \quad =\frac{I}{2}\sin\alpha_C\sin\beta_C \qquad (5.25b)$$

$$\text{Circularity } S_C=\frac{I}{2}\sin\alpha_A\sin\beta_A \quad =\frac{I}{2}\cos\alpha_B\sin\beta_B=\frac{I}{2}\cos\beta_C \qquad (5.25c)$$

To find the *C*-axis polar angle β_C in terms of *A*-axis angles α_A and β_A, we use (5.25 c).

The C-view in {x_R,x_L}-basis

The orbit can be expressed in right and left circular polarization $\{x_R,x_L\}$-bases using angles $(\alpha_C,\beta_C,\gamma_C)$.

$$\begin{pmatrix} a_R \\ a_L \end{pmatrix} = A \begin{pmatrix} e^{-i\alpha_C/2}\cos\frac{\beta_C}{2} \\ e^{+i\alpha_C/2}\sin\frac{\beta_C}{2} \end{pmatrix} e^{-i\frac{\gamma_C}{2}} = \begin{pmatrix} x_R+ip_R \\ x_R+ip_R \end{pmatrix} \tag{5.26}$$

Angles (α_C,β_C) are found quickly using (5.25). *C*-axial polar angle β_C uses (5.25c). See β_C in Fig. 5.4b.

$$\sin\alpha_A \sin\beta_A = \cos\beta_C \qquad \text{or:} \quad \beta_C = ACS(\sin\alpha_A \sin\beta_A) = ACS(\frac{\sqrt{3}}{2}\cdot\frac{\sqrt{3}}{2}) = 41.4° \tag{5.27}$$

C-axis azimuth angle α_C relates to *A*-axis angles α_A and β_A by (5.25a) and (5.25b). See α_C in Fig. 5.4b.

$$\frac{\cos\alpha_A \sin\beta_A}{\cos\beta_A} = \tan\alpha_C \quad \text{or:} \quad \alpha_C = ATN(\cos\alpha_A \sin\beta_A / \cos\beta_A) = ATN2(\frac{1}{2}\cdot\frac{\sqrt{3}}{2},\frac{1}{2}) = 40.9° \tag{5.28}$$

Half the azimuth angle α_C is the ellipse tipping angle $\varphi=\alpha_C/2$, and half –polar-elevation $2\psi=\pi/2-\beta_C$ is the ellipse diagonal half-angle ψ as seen in Fig. 5.4a. Recall, *2D* angles are $\frac{1}{2}$ the corresponding *3D* ones.

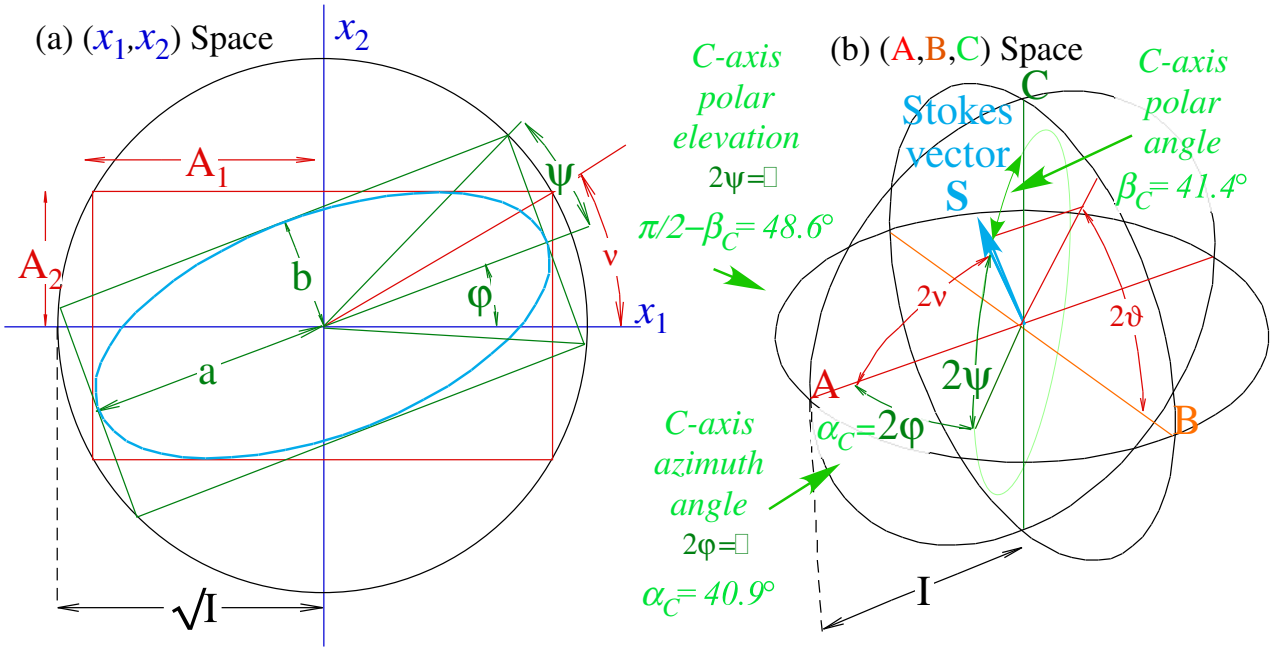

Fig. 5.4 Polarization described by (a) circular-RL bases and (b) C-axis polar angles of Stokes vector.

A 90° *B* –rotation $\mathbf{R}(\pi/4)|x_1\rangle = |x_R\rangle$ of axis *A* into *C* gets $(\alpha_C,\beta_C,\gamma_C)$ from $(\alpha_A,\beta_A,\gamma_A)$ all at once.

$$\begin{pmatrix} \cos\frac{\pi}{4} & i\sin\frac{\pi}{4} \\ i\sin\frac{\pi}{4} & \cos\frac{\pi}{4} \end{pmatrix}\begin{pmatrix} x_1+ip_1 \\ x_2+ip_2 \end{pmatrix} = \frac{\sqrt{2}}{2}\begin{pmatrix} 1 & i \\ i & 1 \end{pmatrix}\begin{pmatrix} Ae^{-i\alpha_A/2}\cos\frac{\beta_A}{2} \\ Ae^{+i\alpha_A/2}\sin\frac{\beta_A}{2} \end{pmatrix} e^{-i\frac{\gamma_A}{2}} = \begin{pmatrix} Ae^{-i\alpha_C/2}\cos\frac{\beta_C}{2} \\ Ae^{+i\alpha_C/2}\sin\frac{\beta_C}{2} \end{pmatrix} e^{-i\frac{\gamma_C}{2}} = \begin{pmatrix} x_R+ip_R \\ x_R+ip_R \end{pmatrix} \tag{5.29}$$

Circular polarization is natural for things with *chirality* or "handedness" such as magnetic fields or Coriolis rotational effects. Then the *C*-axis becomes the "special *z*-one" as indicated in Fig. 5.5.

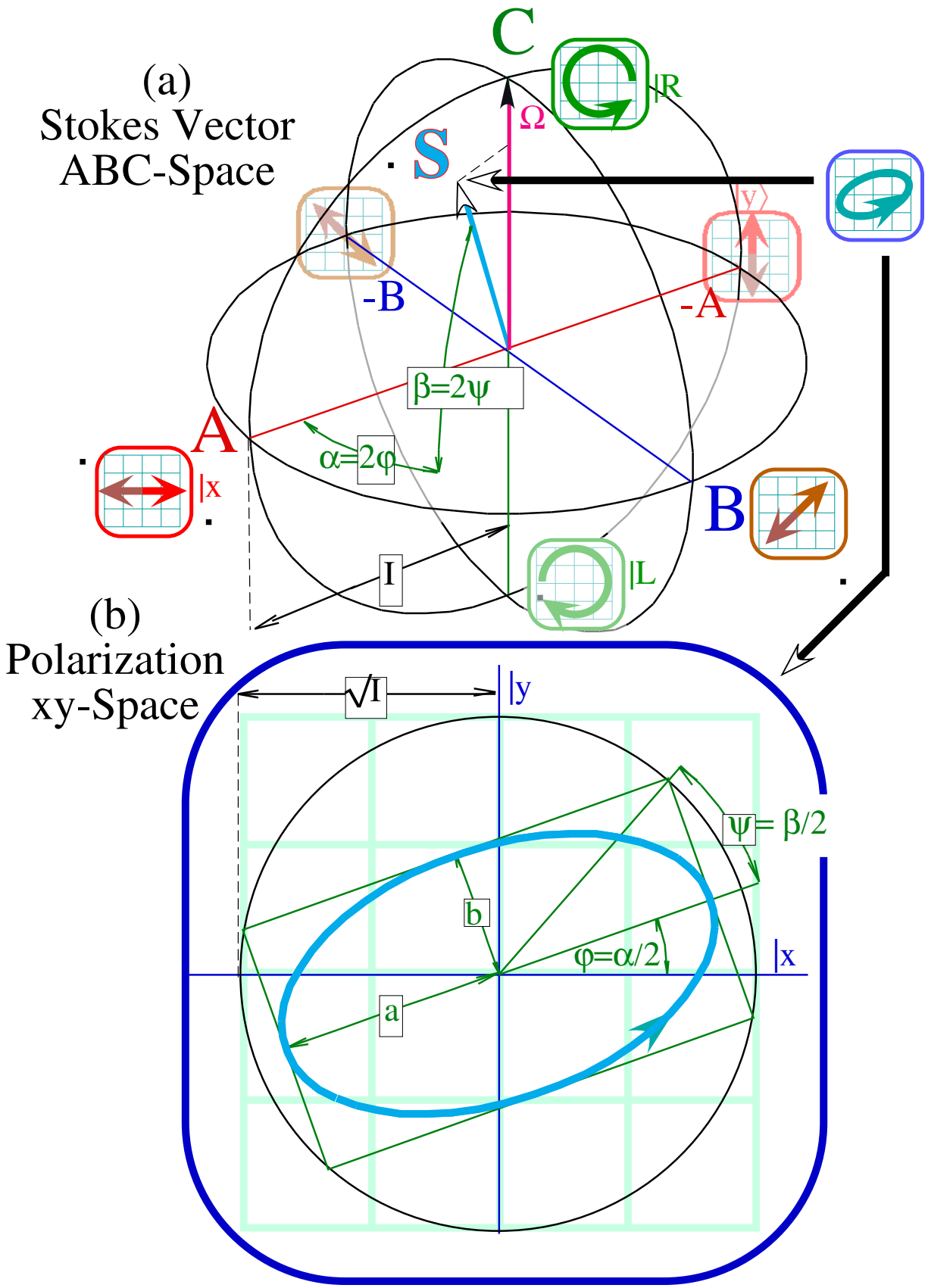

Fig. 5.5 Polarization variables (a) Stokes real-vector space (ABC) (b) Complex xy-spinor-space (x_1,x_2).

(c) How spinors give eigensolutions *(Gone in 60 seconds!)*

Can you write down all eigensolutions to the following **H** -matrix in 60 seconds?

$$\mathbf{H}=\begin{pmatrix} 10+4\cos\frac{\pi}{3} & 4\cos\frac{\pi}{4}\sin\frac{\pi}{3}-i4\sin\frac{\pi}{4}\sin\frac{\pi}{3} \\ 4\cos\frac{\pi}{4}\sin\frac{\pi}{3}+i4\sin\frac{\pi}{4}\sin\frac{\pi}{3} & 10-4\cos\frac{\pi}{3} \end{pmatrix}=\begin{pmatrix} 12 & \sqrt{6}(1-i) \\ \sqrt{6}(1+i) & 8 \end{pmatrix}$$

We're not just asking for eigen*values* in 60 minutes, but *all* eigen*solutions*, vectors *and* values, in *60 seconds flat*! If you know your spinors, it's as easy as π. Here they are.

$$\underline{|eigenvalue-1}$$

$$\omega_{\uparrow}=10+\sqrt{\left(\frac{12-8}{2}\right)^2+\left(\sqrt{6}\right)^2+\left(\sqrt{6}\right)^2}$$

$$=10+4=14$$

$$\underline{|eigenvector-1}$$

$$|\uparrow\rangle=\begin{pmatrix} e^{-i\frac{\pi}{8}}\cos\frac{\pi}{6} \\ e^{+i\frac{\pi}{8}}\sin\frac{\pi}{6} \end{pmatrix}=\begin{pmatrix} 1 \\ e^{i\frac{\pi}{4}}\frac{\sqrt{3}}{3} \end{pmatrix}\frac{e^{-i\frac{\pi}{8}}\sqrt{3}}{2}$$

$$\underline{|eigenvalue-2}$$

$$\omega_{\downarrow}=10-\sqrt{\left(\frac{12-8}{2}\right)^2+\left(\sqrt{6}\right)^2+\left(\sqrt{6}\right)^2}$$

$$=10-4=6$$

$$\underline{|eigenvector-2}$$

$$|\downarrow\rangle=\begin{pmatrix} -e^{-i\frac{\pi}{8}}\sin\frac{\pi}{6} \\ e^{+i\frac{\pi}{8}}\cos\frac{\pi}{6} \end{pmatrix}=\begin{pmatrix} -e^{i\frac{\pi}{4}}\frac{\sqrt{3}}{3} \\ 1 \end{pmatrix}\frac{e^{-i\frac{\pi}{8}}\sqrt{3}}{2}$$

The trick: Get the **H** crank vector $\vec{\mathbf{\Omega}}$ polar angles of azimuth φ, polar ϑ, and rate Ω. Here $\Omega=8$.

$$\vec{\mathbf{\Omega}}=[(A-D),2B,2C]=\Omega[\cos\vartheta,\cos\varphi\sin\vartheta,\sin\varphi\sin\vartheta] \quad \text{where:} \quad \Omega=\sqrt{(A-D)^2+(2B)^2+(2C)^2} \qquad (5.30a)$$

$$\mathbf{H}=\begin{pmatrix} \frac{A+D}{2}+\frac{\Omega}{2}\cos\vartheta & \frac{\Omega}{2}\cos\varphi\sin\vartheta-i\frac{\Omega}{2}\sin\varphi\sin\vartheta \\ \frac{\Omega}{2}\cos\varphi\sin\vartheta+i\frac{\Omega}{2}\sin\varphi\sin\vartheta & \frac{A+D}{2}-\frac{\Omega}{2}\cos\vartheta \end{pmatrix}=\begin{pmatrix} A & B-iC \\ B+iC & D \end{pmatrix} \qquad (5.30b)$$

Eigenstate $|\uparrow\rangle$ spin vector $\vec{\mathbf{s}}$ has Euler angles of azimuth $\alpha=\varphi$, pole $\beta=\vartheta$, and any phase $(\text{let:}\gamma=0)$.

$$|\uparrow\rangle=\begin{pmatrix} e^{-i\frac{\alpha}{2}}\cos\frac{\beta}{2} \\ e^{+i\frac{\alpha}{2}}\sin\frac{\beta}{2} \end{pmatrix}e^{-i\frac{\gamma}{2}}=\begin{pmatrix} e^{-i\frac{\varphi}{2}}\cos\frac{\vartheta}{2} \\ e^{+i\frac{\varphi}{2}}\sin\frac{\vartheta}{2} \end{pmatrix} \qquad |\downarrow\rangle=\begin{pmatrix} e^{-i\frac{\alpha}{2}}\cos\frac{\beta}{2} \\ e^{+i\frac{\alpha}{2}}\sin\frac{\beta}{2} \end{pmatrix}e^{-i\frac{\gamma}{2}}=\begin{pmatrix} -e^{-i\frac{\varphi}{2}}\sin\frac{\vartheta}{2} \\ e^{+i\frac{\varphi}{2}}\cos\frac{\vartheta}{2} \end{pmatrix} \qquad (5.30c)$$

has eigenvalue: $\omega_{\uparrow}=\frac{A+D}{2}+\frac{\Omega}{2}$ has eigenvalue: $\omega_{\downarrow}=\frac{A+D}{2}-\frac{\Omega}{2}$

Eigenstate $|\downarrow\rangle$ spin vector $-\vec{\mathbf{s}}$ has same azimuth $\alpha=\varphi$, flipped pole $\beta=\vartheta\pm\pi$, and any phase.

It doesn't get much easier! You just line up state spin vector-$\vec{\mathbf{s}}$ angles (α,β) and (φ,ϑ) of Hamiltonian crank vector to get the first (spin-up) eigenstate, and then stick $\vec{\mathbf{s}}$ the other way to get an orthogonal (spin-down) eigenstate. But, don't goof the **H** angles. Use *atan2* or $Rct\rightleftharpoons Pol$.

$$\varphi=atan2(C,B) \quad [\tan^{-1}(C\ /\ B)\ is\ unreliable] \qquad \vartheta=atan2(2\sqrt{B^2+C^2},A-D)$$

Simple arc-functions like *arctan(C/B)* are unreliable due to their multi-valued quadrant ambiguity.

(d) How spinors give time evolution

Can you just as quickly write down the evolution operator of that Hamiltonian?

$$\mathbf{U}(0,t) = e^{-i\mathbf{H}t/\hbar} = e^{-i\begin{pmatrix} 12 & \sqrt{6}(1-i) \\ \sqrt{6}(1+i) & 8 \end{pmatrix}t/\hbar} = \begin{pmatrix} ? & ? \\ ? & ? \end{pmatrix}$$

A formal exponential is pretty useless unless you expand it using the **H** -crank $\vec{\mathbf{\Omega}}$ in (5.15c).

$$e^{-i(\sigma\bullet\vec{\mathbf{\Omega}}t)/2} = e^{-i\mathbf{S}\bullet\vec{\mathbf{\Omega}}t} = \mathbf{1}\cos\frac{\Omega t}{2} - i\ (\sigma\bullet\hat{\mathbf{\Omega}})\sin\frac{\Omega t}{2}$$

This is the $e^{-i\mathbf{S}\bullet\vec{\Theta}}$ formula (5.15a) with whirl rate-times-time $\vec{\mathbf{\Omega}}t = \vec{\mathbf{\Theta}}$ replacing turn-axis vector $\vec{\mathbf{\Theta}}$.

$$\mathbf{U}(0,t) = e^{-i(\sigma\bullet\vec{\mathbf{\Omega}}t)/2} = \mathbf{1}\cos\frac{\Omega t}{2} - i\ (\sigma\bullet\hat{\mathbf{\Omega}})\sin\frac{\Omega t}{2} \qquad \left(\begin{array}{l}\text{The overall phase factor } e^{-i\frac{A+D}{2}t} \\ \text{may be attached later. (Or ignored)}\end{array}\right) \tag{5.31a}$$

(The *unit* crank vector $\hat{\mathbf{\Omega}} = [(A-D), 2B, 2C]/\Omega = [\cos\vartheta, \cos\varphi\sin\vartheta, \sin\varphi\sin\vartheta]$ is also *unit* $\hat{\mathbf{\Theta}}$.)

$$\begin{aligned}\mathbf{U}(0,t) &= \mathbf{1}\cos\frac{\Omega t}{2} - i\,(\sigma_A\cos\vartheta + \sigma_B\cos\varphi\sin\vartheta + \sigma_C\sin\varphi\sin\vartheta)\sin\frac{\Omega t}{2} \\ &= \begin{pmatrix}1&0\\0&1\end{pmatrix}\cos\frac{\Omega t}{2} - i\,(\begin{pmatrix}1&0\\0&-1\end{pmatrix}\cos\vartheta + \begin{pmatrix}0&1\\1&0\end{pmatrix}\cos\varphi\sin\vartheta + \begin{pmatrix}0&-i\\i&0\end{pmatrix}\sin\varphi\sin\vartheta)\sin\frac{\Omega t}{2}\end{aligned} \tag{5.31b}$$

Sum this all into a single matrix and you get a useful general evolution operator.

$$\begin{aligned}\mathbf{U}(0,t) &= \begin{pmatrix} \cos\frac{\Omega t}{2} - i\cos\vartheta\sin\frac{\Omega t}{2} & -i(\cos\varphi - i\sin\varphi)\sin\vartheta\sin\frac{\Omega t}{2} \\ -i(\cos\varphi - i\sin\varphi)\sin\vartheta\sin\frac{\Omega t}{2} & \cos\frac{\Omega t}{2} + i\cos\vartheta\sin\frac{\Omega t}{2}\end{pmatrix} \\ &= \begin{pmatrix} \cos\frac{\Omega t}{2} - i\cos\vartheta\sin\frac{\Omega t}{2} & -ie^{-i\varphi}\sin\vartheta\sin\frac{\Omega t}{2} \\ -ie^{+i\varphi}\sin\vartheta\sin\frac{\Omega t}{2} & \cos\frac{\Omega t}{2} + i\cos\vartheta\sin\frac{\Omega t}{2}\end{pmatrix} = \begin{pmatrix} \cos\frac{\Omega t}{2} - i\hat{\Omega}_A\sin\frac{\Omega t}{2} & -i(\hat{\Omega}_B - i\hat{\Omega}_C)\sin\frac{\Omega t}{2} \\ -i(\hat{\Omega}_B + i\hat{\Omega}_C)\sin\frac{\Omega t}{2} & \cos\frac{\Omega t}{2} + i\hat{\Omega}_A\sin\frac{\Omega t}{2}\end{pmatrix}\end{aligned} \tag{5.31c}$$

Our numerical crank rate is $\Omega = 8$. Our *unit* crank rate vector $\hat{\mathbf{\Omega}}$ fills in the numbers for $\mathbf{U}(0,t)$.

$$\hat{\mathbf{\Omega}} = \frac{[(12-8), 2\sqrt{6}, 2\sqrt{6}]}{\Omega} = \left[\frac{1}{2}, \frac{\sqrt{6}}{4}, \frac{\sqrt{6}}{4}\right] = [\cos\vartheta, \cos\varphi\sin\vartheta, \sin\varphi\sin\vartheta] = [\hat{\Omega}_A, \hat{\Omega}_B, \hat{\Omega}_C]$$

$$\mathbf{U}(0,t) = \begin{pmatrix} \cos 4t - i\frac{1}{2}\sin 4t & -i(1-i)\frac{\sqrt{6}}{4}\sin 4t \\ -i(1+i)\frac{\sqrt{6}}{4}\sin 4t & \cos 4t + i\frac{1}{2}\sin 4t\end{pmatrix}$$

Starting from any initial state like $|\Psi(0)\rangle = \begin{pmatrix}1\\0\end{pmatrix}$ we compute what it will be at time *t*.

$$|\Psi(t)\rangle = \mathbf{U}(0,t)|\Psi(0)\rangle = \begin{pmatrix} \cos 4t - i\frac{1}{2}\sin 4t & -i(1-i)\frac{\sqrt{6}}{4}\sin 4t \\ -i(1+i)\frac{\sqrt{6}}{4}\sin 4t & \cos 4t + i\frac{1}{2}\sin 4t \end{pmatrix}\begin{pmatrix} 1 \\ 0 \end{pmatrix} = \begin{pmatrix} \cos 4t - i\frac{1}{2}\sin 4t \\ (1-i)\frac{\sqrt{6}}{4}\sin 4t \end{pmatrix}$$

B-Type Oscillation: Simple examples of balanced beats

Resonant beats in Fig. 3.9 are super-positions of a 0°-in-phase mode (○→ ○→) of slower frequency ω_{slow} and a 180°-out-of-phase mode (○→ ←○) of faster frequency ω_{fast}. Transverse 0°-in-phase modes $\begin{pmatrix}\circ\!\!\rightarrow\\ \circ\!\!\rightarrow\end{pmatrix}$ and 180°-out-of-phase modes $\begin{pmatrix}\circ\!\!\rightarrow\\ \leftarrow\!\!\circ\end{pmatrix}$ do the same. Each mode is denoted by complex amplitude vectors $e^{-i\omega_{slow}t}\begin{pmatrix}1\\1\end{pmatrix}$ and $e^{-i\omega_{fast}t}\begin{pmatrix}1\\-1\end{pmatrix}$, respectively.

Let's add them half-and-half or 50-50. (We let slow and fast phases be $s=-\omega_{slow}t$ and $f=-\omega_{fast}t$.)

$$\begin{pmatrix}a_1^{50-50}\\ a_2^{50-50}\end{pmatrix}=\frac{1}{2}e^{-i\omega_{slow}t}\begin{pmatrix}1\\1\end{pmatrix}+\frac{1}{2}e^{-i\omega_{fast}t}\begin{pmatrix}1\\-1\end{pmatrix}=\frac{1}{2}e^{is}\begin{pmatrix}1\\1\end{pmatrix}+e^{if}\begin{pmatrix}1\\-1\end{pmatrix}=\frac{1}{2}\begin{pmatrix}e^{is}+e^{if}\\ e^{is}-e^{if}\end{pmatrix} \qquad (5.32)$$

We could write the complex numbers in Cartesian form: $e^{is}=\cos s+i\sin s$ and $e^{if}=\cos f+i\sin f$.

$$\begin{pmatrix}a_1^{50-50}\\ a_2^{50-50}\end{pmatrix}=\frac{1}{2}\begin{pmatrix}e^{is}+e^{if}\\ e^{is}-e^{if}\end{pmatrix}=\frac{1}{2}\begin{pmatrix}\cos s+i\sin s+\cos f+i\sin f\\ \cos s+i\sin s-\cos f-i\sin f\end{pmatrix}=\frac{1}{2}\begin{pmatrix}\left(\cos s+\cos f\right)+i\left[\sin s+\sin f\right]\\ \left(\cos s-\cos f\right)+i\left[\sin s-\sin f\right]\end{pmatrix}=\begin{pmatrix}X_1+iP_1\\ X_2+iP_2\end{pmatrix}$$

Cartesian $X_1=Re\ a_1$, $P_1=Im\ a_1$, $X_2=Re\ a_2$, $P_2=Im\ a_2$ are then given. A factored polar form is better:

$$\begin{pmatrix}a_1^{50-50}\\ a_2^{50-50}\end{pmatrix}=\frac{1}{2}\begin{pmatrix}e^{is}+e^{if}\\ e^{is}-e^{if}\end{pmatrix}=\frac{1}{2}\begin{pmatrix}e^{i\frac{s+f}{2}}\left(e^{i\frac{s-f}{2}}+e^{-i\frac{s-f}{2}}\right)\\ e^{i\frac{s+f}{2}}\left(e^{i\frac{s-f}{2}}-e^{-i\frac{s-f}{2}}\right)\end{pmatrix}=\begin{pmatrix}e^{i\frac{s+f}{2}}\cos\frac{s-f}{2}\\ e^{i\frac{s+f}{2}}i\sin\frac{s-f}{2}\end{pmatrix} \quad \text{where:} \quad \cos A=\frac{e^{iA}+e^{-iA}}{2},\quad i\sin A=\frac{e^{iA}-e^{-iA}}{2}$$

Note: this trick easily gives four *sin-cos* identities like $\cos\frac{s+f}{2}\cos\frac{s-f}{2}=\frac{1}{2}(\cos s+\cos f)$. Now we factor out overall phase and compute the (get real!) Stokes vector $\mathbf{S}=(S_A, S_B, S_C)$ as functions of time.

$\begin{pmatrix}a_1^{50-50}\\ a_2^{50-50}\end{pmatrix}=e^{i\frac{s+f}{2}}\begin{pmatrix}\cos\frac{s-f}{2}\\ i\sin\frac{s-f}{2}\end{pmatrix}=e^{i\frac{s+f}{2}}\begin{pmatrix}\cos\frac{\Delta}{2}\\ i\sin\frac{\Delta}{2}\end{pmatrix}$ gives the following where: $\Delta=s-f=-\left(\omega_{fast}-\omega_{slow}\right)t$.

$$S_A=\begin{pmatrix}\cos\frac{\Delta}{2} & i\sin\frac{\Delta}{2}\end{pmatrix}^*\begin{pmatrix}1&0\\0&-1\end{pmatrix}\begin{pmatrix}\cos\frac{\Delta}{2}\\ i\sin\frac{\Delta}{2}\end{pmatrix}=\begin{pmatrix}\cos\frac{\Delta}{2} & -i\sin\frac{\Delta}{2}\end{pmatrix}\begin{pmatrix}\cos\frac{\Delta}{2}\\ -i\sin\frac{\Delta}{2}\end{pmatrix}=\cos^2\frac{\Delta}{2}-\sin^2\frac{\Delta}{2}=\cos\Delta=\cos(s-f)$$

$$S_B=\begin{pmatrix}\cos\frac{\Delta}{2} & i\sin\frac{\Delta}{2}\end{pmatrix}^*\begin{pmatrix}0&1\\1&0\end{pmatrix}\begin{pmatrix}\cos\frac{\Delta}{2}\\ i\sin\frac{\Delta}{2}\end{pmatrix}=\begin{pmatrix}\cos\frac{\Delta}{2} & -i\sin\frac{\Delta}{2}\end{pmatrix}\begin{pmatrix}i\sin\frac{\Delta}{2}\\ \cos\frac{\Delta}{2}\end{pmatrix}=i\cos\frac{\Delta}{2}\sin\frac{\Delta}{2}-i\sin\frac{\Delta}{2}\cos\frac{\Delta}{2}=0$$

$$S_C=\begin{pmatrix}\cos\frac{\Delta}{2} & i\sin\frac{\Delta}{2}\end{pmatrix}^*\begin{pmatrix}0&-i\\i&0\end{pmatrix}\begin{pmatrix}\cos\frac{\Delta}{2}\\ i\sin\frac{\Delta}{2}\end{pmatrix}=\begin{pmatrix}\cos\frac{\Delta}{2} & -i\sin\frac{\Delta}{2}\end{pmatrix}\begin{pmatrix}\sin\frac{\Delta}{2}\\ i\cos\frac{\Delta}{2}\end{pmatrix}=\cos\frac{\Delta}{2}\sin\frac{\Delta}{2}+\sin\frac{\Delta}{2}\cos\frac{\Delta}{2}=\sin\Delta=\sin(s-f)$$

It is a B-axial rotation of Stokes vector $\mathbf{S}=(S_A, S_B, S_C)=(\cos\Delta,0,\sin\Delta)$ past ±A and ±C-axes as in Fig. 5.6.

The angular frequency $|\Delta|=|\omega_{fast}-\omega_{slow}|$ of the rotation is called a *beat frequency* . In quantum theory it is the *Rabi rotation frequency* or the *NMR precession frequency* in spin resonance that Rabi pioneered. It is simply the relative angular velocity between two phasors having a race around the clock. It is twice that of the half-difference $|\Delta|/2=|\omega_{fast}-\omega_{slow}|/2$ seen in phasor space. That mysterious factor of *1/2* discussed after (5.14) appears again and makes us sharpen our view of space and time.

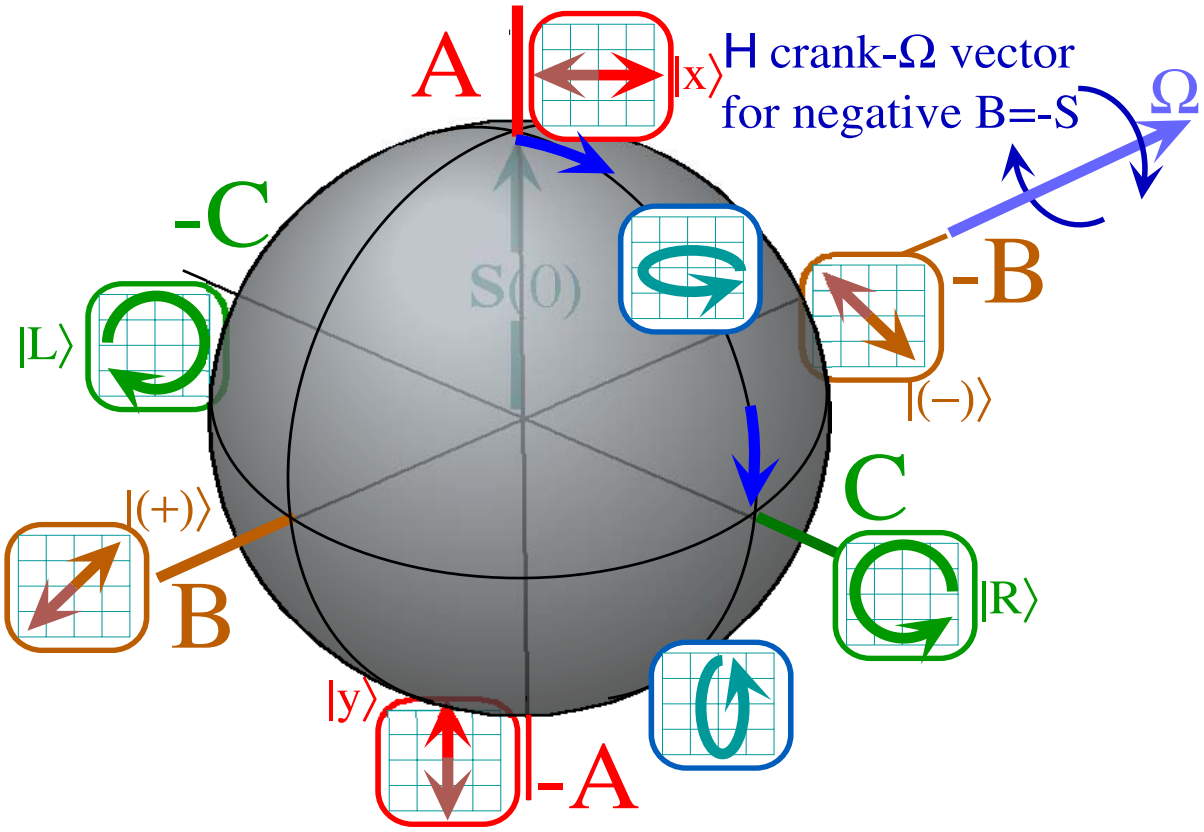

Fig. 5.6 Time evolution of a B-type beat. **S***-vector rotates from A to C to -A to -C and back to A..*

For example if you follow the rotation in the $X_1=Re\ a_1$, $P_1=Im\ a_1$, $X_2=Re\ a_2$, $P_2=Im\ a_2$ space you will see that one rotation by 360° in ABC-space is only half way back to the starting line, and another 360° rotation (either way) is needed in ABC-space to get a full 360° rotation in phasor xy-space. That is, a rotation of 720° or 0° in the Stokes ABC-space is needed to return to where they started in *xy*-space.

Points that are separated by 180° in ABC-vector-space map onto phasor (2D-spinor) base vectors that are only 90° apart since in *xy*-space $|x\rangle$ and $|y\rangle$ are orthogonal. So a 180° separation in *xy*-space, that is, a 180° phase factor $e^{\pm i\pi}=-1$, maps onto the *same* Stokes-vector in ABC space. Another way to see this strange phase shift is to look at a C-rotation that happens in Circular polarization environments, or in a Cyclotron oscillator, or in the presence of a Coriolis or Chiral force of Earth rotation. (Notice all the C's including Complex that are used to describe the circular case.) The Fig. 5.7 shows how +*x*-polarization returns first to –*x*-polarization, that is 180° out of phase and needs another 360° rotation around the C-axis

to really be back to +*x*-polarization. The *xy*-spinor rotates by half the angle its S-vector turns in ABC-space so *xy*-oscillation vector returns to the North pole "pointing backwards" with a 180° phase shift.

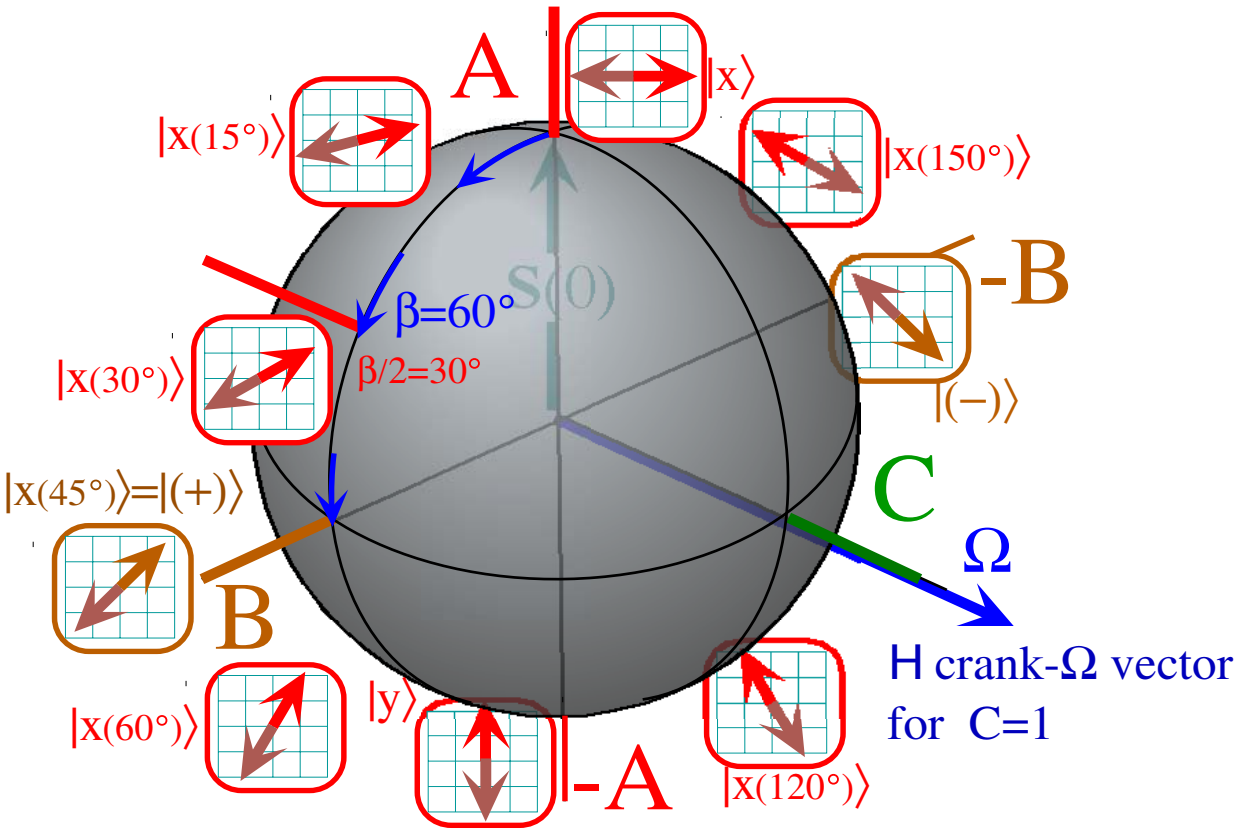

Fig. 5.7 Time evolution of a C-type beat. **S***-vector rotates from A to B to -A to -B and back to A.*

Chapter 6 Multiple Oscillators and Wave Motion

Two mass-m-spring-k oscillators coupled by spring-k_{12} feel a force vector $\mathbf{F}=(F_1,F_2)$ given by

$$-\begin{pmatrix}F_1\\F_2\end{pmatrix}=\begin{pmatrix}k+k_{12} & -k_{12}\\ -k_{12} & k+k_{12}\end{pmatrix}\bullet\begin{pmatrix}x_1\\x_2\end{pmatrix} \quad \text{or :-}\mathbf{F}=\mathbf{K}\bullet\mathbf{x} \qquad (3.4)_{repeated}$$

at position vector $\mathbf{x}=(x_1,x_2)$. (Recall discussion around (3.4).) Unless force $\mathbf{F}$ points down the vector $\mathbf{x}$, as it does for special directions $\mathbf{u}_+$ (beginner slope) or $\mathbf{u}_-$ (advanced slope), complicated beating motion seen in Fig. 5.5 results. The directions $\mathbf{u}_\pm$ giving $-\mathbf{F}=\mathbf{K}\bullet\mathbf{u}_\pm=k_\pm\mathbf{u}_\pm$ are *simple harmonic mode* directions.

$$\mathbf{K}\bullet\mathbf{u}_+=\begin{pmatrix}k+k_{12} & -k_{12}\\ -k_{12} & k+k_{12}\end{pmatrix}\bullet\begin{pmatrix}1\\1\end{pmatrix}=k_+\begin{pmatrix}1\\1\end{pmatrix} \qquad \text{Eigenvalue: } k_+=k, \qquad \text{Eigenfrequency: } \omega_+=\sqrt{\frac{k_+}{m}} \qquad (6.1a)$$

$$\mathbf{K}\bullet\mathbf{u}_-=\begin{pmatrix}k+k_{12} & -k_{12}\\ -k_{12} & k+k_{12}\end{pmatrix}\bullet\begin{pmatrix}1\\-1\end{pmatrix}=k_-\begin{pmatrix}1\\-1\end{pmatrix} \qquad \text{Eigenvalue: } k_-=k+2k_{12}, \quad \text{Eigenfrequency: } \omega_-=\sqrt{\frac{k_-}{m}} \qquad (6.1b)$$

The $\mathbf{u}_\pm$'s are called *eigenvectors* and the proportionality factors $k_\pm$ are called *eigenvalues* $k_\pm$ and lead to the *eigenfrquencies* $\omega_\pm$ in (6.1). This solves two-oscillator motion. Now we consider N oscillators.

(a) The Shower Curtain Model

What if we hook up N oscillators in a ring? Let's imagine rings of N masses in Fig. 6.1 like lead weights at the bottom of a shower curtain. An N-dimensional $\mathbf{K}$ matrix like (3.4) gives forces F_m.

$$-\begin{pmatrix}F_0\\F_1\\F_2\\F_3\\F_4\\\vdots\\F_{N-1}\end{pmatrix}=\begin{pmatrix}K & -k_{12} & . & . & . & \cdots & -k_{12}\\ -k_{12} & K & -k_{12} & . & . & \cdots & .\\ . & -k_{12} & K & -k_{12} & . & \cdots & .\\ . & . & -k_{12} & K & -k_{12} & \cdots & .\\ . & . & . & -k_{12} & K & \cdots & .\\ \vdots & \vdots & \vdots & \vdots & \vdots & \ddots & -k_{12}\\ -k_{12} & . & . & . & . & -k_{12} & K\end{pmatrix}\bullet\begin{pmatrix}x_0\\x_1\\x_2\\x_3\\x_4\\\vdots\\x_{N-1}\end{pmatrix} \quad \text{where:} \quad \begin{matrix}K=k+2k_{12}\\ k=\dfrac{Mg}{\ell}\\ (\cdot)=0\end{matrix} \qquad (6.2)$$

Each mass-M connects through a k_{12} spring to its two nearest neighbors. The mass at origin coordinate x_0 connects to x_1 on its right and x_{N-1} on its left. Then the first mass to the right of origin with coordinate x_1 connects to x_2 on its right and x_1 on its left, and so on around the loop. If all in (6.2) are fixed except x_0 (Let x_0 vary but fix $0=x_1=x_2=\ldots x_{N-1}$) then x_0 has its pendulum oscillation frequency $\omega=\sqrt{\frac{k}{M}}=\sqrt{\frac{g}{\ell}}$ plus that of two k_{12}-springs connecting it to fixed neighbors with restoring force $-F_0=Kx_0=(k+2k_{12})x_0$ from (6.2).

This circular *shower curtain model* may be solved using complex arithmetic and symmetry arguments. This seemingly silly system helps in Unit 3 to learn some things about the relativistic quantum universe, another seemingly *very* silly system! Be prepared to learn a lot in a rather short time. If you have understood what has gone before in this book then what follows will not be so difficult.

We now use symmetry to find eigenvectors $\mathbf{u}_m$ of the $\mathbf{K}$-matrix in (6.2) for which $\mathbf{K}\bullet\mathbf{u}_m=k_m\mathbf{u}_m$. The $\mathbf{u}_m$ give directions in $\mathbf{u}$-space that are invariant to spring-force matrix $\mathbf{K}$ and thus don't change in time.

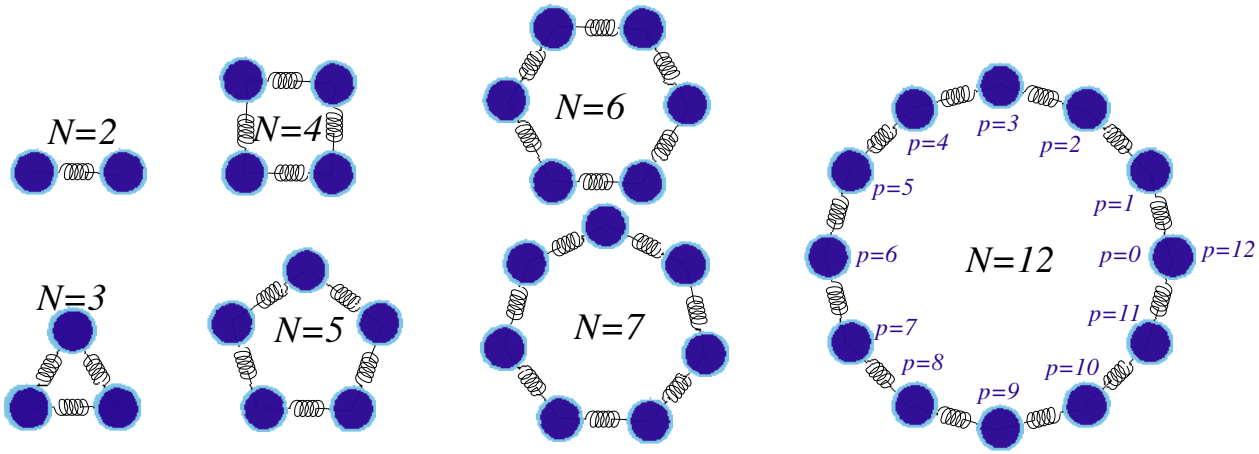

Fig. 6.1 N-Coupled Pendulums. (Viewed from above.)

N^{th} Roots of unity

The eigenvectors and eigenvalues of the *N-by-N*-matrix **K** (6.2) are made of the complex *N^{th}-roots of unity*, that are solutions to the equation $x^N=1$. The 2-mass solutions (6.1) use 2nd or square roots ± 1 of 1. Euler's exponential leads to the N^{th} roots of $1=e^{2\pi i}$, that is, exactly N *different* solutions to $x^N= e^{2\pi i}$.

$$x^N = 1 = e^{2\pi i} \quad \text{implies : } x = \left(e^{2\pi i}\right)^{\frac{1}{N}} = e^{\frac{2\pi i}{N}} \quad \text{and: } \quad x^m = e^{\frac{2\pi i}{N}m} \quad \text{satisfies: } \left(x^m\right)^N = 1 \qquad (6.3)$$

Square, cubic, quartic, quintic*(5^{th})*, hexaic *(6^{th})*, and duodecaic *(12^{th})* roots of 1 are plotted in Fig. 6.2. They form regular polygons whose vertices are powers $(\psi_N)^m$ of a *fundamental N^{th} root $\psi_N=e^{2\pi i/N}$*.

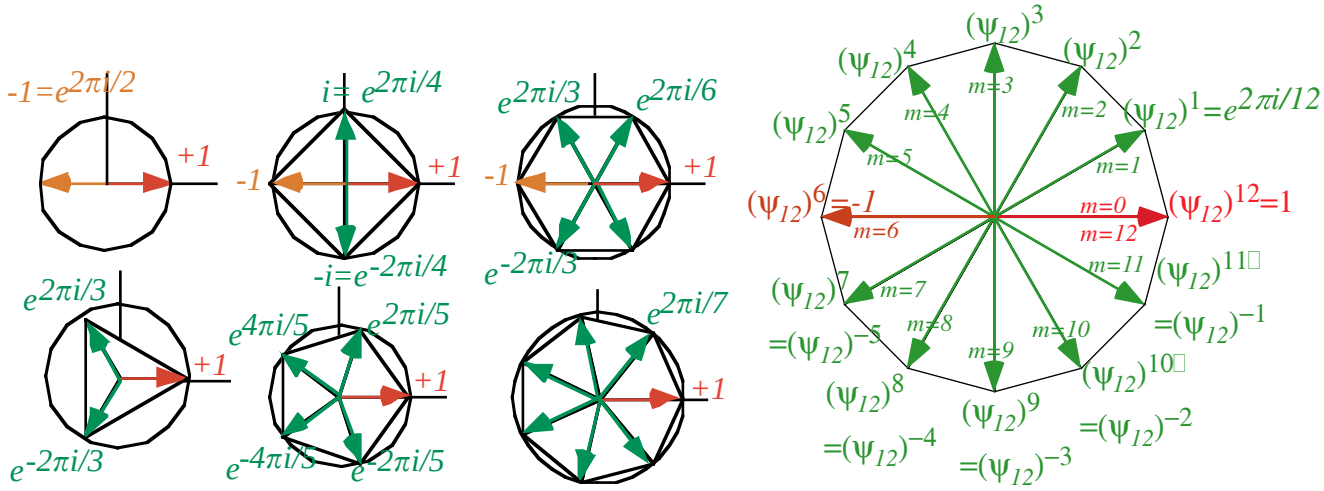

Fig. 6.2 N^{th}-Roots of Unity. Collections of Fourier coefficients for discrete N=2,3,4,5,6.7, and 12.

We'll use *N=12* since it's easy to picture clock numerals. Note that *0* and *12 o'clock* share a point $(\psi_{12})^0=e^{i0}=(e^{i2\pi/12})^{12}=(\psi_{12})^{12}$ as do $(\psi_{12})^{-1}=(\psi_{12})^{11}$, and $(\psi_{12})^{-2}=(\psi_{12})^{10}$, and so on down to the *6 o'clock* point $(\psi_{12})^{-6}=-1=(\psi_{12})^6$. Real axis (*6 and 12 o'clock*) is horizontal in Fig. 6.2 but vertical in later Fig. 6.3.

(b) Solving shower curtain models by symmetry

Eigenvectors of *rotate-shuffle-ops* **r** and $\mathbf{r}^{-1}$ are also eigenvectors of **K**-matrix (6.2).

$$\mathbf{K} = K\cdot\mathbf{1} - k_{12}\cdot\mathbf{r} - k_{12}\cdot\mathbf{r}^{-1} \quad \text{where:} \quad \mathbf{1}=\text{unit matrix , and :} \tag{6.4a}$$

$$\mathbf{r}\bullet\mathbf{x} = \begin{pmatrix} . & . & . & . & . & \cdots & 1 \\ 1 & . & . & . & . & \cdots & . \\ . & 1 & . & . & . & \cdots & . \\ . & . & 1 & . & . & \cdots & . \\ . & . & . & 1 & . & \cdots & . \\ \vdots & \vdots & \vdots & \vdots & \vdots & \ddots & . \\ . & . & . & . & . & 1 & . \end{pmatrix} \bullet \begin{pmatrix} x_0 \\ x_1 \\ x_2 \\ x_3 \\ x_4 \\ \vdots \\ x_{N-1} \end{pmatrix} = \begin{pmatrix} x_{N-1} \\ x_0 \\ x_1 \\ x_2 \\ x_3 \\ \vdots \\ x_{N-2} \end{pmatrix}, \quad \mathbf{r}^{-1}\bullet\mathbf{x} = \begin{pmatrix} . & 1 & . & . & . & \cdots & . \\ . & . & 1 & . & . & \cdots & . \\ . & . & . & 1 & . & \cdots & . \\ . & . & . & . & 1 & \cdots & . \\ . & . & . & . & . & \cdots & . \\ \vdots & \vdots & \vdots & \vdots & \vdots & \ddots & 1 \\ 1 & . & . & . & . & . & . \end{pmatrix} \bullet \begin{pmatrix} x_0 \\ x_1 \\ x_2 \\ x_3 \\ x_4 \\ \vdots \\ x_{N-1} \end{pmatrix} = \begin{pmatrix} x_1 \\ x_2 \\ x_3 \\ x_4 \\ x_5 \\ \vdots \\ x_0 \end{pmatrix} \tag{6.4b}$$

So let's find vectors $\mathbf{u}_m=(x_0,x_1,x_2,x_3,\ldots)$ that are the same after a rotate-shuffle except for a factor f_m.

$$\mathbf{r}^{-1}\bullet\mathbf{u}_m=\mathbf{r}^{-1}(x_0,x_1,x_2,x_3,\ldots) = (x_1,x_2,x_3,x_4,\ldots) = f_m\,(x_0,x_1,x_2,x_3,\ldots) = f_m\mathbf{u}_m \tag{6.4c}$$

Factors f_m will be the desired eigenvalues and we'll have solved $\mathbf{r}^{-1}$, $\mathbf{r}$ *and* $\mathbf{K}$!

The $N=2$ eigenvector $\mathbf{u}_+=(1,1)$ in (6.1a) gives us a clue for $N=12$. Fig. 6.3(g) shows all the pendulums swinging together in the $(m_{12})=0_{12}$ wave (All phasors set to 0^{th}-root $(\psi_{12})=1$) or π-out-of-phase in a $(m_{12})=6_{12}$ wave (x_p set to the p^{th} power of 6^{th}-root $(\psi_{12})=-1$) like (6.1b) vector $\mathbf{u}_-=(1,-1)$.

$$\mathbf{u}_0 = (1,1,1,1,1,1,\ldots) \tag{6.5a}$$

$$\mathbf{u}_6 = (1,-1,1,-1,1,-1,\ldots) \tag{6.5b}$$

To understand general $\mathbf{u}_m$ eigenvectors consider the $(m_{12})=1_{12}$ and 2_{12} vectors plotted in Fig. 6.3(g).

x_p:	x_0	x_1	x_2	x_3	x_4	x_5	x_6	x_7	x_8	x_9	x_{10}	x_{11}	x_{12}	$e^{ik_1}=e^{2\pi i/12}$
$\mathbf{u}_1=$	(1	$e^{ik_1 1}$	$e^{ik_1 2}$	$e^{ik_1 3}$	$e^{ik_1 4}$	$e^{ik_1 5}$	$e^{ik_1 6}$	$e^{-ik_1 5}$	$e^{-ik_1 4}$	$e^{-ik_1 3}$	$e^{-ik_1 2}$	$e^{-ik_1 1}$	1)	
$\mathbf{u}_2=$	(1	$e^{ik_1 2}$	$e^{ik_1 4}$	$e^{ik_1 6}$	$e^{ik_1 8}$	$e^{ik_1 10}$	1	$e^{ik_1 2}$	$e^{ik_1 4}$	$e^{ik_1 6}$	$e^{ik_1 8}$	$e^{ik_1 10}$	1)	$e^{i12k_1}=1$

Each phasor in wave $\mathbf{u}_1$ leads the phasor to the left of it by 1-hour. Clocks are set *12 o'clock, 1 o'clock, 2 o'clock, 3 o'clock, 4 o'clock, 5 o'clock,* and so on for <u>one</u> complete *12 hr*. day going around the "world." Each phasor in wave $\mathbf{u}_2$ leads the phasor to the left of it by <u>2</u>-hours. Clocks are set *12 o'clock, 2 o'clock, 4 o'clock, 6 o'clock, 8 o'clock, 10 o'clock,* and so on for <u>two</u> complete *12 hr*. days going around the loop. This means the $\mathbf{u}_{\pm m}$ eigenvalues of the shuffle-ops $\mathbf{r}^{-1}$ and $\mathbf{r}$ are the *single-step phase-factor* $f_m = e^{\pm ik_1 m}$.

$$\mathbf{r}^{-1}\bullet\mathbf{u}_m = e^{ik_1 m}\mathbf{u}_m \tag{6.6a}$$

$$\mathbf{r}\bullet\mathbf{u}_m = e^{-ik_1 m}\mathbf{u}_m \tag{6.6b}$$

Here $k_1=2\pi/N=2\pi/12$. The **K**-matrix has the same eigenvalue and frequency for a $\mathbf{u}_{+m}$ wave as for $\mathbf{u}_{-m}$.

$$\mathbf{K}\bullet\mathbf{u}_m = \left[K\mathbf{1} - k_{12}\left(\mathbf{r}^{-1}+\mathbf{r}\right)\right]\bullet\mathbf{u}_m = \left[K - k_{12}\left(e^{ik_1 m}+e^{-ik_1 m}\right)\right]\mathbf{u}_m = \left[K - 2k_{12}\cos k_1 m\right]\mathbf{u}_m \tag{6.6c}$$

This gives the *wave* or *spectral dispersion function*. An $\omega(k)$ is a "bottom-line" for wave theory.

$$\omega_m = \sqrt{\frac{K-2k_{12}\cos k_1 m}{M}} = \sqrt{\frac{k+2k_{12}-2k_{12}\cos\left(2\pi m/N\right)}{M}} \tag{6.7}$$

Linear wave motions, velocity, and spreading (dispersion) are ruled by dispersion functions of some kind. The K-pendulum dispersion function ω_m above is a good example and is plotted with others in Fig. 6.6.

An $\omega(k)$ plot is a graph of *per-time* (frequency ω) versus *per-space* (wavevector k). In other words it is a *per-space-time* graph. Let's see how these *"winks-vs-kinks"* functions determine wave physics.

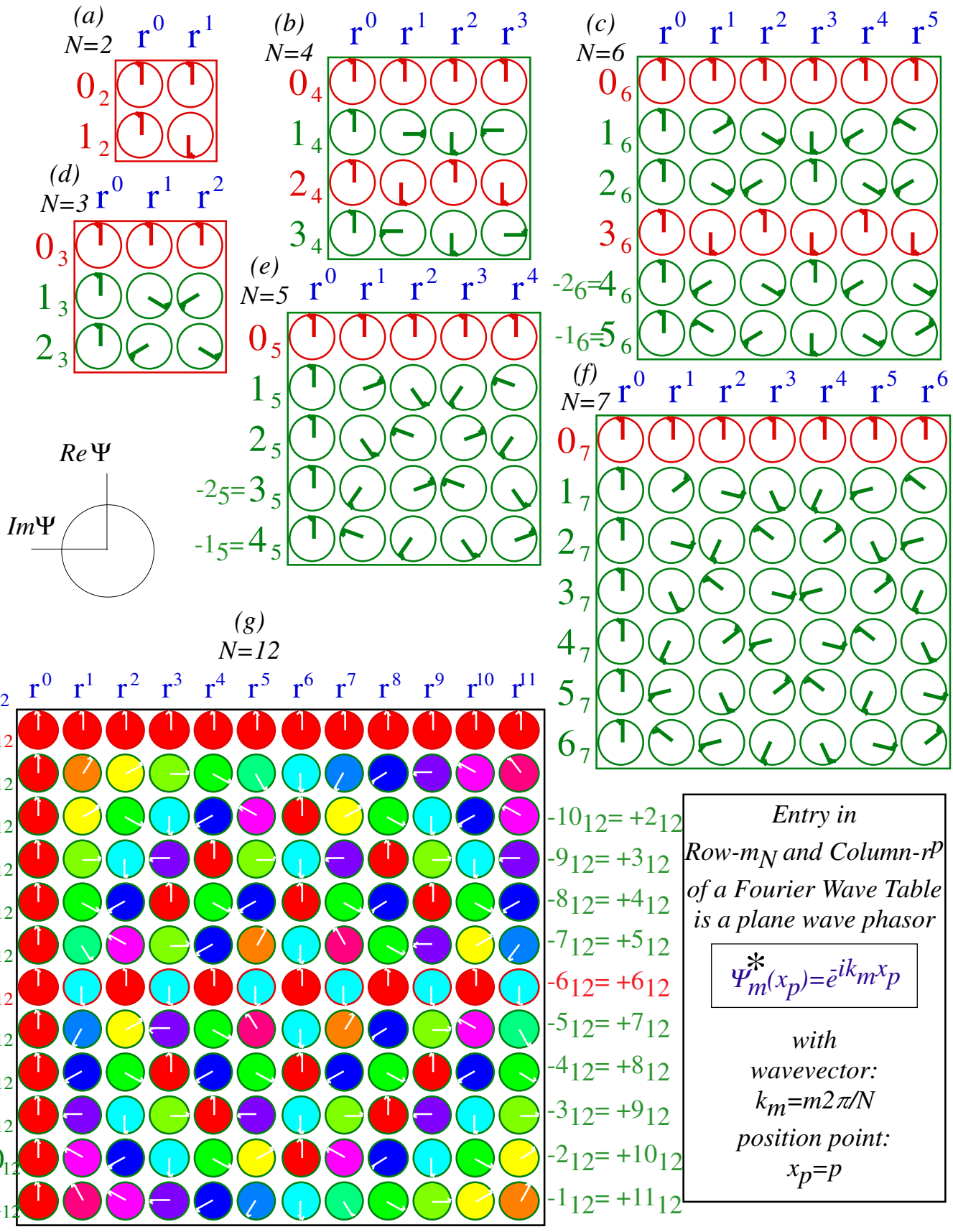

Fig. 6.3 Discrete wave phasor or Fourier transform tables for N=2,3,4,5,6,7, and 12.

(c) Wave structure and dynamics

When watching phasor waves in motion (You should view *WaveIt* and *BohrIt* animations in order to see what's going on here!) we are struck by the impression that some "spirit" is going through the phasors. That, like many spooky notions, is an illusion because only the individual phasors determine the motion of their respective oscillator. But their synchrony begs an explanation and our mind provides one.

To honor our spooky illusion we construct what's called a *wavefunction*. We simply "fill in" the space between each x_p-phasor point $p=0,1,2\ldots$ with the continuous *plane wave function* e^{ikx} of a continuous coordinate x. That is easy to since we are given discrete functions $\Psi_m(x_p)=e^{ik_m x_p}$ in Fig. 6.3 and it is easy to replace x_p with x and plot the resulting $\Psi_m(x)=e^{ik_m x}$. Wavevector k_m is still discrete.

$$\Psi_m(x)=e^{ik_m x}=\cos k_m x+i\sin k_m x \quad \text{where: } k_m=m\frac{2\pi}{N}. \tag{6.8a}$$

This is done in Fig. 6.4 with the real part of the wave plotted darkly and the imaginary part shaded.

Distinguishing Ψ and Ψ: Conjugation and time reversal*

OK! It's time to tell about some symmetry conventions. The wave phasors plotted in Fig. 5.3 are for what's called the *conjugate* **Ψ*** or *time-reversed-wave*. Its phasors run *backwards* like the engineers' phasors. Conjugation (*), if you recall from (5.19a), means reverse imaginary part ±sign.

$$\Psi_m{}^*(x)=e^{-ik_m x}=\cos k_m x-i\sin k_m x \quad \text{where: } k_m=m\frac{2\pi}{N}. \tag{6.8b}$$

Wave tables with wavevector k_m or m-number as a row label must contain the conjugate $(e^{ikx})^*=e^{-ikx}$. Since we're plotting real Re Ψ in the vertical-up direction and Im Ψ in the horizontal-left direction, the act of conjugation *(*)* reflects the horizontal direction of phasor arrows. (This will make more sense later on! It has to do with Dirac's bra-ket notation $\langle x|\Psi_m\rangle=\Psi_m(x)=\langle\Psi_m|x\rangle^*$ which demands that "bras" or "row-vectors" carry a star *(*)* and sounds like sex-discrimination!)

It helps to remember the sine-phase-lag rule from (1.10): *A leading phasor feeds its follower.* That's the wave propagation direction: from leader to follower. A main idea of plane wave eigenvectors is that they are eigenvectors of the shuffle-op r in (6.4). So each phasor is equally a leader over one side and a follower by the same lag of the other side. Whatever is taken gets passed on with no chance to swallow and get fatter! Thus all phasors in a **K**-matrix eigenvector stay the same area forever. Thus each $\Psi_m(x)$ is what we call a *stationary state* or *eigenstate* wave. Recall the mnemonic stated after (10.19) in Unit 1: *Imagination precedes reality by one quarter.* The imaginary wave (gray) precedes the real one by a *1/4*-wavelength. ImΨ is the "*gonna'be*" and ReΨ "*is*."

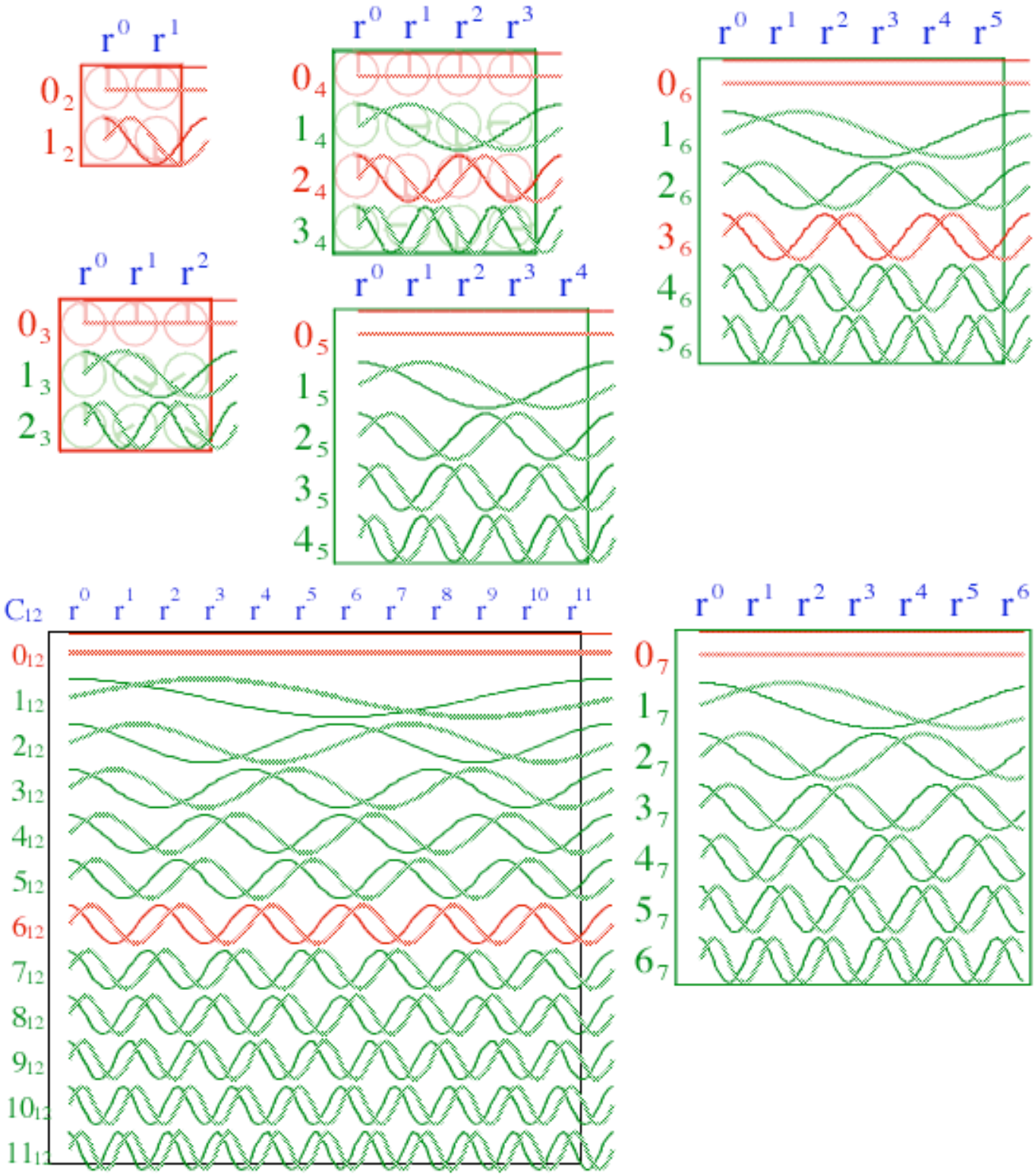

Fig. 6.4 Continuous "spirit" wavefunctions for N=2-7, and 12. NOTE:Gray Im Ψ is for Ψ <u>not</u> Ψ^*.

(d) Wave superposition

Suppose we add a $\Psi_{m=1}(x_p)$ wave to a $\Psi_{m=2}(x_p)$ wave of the same amplitude. The construction in Steps 1-5 of Fig. 6.5 does this phasor-by-phasor at time *t=0*, showing both their real and imaginary components. A vector sum is performed to obtain a resultant phasor at each of 12 points x_0, x_1, x_2, … x_{11}, where starting point is $x_0=x_{12}$. The algebraic sum is done by the expo-sine-cosine identities (4.10)

$$\Psi_{m=1}(x_p)+\Psi_{m'=2}(x_p)=e^{imp\frac{2\pi}{12}}+e^{im'p\frac{2\pi}{12}}=e^{ip\frac{m+m'}{2}\frac{\pi}{6}}\left(e^{ip\frac{m-m'}{2}\frac{\pi}{6}}+e^{-ip\frac{m-m'}{2}\frac{\pi}{6}}\right)=2e^{ip\frac{m+m'}{2}\frac{\pi}{6}}\cos p\frac{m-m'}{12}\pi$$

$$\Psi_{m=1}(x_p)+\Psi_{m'=2}(x_p)=e^{ip\frac{\pi}{6}}+e^{i2p\frac{\pi}{6}}=e^{ip\frac{1+2}{2}\frac{\pi}{6}}\left(e^{ip\frac{1-2}{2}\frac{\pi}{6}}+e^{-ip\frac{1-2}{2}\frac{\pi}{6}}\right)=2e^{ip\frac{\pi}{4}}\cos\frac{p\pi}{12} \qquad (6.9)$$

The overall phase factor $e^{ip\frac{\pi}{4}}=e^{i\frac{3}{2}p\frac{2\pi}{12}}$ turns 1.5 times while the envelope factor $\cos\frac{p\pi}{12}=\cos\frac{1}{2}\frac{p2\pi}{12}$ does half a turn in the space between *p=0* and *p=12*.

Fig. 6.5 reveals a beat that appears at first glance to be 100% complete, but the $\cos\frac{p\pi}{12}$ envelope is twisted π-out of phase at *p=12*, a kind of half-beat like the example in Fig. 4.8(a). The real wave *inside* the envelope does *1/2* phasor turn by *p=4*, which is *1/3* of the ring circumference from *p=0* to *p=12*. So it's doing *3/2* turns per *12* units, but the twist of the envelope makes that look like two *full* turns.

Wave phase velocity

Each wave-k_m phasor turns clockwise with time in *Step 6* according to its frequency ω_m.

$$\Psi_m(x_p,t)=\Psi_m(x_p,0)e^{-i\omega_m t}=e^{ik_m x_p}e^{-i\omega_m t}=e^{i(k_m x_p-\omega_m t)} \qquad (6.10a)$$

The wave appears to move. The point where phase $k_m x_p-\omega_m t=0$ moves at *phase velocity* V_{phase}.

$$V_{phase}(\text{1 plane wave})=\frac{x_p}{t}=\frac{\omega_m}{k_m} \qquad (6.10b)$$

Phase velocity is *time wink rate over spatial kink setting*, ω over k. The wink rate ω_m is given in terms of kink setting or *wavevector* $k_m=k_1 m$ by a dispersion function like (6.7). For low k_m, ω_m is linear: $\omega_m=C\cdot k_m$.

$$\omega_m=\sqrt{\frac{2k_{12}-2k_{12}\cos k_m}{M}}=2\sqrt{\frac{k_{12}}{M}}\sin\frac{k_m}{2}\approx Ck_m,\ \text{where: } C=V_{phase}=\sqrt{\frac{k_{12}}{M}}\ \text{for: } k_m=m\frac{2\pi}{N}<<1 \qquad (6.10c)$$

(Note: gravity *g* and $k=\frac{Mg}{\ell}$ are zero here.) Short waves, like dogs with short legs, must walk faster to keep up a speed *C*. If long wave-$k_{m=1}$ advances all its phasor by one tick, then twice-as-kinky and half-as-short wave-$k_{m=2}$ must do *two ticks* to keep up in *Step 6-8* of Fig. 6.5 and make the beat pattern move rigidly. Otherwise, wave patterns disperse as we'll see. That's why $\omega_m(k_m)$ is called a *dispersion* function.

Step-1 Construct 4 rows of 13 radius-2unit phasor circles with center-to-center distance of 5-units
(For sideways paper 5-units=1 inch. For normal vertical paper: 5-units=1/2 inch)

Label points p=0, 1, 2, 3, ...11, 12

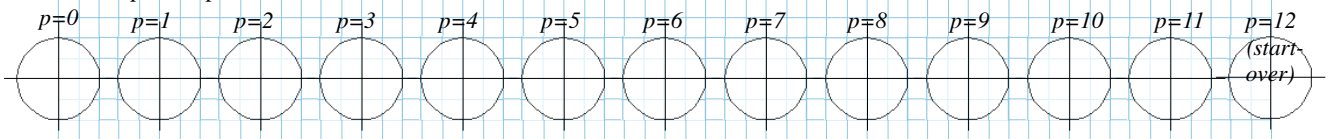

Step-2 Construct 12 equal time tics on first (p=0) and last (p=12). Connect them with light horizontal lines

Step-3 Construct and label the $m_{12}=1_{12}$ or k=1 wave by setting phasors back 1 hr. for each p to 0, -1, -2, -3, ...
(12, 11, 10, 9 ..)
Sketch real and imaginary "spirit" waves Re Ψ_m and Im Ψ_m

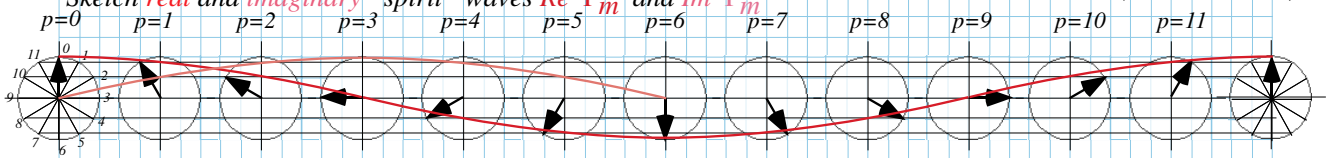

Step-4 Construct and label the $m_{12}=2_{12}$ or k=2 wave by setting phasors back 2 hr. for each p to 0, -2, -4, -6, ...
(12, 10, 8, 6 ..)
Sketch real and imaginary "spirit" waves Re Ψ_m and Im Ψ_m

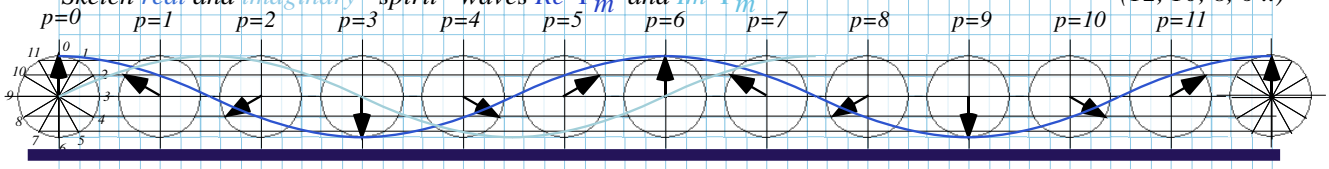

Step-5 Add phasors of k=1 wave to k=2 wave

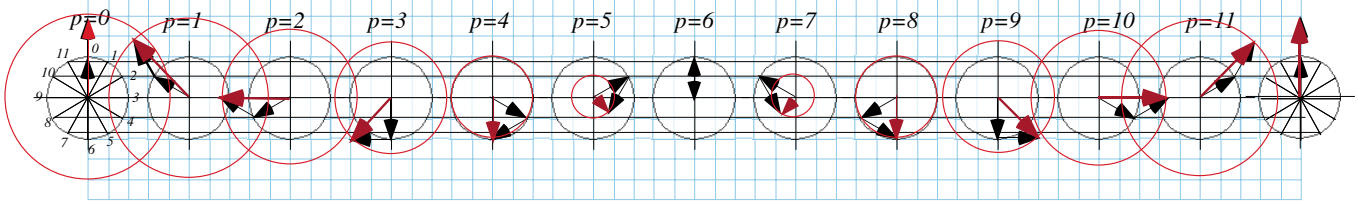

Step-6 Advanceall $m_{12}=1_{12}$ or k=1 phasors by 1 hr.
Sketch real and imaginary "spirit" waves Re Ψ_m and Im Ψ_m

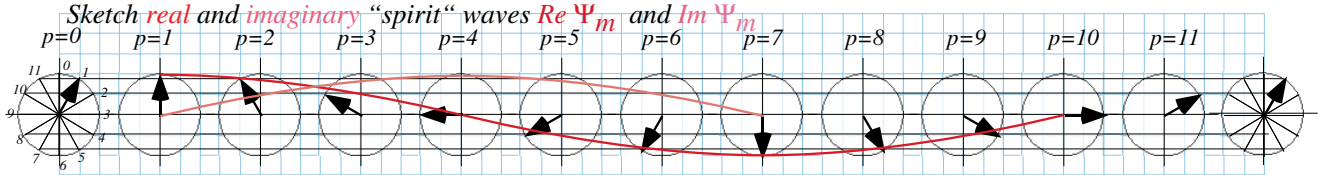

Step-7 Advance all $m_{12}=2_{12}$ or k=2 phasors by 2 hr.
Sketch real and imaginary "spirit" waves Re Ψ_m and Im Ψ_m

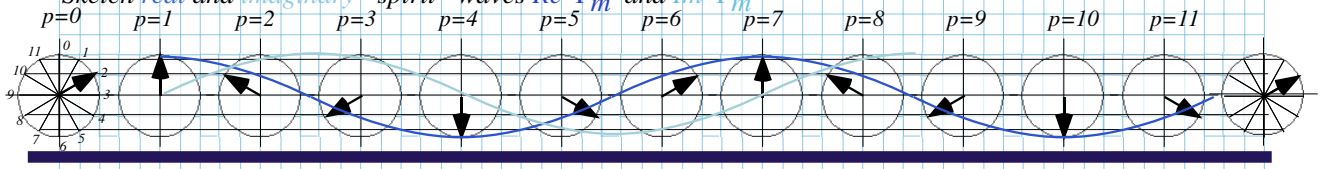

Step-8 Add phasors of k=1 wave to k=2 wave

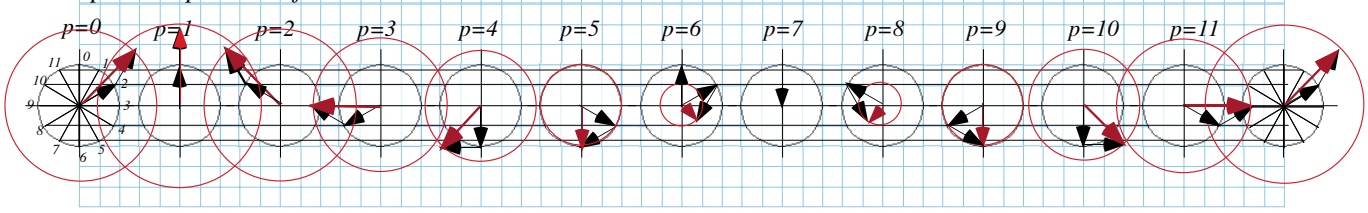

Fig. 6.5 Adding (m=1) and (m=2) waves. Step 1-5 is initial time t=0. Step 6-8 is later time t=1 tick.

Group velocity and mean phase velocity

A sum of two waves forms patterns that don't resemble either wave and the patterns may change or disperse over time. If an *m*-wave and *n*-wave have equal amplitude their sum is easy by (4.10e).

$$\Psi_{k_m}(x_p,t)+\Psi_{k_n}(x_p,t)=e^{i(k_m x_p-\omega_m t)}+e^{i(k_n x_p-\omega_n t)}=2e^{i\left(\frac{k_m+k_n}{2}x_p-\frac{\omega_m+\omega_n}{2}t\right)}\cos\left(\frac{k_m-k_n}{2}x_p-\frac{\omega_m-\omega_n}{2}t\right) \quad (6.11)$$

The sum wave has two velocities, one for the cosine envelope, and one for the exponential phase inside. Zeroing the *cos(.)* phase gives *exterior envelope velocity* $V_{envelope}$ or *group velocity* V_{group}.

$$\left(\frac{k_m-k_n}{2}x_p-\frac{\omega_m-\omega_n}{2}t\right)=0 \text{ implies: } x_p=\frac{\omega_m-\omega_n}{k_m-k_n}t \text{ or: } V_{envelope}=\frac{\omega_m-\omega_n}{k_m-k_n}=V_{group} \quad (6.12)$$

Zeroing the $e^{i(.)}$ phase gives an *interior wave velocity* $V_{interior}$ or *mean phase velocity* $V_{mean\ phase}$.

$$\left(\frac{k_m+k_n}{2}x_p-\frac{\omega_m+\omega_n}{2}t\right)=0 \text{ implies: } x_p=\frac{\omega_m+\omega_n}{k_m+k_n}t \text{ or: } V_{interior}=\frac{\omega_m+\omega_n}{k_m+k_n}=V_{mean\ phase} \quad (6.13)$$

A linear dispersion ($\omega_m = Ck_m$ as in Fig. 3.5) makes a sum wave move rigidly, that is, its interior and envelope wave go the same speed *C*. By (6.10c), individual wavespeed is C, too. ($\omega_m/k_m=C=const.$)

$$V_{interior}=\frac{Ck_m+Ck_n}{k_m+k_n}=C=\frac{Ck_m-Ck_n}{k_m-k_n}=V_{envelope} \text{ if: } \omega_m=Ck_m \text{ for all } m. \quad (6.14)$$

For nonlinear dispersion, speed $V_{interior}$ of a wave's "guts" differs from speed $V_{envelope}$ of its "skin." (Imagine a slithering boa constrictor swallowing live rabbits that continuously hop along inside it!)

Absolute square $|\Psi|^2=\Psi^*\Psi$ of equi-amplitude sum $\Psi=\psi_m+\psi_n$ (6.11) is just a cosine squared.

$$|\Psi|^2=\left|e^{i(k_m x_p-\omega_m t)}+e^{i(k_n x_p-\omega_n t)}\right|^2=\cos^2\left(\frac{k_m-k_n}{2}x_p-\frac{\omega_m-\omega_n}{2}t\right) \quad (6.15a)$$

The mean phase of $e^{i(.)}$ cancels ($e^{i(.)}*e^{i(.)}=e^{-i(.)}e^{i(.)}=1$) leaving envelope wave $|\Psi|=\sqrt{(\Psi^*\Psi)}$. Envelope $|\Psi|$ is more complicated for a sum of waves with unequal amplitudes ($A_m \neq A_n$). (Recall (4.12).)

$$|\Psi|=\sqrt{\Psi^*\Psi}=\sqrt{\left|A_m e^{i(k_m x_p-\omega_m t)}+A_n e^{i(k_n x_p-\omega_n t)}\right|^2}=\sqrt{|A_m|^2+|A_n|^2+2|A_m||A_n|\cos^2\left(\frac{k_m-k_n}{2}x_p-\frac{\omega_m-\omega_n}{2}t\right)} \quad (6.15b)$$

Both (6.15a) and (6.15b) have the same *cos(.)* and envelope velocity V_{group} but internal phase behavior is very different and "gallops" at a rate that depends on SWR (4.6). (The rabbits try to hop out of the boa!)

Fig. 6.6 plots archetypical dispersion functions $\omega(k_m)$. *Constant dispersion* ($\omega=K=Mg/l$) describes uncoupled ($k_{12}=0$) pendulums. Weak coupling but no gravity ($g=0$) is approximated by *linear dispersion* ($\omega_m=Ck_m$)(6.10c), and *quadratic dispersion* ($\omega_m=B+Ck_m^2$) approximates weak coupling with gravity for low wavevector $k_m<<\pi$. Next we will see how any *per-space-time* $\omega(k)$ dispersion graph is related to a *space-time* $x(t)$ graph of paths of wave peaks and zeros.

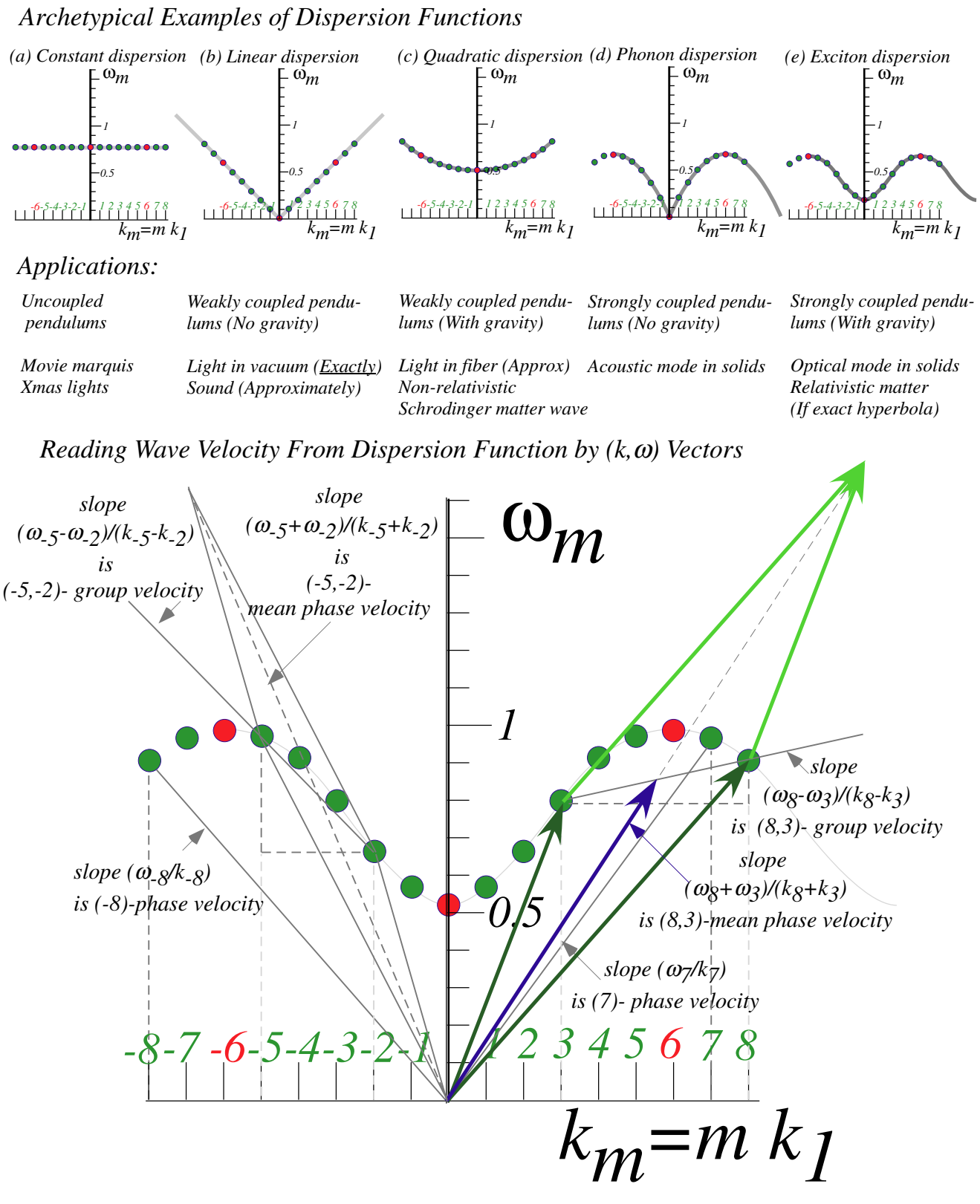

Fig. 6.6 Types of dispersion ω(k) functions and geometry of phase and group velocity.

Wave-zero (WZ) and pulse-peak (PP) space-time coordinate grids

Fig. 6.7 and 6.8 compare and superimpose time-*vs*-space *(x,t)*-plots of group and phase waves and their inverse *per-time-space* or *reciprocal space-time* plots of frequency-*vs*-wavevector *(ω,k)*.

The plots apply to all waves and not just to light. The example in Fig. 6.7 begins by picking four random numbers, say, *1,2,4,* and *4* to insert into frequency-wavevector $\mathbf{K}_2 = (\omega_2,k_2)=(1,2)$ of a mythical *source-2* and frequency-wavevector $\mathbf{K}_4 = (\omega_4,k_4)=(4,4)$ of another mythical *source-4*. Velocity $c_2=\omega_2/k_2 = 1/2$ of *source-2* and $c_4=\omega_4/k_4 = 1$ of *source-4* are unequal. For light waves in Fig. 6.8, c_2 equals c_4.

Let the continuous waves (CW) from the two sources interfere in a 2-CW sum.

$$\Psi^{2-CW} = (e^{i(k_4x-\omega_4t)} + e^{i(k_2x-\omega_2t)})/2 \tag{6.16a}$$

To solve for zeros of this sum we first factor it into a phase-wave e^{ip} and a group-wave *cos g* factor.

$$\begin{aligned}\Psi^{2-CW} &= e^{i\left(\frac{k_4+k_2}{2}x-\frac{\omega_4+\omega_2}{2}t\right)}\left(e^{i\left(\frac{k_4-k_2}{2}x-\frac{\omega_4-\omega_2}{2}t\right)} + e^{-i\left(\frac{k_4-k_2}{2}x-\frac{\omega_4-\omega_2}{2}t\right)}\right)/2 \\ &= e^{i(k_px-\omega_pt)}\cos\left(k_gx - \omega_gt\right) \equiv e^{ip}\cos g\end{aligned} \tag{6.16b)}$$

Phase factor e^{ip} uses the half-sum *(ω,k)*-vector $\mathbf{K}_{phase}=(\mathbf{K}_4+\mathbf{K}_2)/2$ in its argument $p = k_px - \omega_pt$. *Group factor cos g* has the half-difference *(ω,k)*-vector $\mathbf{K}_{group}=(\mathbf{K}_4-\mathbf{K}_2)/2$ in its argument $g = k_gx - \omega_gt$.

$$\mathbf{K}_{phase} = \frac{\mathbf{K}_4+\mathbf{K}_2}{2} = \frac{1}{2}\begin{pmatrix}\omega_4+\omega_2\\ k_4+k_2\end{pmatrix} = \begin{pmatrix}\omega_p\\ k_p\end{pmatrix} = \frac{1}{2}\begin{pmatrix}4+1\\ 4+2\end{pmatrix} = \begin{pmatrix}2.5\\ 3.0\end{pmatrix} \tag{6.16c}$$

$$\mathbf{K}_{group} = \frac{\mathbf{K}_4-\mathbf{K}_2}{2} = \frac{1}{2}\begin{pmatrix}\omega_4-\omega_2\\ k_4-k_2\end{pmatrix} = \begin{pmatrix}\omega_g\\ k_g\end{pmatrix} = \frac{1}{2}\begin{pmatrix}4-1\\ 4-2\end{pmatrix} = \begin{pmatrix}1.5\\ 1.0\end{pmatrix} \tag{6.16d}$$

The *(ω,k)*-vectors $\mathbf{K}_n$ define paths and coordinate lattices for pulse peaks and wave zeros in Fig. 6.7a.

Real zeros ($\mathrm{Re}\Psi=0$) have velocity V_{phase} on $\mathbf{K}_{phase}$ paths. Group zeros ($|\Psi|=0$) move at V_{group} on $\mathbf{K}_{group}$.

$$V_{phase} = \frac{\omega_p}{k_p} = \frac{\omega_4+\omega_2}{k_4+k_2} = \frac{2.5}{3.0} = 0.83 \tag{6.17a}$$

$$V_{group} = \frac{\omega_g}{k_g} = \frac{\omega_4-\omega_2}{k_4-k_2} = \frac{1.5}{1.0} = 1.5 \tag{6.17b}$$

Zeros of phase factor real part $\mathrm{Re}\,e^{ip} = \mathrm{Re}\,e^{i(k_px-\omega_pt)} = \cos p$ lie on *phase-zero paths* where angle *p* is *N(odd)·π/2*.

$$k_px - \omega_pt = p = N_p\pi/2 \quad (N_p = \pm1,\pm3...).$$

Zeros of group amp-factor $\cos g = \cos(k_gx - \omega_gt)$ lie on *group-zero* or *nodal paths* where angle *g* is *N(odd)·π/2*.

$$k_gx - \omega_gt = g = N_g\pi/2 \quad (N_g = \pm1,\pm3...).$$

Both factors are zero at *wave zero (WZ) lattice points (x,t)*. This defines the lattice vectors in Fig. 6.7a.

$$\begin{pmatrix}k_p & -\omega_p\\ k_g & -\omega_g\end{pmatrix}\begin{pmatrix}x\\ t\end{pmatrix} = \begin{pmatrix}p\\ g\end{pmatrix} = \begin{pmatrix}N_p\\ N_g\end{pmatrix}\frac{\pi}{2} \tag{6.18a}$$

Solving gives *spacetime (x,t)* zero-path lattice that are white lines in Fig. 6.7a. Each lattice intersection point is an odd-integer (N_p, N_g) combination of wave-vectors $\mathbf{P} = \pi \mathbf{K}_{phase} / 2D$ and $\mathbf{G} = \pi \mathbf{K}_{group} / 2D$.

$$\begin{pmatrix} x \\ t \end{pmatrix} = \frac{\begin{pmatrix} -\omega_g & \omega_p \\ -k_g & k_p \end{pmatrix}\begin{pmatrix} p \\ g \end{pmatrix}}{\omega_p k_g - \omega_g k_p} = \frac{-p\begin{pmatrix} \omega_g \\ k_g \end{pmatrix} + g\begin{pmatrix} \omega_p \\ k_p \end{pmatrix}}{\omega_p k_g - \omega_g k_p} = \frac{\pi}{2D}(-N_p \mathbf{K}_{group} + N_g \mathbf{K}_{phase}) \qquad (6.18b)$$

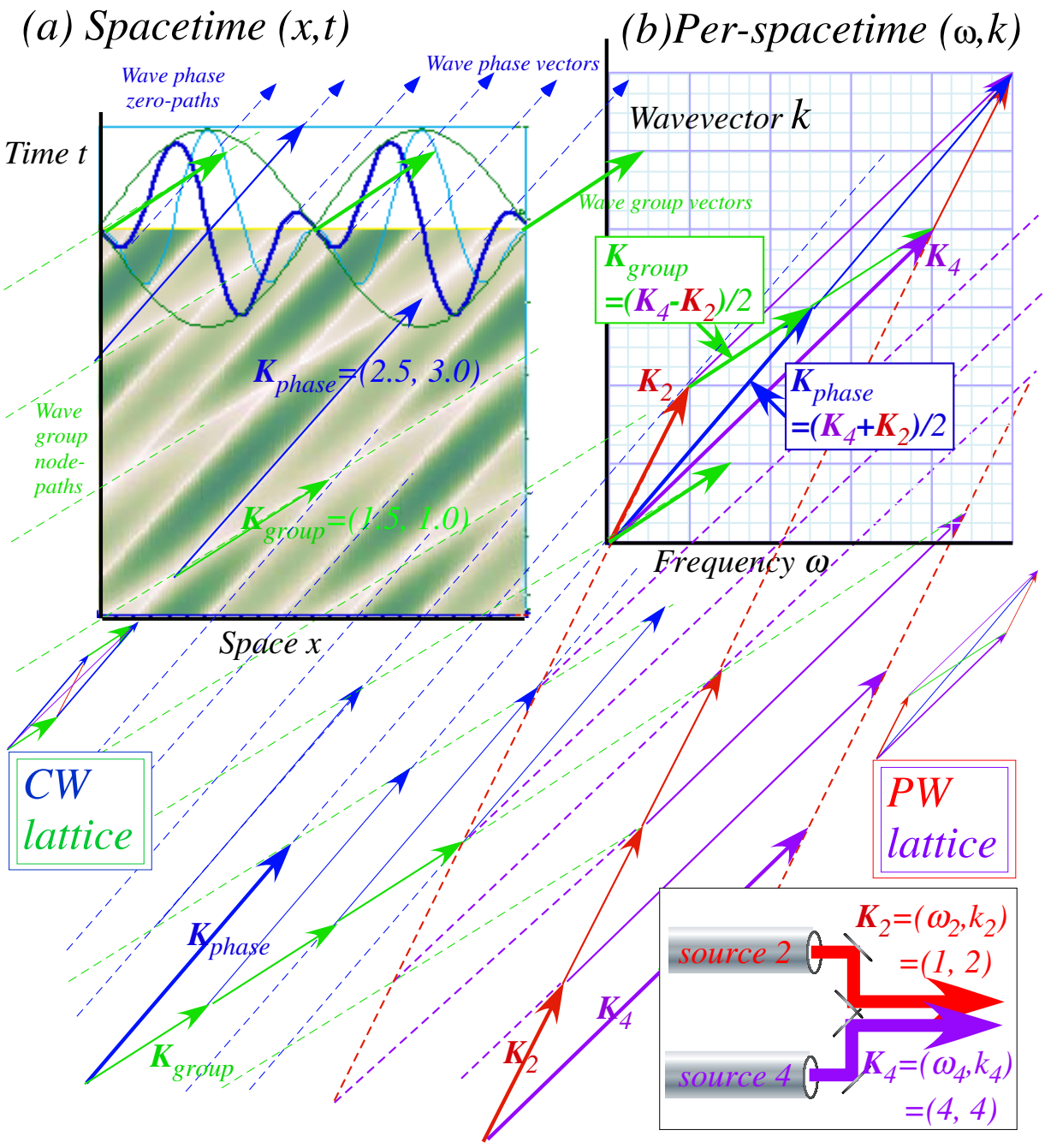

Fig. 6.7 "Mythical" sources and their wave coordinate lattices in (a) Spacetime and (b) Per-spacetime.

CW lattices of phase-zero and group-node paths intermesh with PW lattices of pulse, packet, or "particle" paths.

Scaling factor $2D/\pi = 2(\omega_p k_g - \omega_g k_p)/\pi$ converts *(per-time, per-space)* vectors $\mathbf{K}_{group}$ or $\mathbf{K}_{phase}$ into *(space, time)* vectors $\mathbf{P} = \binom{x}{t}_p$ or $\mathbf{G} = \binom{x}{t}_g$. (Plot units are set so $2D/\pi = 1$ or $D = \pi/2$. *This works only if D* is *non*-zero.)

Fig. 6.7b is a lattice of source vectors $\mathbf{K}_2$ and $\mathbf{K}_4$ (the difference and sum of $\mathbf{K}_{group}$ and $\mathbf{K}_{phase}$).

$$\mathbf{K}_2 = \mathbf{K}_{phase} - \mathbf{K}_{group} = \begin{pmatrix} \omega_2 \\ k_2 \end{pmatrix} = \begin{pmatrix} 1 \\ 2 \end{pmatrix} \qquad (6.19a)$$

$$\mathbf{K}_4 = \mathbf{K}_{phase} + \mathbf{K}_{group} = \begin{pmatrix} \omega_4 \\ k_4 \end{pmatrix} = \begin{pmatrix} 4 \\ 4 \end{pmatrix} \qquad (6.19b)$$

Source-2 has phase speed c_2 on $\mathbf{K}_2$ paths of slope c_2. Source-4 has speed c_4 on $\mathbf{K}_4$ paths of slope c_4.

$$c_2 = \frac{\omega_2}{k_2} = \frac{1}{2} = 0.5 \qquad (6.20a)$$

$$c_4 = \frac{\omega_4}{k_4} = \frac{1}{1} = 1.0 \qquad (6.20b)$$

One may view the $\mathbf{K}_2$ and $\mathbf{K}_4$ paths from a classical or semi-classical viewpoint if pulse waves (PW) were wave packets (WP) that mimic particles. Newton took a hard-line view of nature and ascribed reality to "corpuscles" but viewed waves as illusory. He misunderstood light if it exhibited interference phenomena and complained that its particles or "corpuscles" were having "fits."

Newtonian corpuscular views are parodied here by imagining that frequency $\upsilon_2 = \omega_2/2\pi$ (or $\upsilon_4 = \omega_4/2\pi$) is the rate at which source-2 (or 4) emits "corpuscles" of velocity c_2 (or c_4). Then the wavelengths $\lambda_2 = 2\pi/k_2$ (or $\lambda_4 = 2\pi/k_4$) are just inter-particle spacing of $\mathbf{K}_2$ (or $\mathbf{K}_4$) lines in Fig. 6.7a. Since wavelength λ_2 (λ_4) separates $\mathbf{K}_2$ ($\mathbf{K}_4$) lattice lines in Fig. 6.7b, one can imagine them as "corpuscle paths." The paths are *diagonals* of the $\mathbf{K}_{group}$($\mathbf{K}_{phase}$) wave-zero lattice in time *vs* space *(x,t)* of Fig. 6.7a.

This development shows wave-particle, wave-pulse, and CW-PW duality in the cells of each CW-PW wave lattice. Each ($\mathbf{K}_2$,$\mathbf{K}_4$)-cell of a PW lattice has a CW vector *2***P** or *2***G** on each diagonal, and each (**P**,**G**)-cell of the CW lattice has a PW vector $\mathbf{K}_2$ or $\mathbf{K}_4$ on each diagonal. This is due to sum and difference relations (6.16d) or (6.19b) between (**P**,**G**)=($\mathbf{K}_{phase}$, $\mathbf{K}_{group}$) and ($\mathbf{K}_2$, $\mathbf{K}_4$).

In order that space-time *(x,t)*-plots can be superimposed on frequency-wavevector *(ω,k)*-plots or *(υ,κ)*-plots, it is necessary to switch axes for one of them. The space-time *t(x)*-plots in Fig. 6.7a follow the convention adopted by most relativity literature for a vertical time ordinate *(t-axis)* and horizontal space abscissa *(x-axis)* that is quite the opposite of Newtonian calculus texts that plot *x(t)* horizontally. However, the frequency-wavevector *k(ω)*-plots in Fig. 6.7b switch axes from the usual *ω(k)* convention so that *t(x)* slope due to space-time velocity *x/t* or *Δx/Δt (meter/second)* in Fig. 6.7a matches that of equal per-time-per-space wave velocity *ω/k* or *Δω/Δk (per-second/per-meter)* in Fig.6.7b.

Superimposing *t(x)*-plots onto *k(ω)*-plots also requires that the latter be rescaled by the scale factor $\pi/2D$ derived in (6.18b), but rescaling fails if cell-area determinant factor *D* is zero.

$$D = \omega_p k_g - \omega_g k_p = \left|\mathbf{K}_{phase} \times \mathbf{K}_{group}\right| \qquad (6.21)$$

Co-propagating light beams $\mathbf{K}_2 = (\omega_2,k_2)=(2c,2)$ and $\mathbf{K}_4 = (\omega_4,k_4)=(4c,4)$ in Fig. 6.8b have $D=0$ since all K-vectors including $\mathbf{K}_{phase}=(\omega_p,k_p)=(3c,3)$ and $\mathbf{K}_{group} = (\omega_g,k_g)=(c,1)$ lie on one c-baseline of speed c that has unit slope $(\omega/ck=1)$ if we rescale (ω,k)-plots to (ω,ck) and (x,t)-plots to (x,ct).

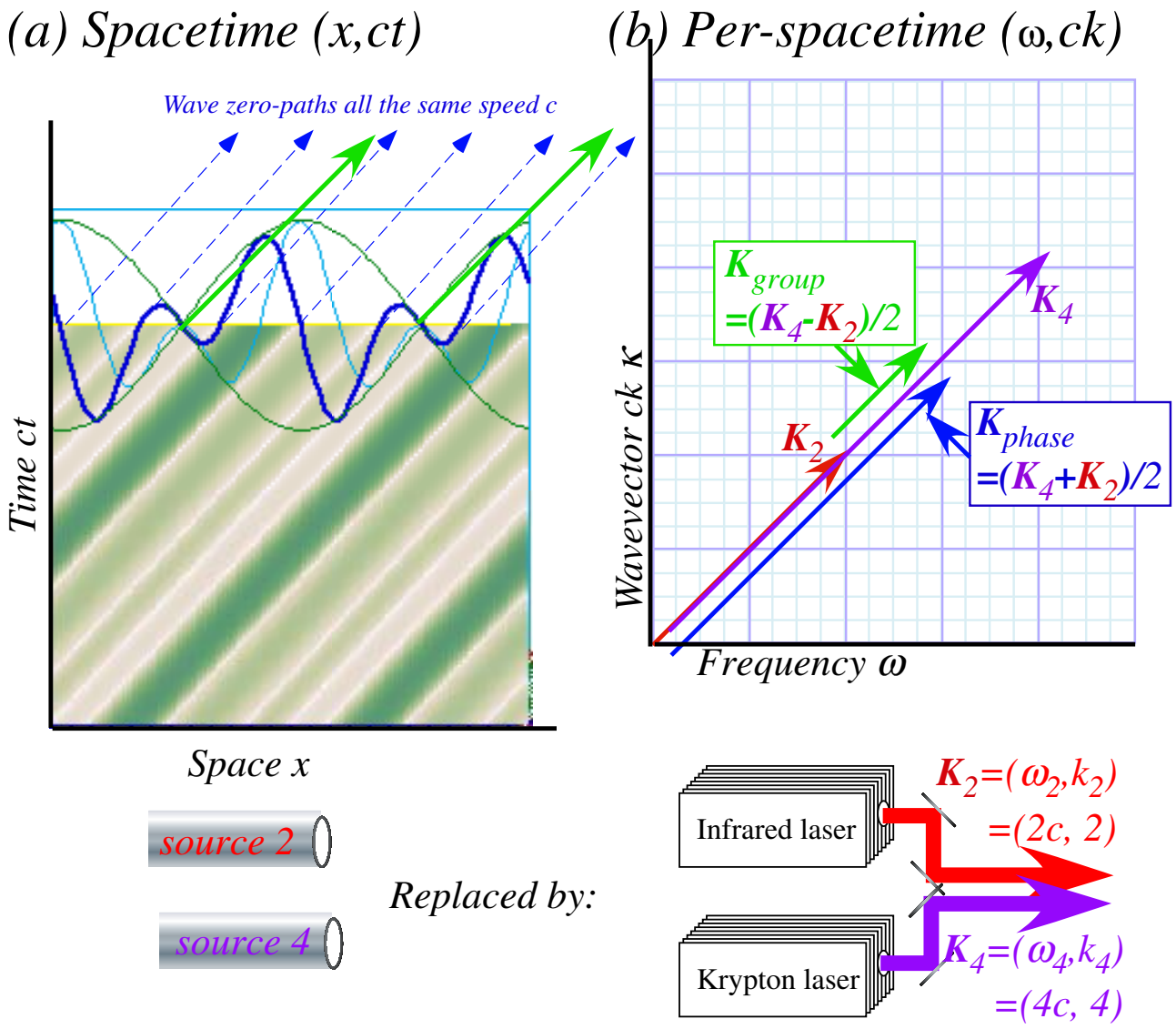

Fig. 6.8 Co-propagating laser beams produce a collapsed wave lattice since all parts have same speed c.

In Unit 3 *counter-propagating* (right-left) light wave vectors $(\mathbf{R},\mathbf{L})= (\mathbf{K}_2,-\mathbf{K}_4)$ are used to make CW bases ($\mathbf{P}= \mathbf{K}_{phase}$, $\mathbf{G}= \mathbf{K}_{group}$) with a non-zero value for area $D =|\mathbf{G}\times\mathbf{P}|$. Opposing PW base vectors are sum and difference $(\mathbf{R},\mathbf{L})=(\mathbf{P}+\mathbf{G},\mathbf{P}-\mathbf{G})$ of CW bases so a PW cell area $|\mathbf{R}\times\mathbf{L}|$ is twice that of CW cell $|\mathbf{G}\times\mathbf{P}|$.

$$|\mathbf{R}\times\mathbf{L}| = |(\mathbf{P}+\mathbf{G})\times(\mathbf{P}-\mathbf{G})| = 2|\mathbf{G}\times\mathbf{P}| \qquad (6.22)$$

Wave cell areas are key geometric invariants for relativity and quantum mechanics.

(e) Counter-propagation: Standing and galloping waves

Counter-propagating light waves include *standing waves* (Fig. 6.9) or *galloping waves* (Fig. 6.10). The latter are the rule rather than the exception. You get galloping unless you turn off one of the lasers! Turning off the right laser gives a pure *right-moving wave* $e^{i(kx-\omega t)}$ that traces *45°* wave zero lines going at a constant lightspeed *c* as shown in the space-time plot of Fig. 6.10(a). Turning on even a small amount of *left-moving wave* $e^{i(-kx-\omega t)}$ results in galloping paths as shown in Fig. 6.10(b-e). The real wave $Re\Psi$ gallops faster than light once each half-cycle as it leap-frogs a similarly galloping $Im\Psi$.

As the relative amount of left moving wave increases, galloping becomes more pronounced, and then, for *exactly* equal left and right amplitudes, the zeros of the real standing wave gallop *infinitely fast* at each moment $Re\Psi$ is zero everywhere. (Being everywhere is tantamount to going infinitely fast.) This is the special case that gives a Cartesian *(x,ct)* grid shown in Fig. 6.9. Finally, for dominant left-moving amplitudes, the galloping reverses sign and then subsides as in Fig. 6.10(e-f).

Counter-propagating laser waves in Fig. 6.10 have the following wave zeros of $Re\Psi$.

$$0 = \mathrm{Re}\,\Psi(x,t) = \mathrm{Re}\left[A_{\rightarrow}e^{i(k_0x-\omega_0t)} + A_{\leftarrow}e^{i(-k_0x-\omega_0t)}\right]$$
$$= A_{\rightarrow}\left[\cos k_0x\ \cos\omega_0t + \sin k_0x\ \sin\omega_0t\right] + A_{\leftarrow}\left[\cos k_0x\ \cos\omega_0t - \sin k_0x\ \sin\omega_0t\right]$$
$$= \left(A_{\rightarrow} + A_{\leftarrow}\right)\left[\cos k_0x\ \cos\omega_0t\right] + \left(A_{\rightarrow} - A_{\leftarrow}\right)\left[\sin k_0x\ \sin\omega_0t\right]$$

Galloping varies according to a *Standing Wave Quotient SWQ* or its inverse *Standing Wave Ratio SWR*.

$$\tan k_0x = -SWQ\cdot\cot\omega_0t \quad (6.23a) \text{ where: } SWQ = \frac{A_{\rightarrow}+A_{\leftarrow}}{A_{\rightarrow}-A_{\leftarrow}} = \frac{1}{SWR} \qquad (6.23b)$$

The time derivative gives upper and lower speed limits in terms of $V_{phase} = \frac{\omega_0}{k_0} = c$ and *SWQ* or *SWR*.

$$\frac{dx}{dt} = c\cdot SWQ\frac{\csc^2\omega_0t}{\sec^2 k_0x} = \frac{c\cdot SWQ}{\cos^2\omega_0t + SWQ^2\cdot\sin^2\omega_0t} = \begin{cases} c\cdot SWQ & \text{for: } t = 0,\ \pi,\ 2\pi\ldots \\ c\cdot SWR & t = \pi/2,\ 3\pi/2,\ldots \end{cases} \qquad (6.23c)$$

These are seen in Fig. 6.10, but the fastest gallop is ±∞ as seen for a "standing" wave in Fig. 6.9.

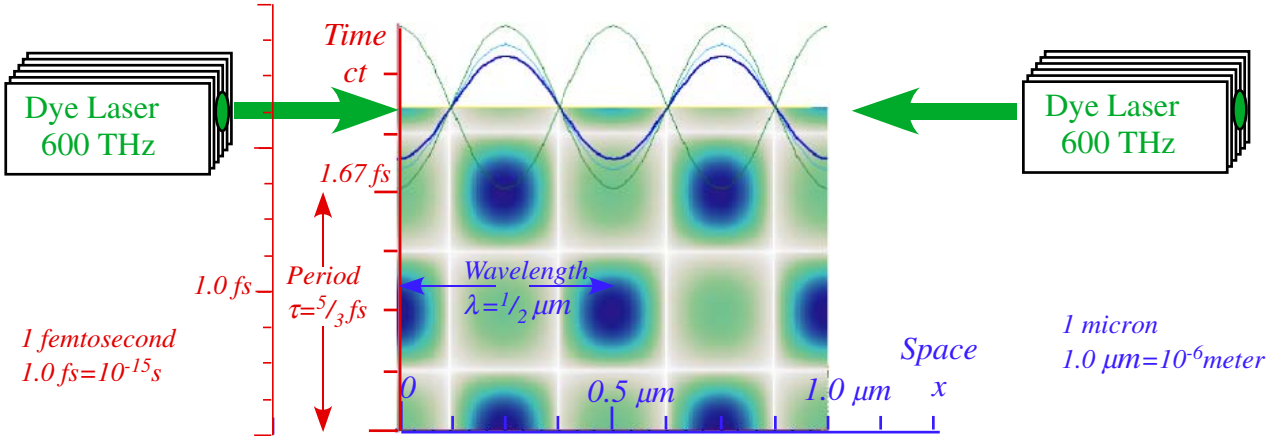

Fig. 6.9 Standing wave (SWR=0) due to counter-propagating 600Thz (green) laser waves.

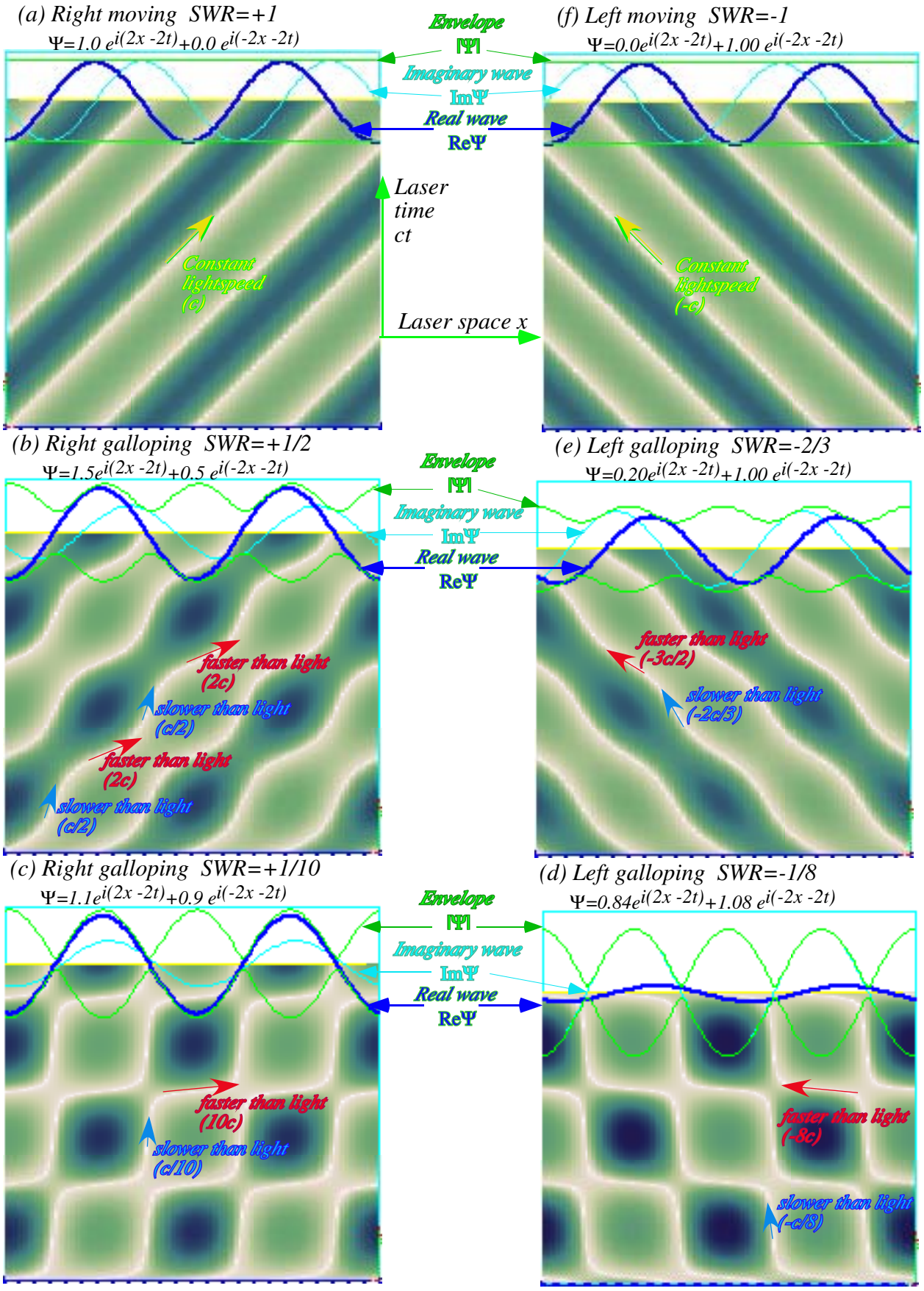

Fig. 6.10 Spacetime plots of monochromatic waves of varying Standing Wave Ratio.

Kepler's Law for galloping

Galloping wave velocity (6.23c) is related to Kepler's Law for isotropic force field orbits, such as in a 2D oscillator orbit constructed by Fig. 6.11 or Fig. 2.1. (Recall Fig. 1.9 in Unit 1.) Clockwise polar angle $\phi(t)$ of ellipse-orbiting point $P=(x=a\sin\omega t, y=a\cos\omega t)$ and orbital phase ωt, relate as follows.

$$\tan\phi(t)=\frac{y}{x}=-\frac{b}{a}\cdot\cot\omega t\,. \qquad (6.24)$$

This resembles the galloping wave equation (6.23a) with the ellipse aspect ratio b/a replacing a standing wave ratio. To conserve orbital angular momentum **rxv** in the absence of torque, the orbital velocity $v(r)$ gallops to a faster $v(b)$ at perigee $(r=b)$ and a slower $v(a)$ at apogee $(r=a)$. In the same way waves in Fig. 6.10 gallop faster through smaller parts of their envelope and slow down as their amplitudes grow.

Analogy of laser wave dynamics (6.23) to classical orbital mechanics (6.24) has physical as well as historical use. Wave galloping shown in Fig. 6.10 happens equally in systems with open or infinite boundaries as it does in closed or periodic (ring laser or Bohr-ring) systems. In fact, Fig. 6.11 are pictures of 2nd lowest $(k_m=\pm 2)$-modes of a micro-ring-laser or the 2nd excited Schrodinger $(m=\pm 2)$-waves on a Bohr-ring. Exactly two wavelengths fit in each space frame and two periods fit in each time frame.

Analogy with polarization ellipsometry

If a frame in Fig. 6.10 were drawn instead for 1st or fundamental $(m=\pm 1)$-waves or $(k_m=\pm 1)$-modes of either ring system it would just be a *1/4*-area square section with only one sine wave per frame. (Recall Fig. 3.1.1(c).) Such a wave has an average dipole moment $\mathbf{p}=\langle p\rangle$ that orbits an ellipse like radius **r** in Fig. 6.11 and is analogous to a polarization figures used to depict states in optical ellipsometry.

In the polarization analogy, purely right-moving $(m=+1)$ or purely left-moving $(m=-1)$ wave states e^{+ikx} and e^{-ikx} are analogous, respectively, to right or left circular polarization states. Equal combinations $e^{+ikx}+e^{-ikx}=2\cos kx$ or $e^{+ikx}-e^{-ikx}=2i\sin kx$ are analogous, respectively, to *x*-plane or *y*-plane polarization. The vast majority of arbitrary combinations $ae^{+ikx}+be^{-ikx}$ are analogous to general elliptical polarization. A polarization vector for elliptic states enjoys the same Kepler galloping described by Fig. 6.11.

Perhaps the simplest explanation of wave galloping in Fig. 6.10 uses an analogy with the elliptical polarization states as in Fig. 6.12. The uniformly spaced ticks on the circular polarization circles are crowded into a traffic jam at the long axes of their elliptic orbits as the aspect ratio *b/a* or *SWR* approaches zero. The ticks near the short axes maintain their spacing in the Kepler geometry. Like a uniformly turning lighthouse beacon viewed edge-on, the beam is seen to gallop by quickly and then slow to a crawl as it swings perpendicular to the line of sight.

An animated simulation of Fig. 6.11 provides an optical illusion of a uniformly rotating circular disc tipped out of the XY plane by an angle of $\sin^{-1}(b/a)$, that is, a perspective projection.

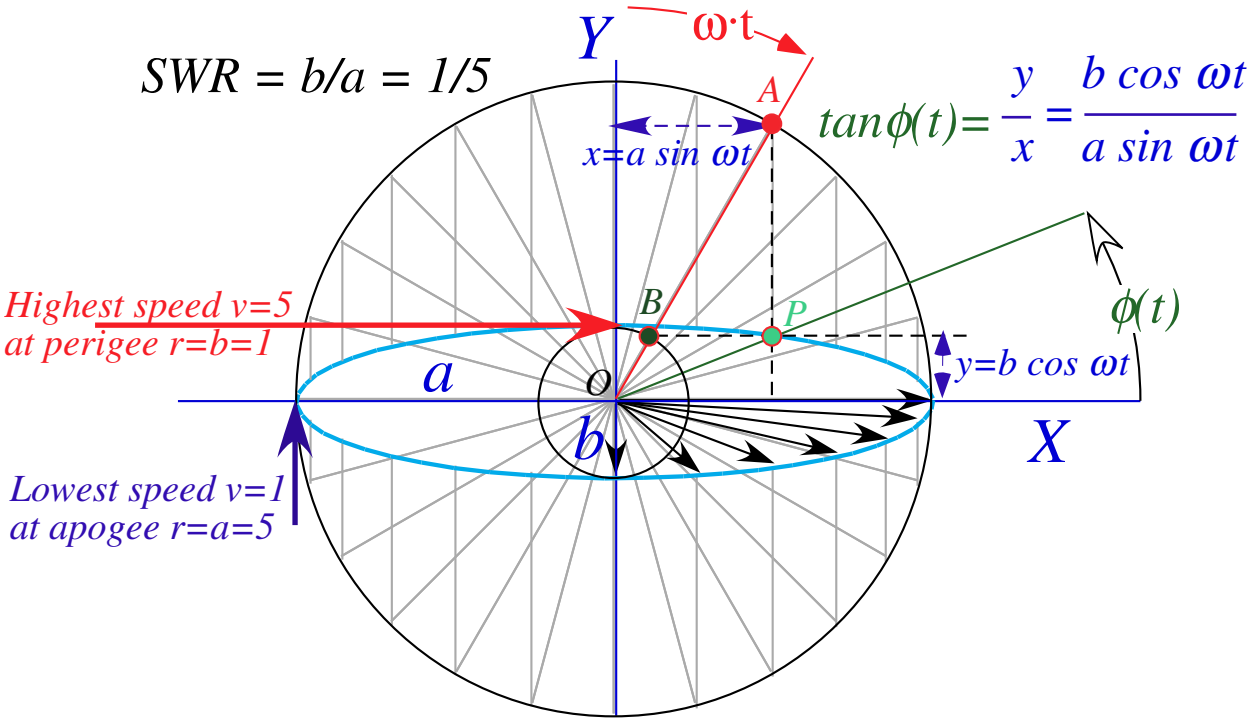

Fig. 6.11 Elliptical oscillator orbit and a Kepler construction

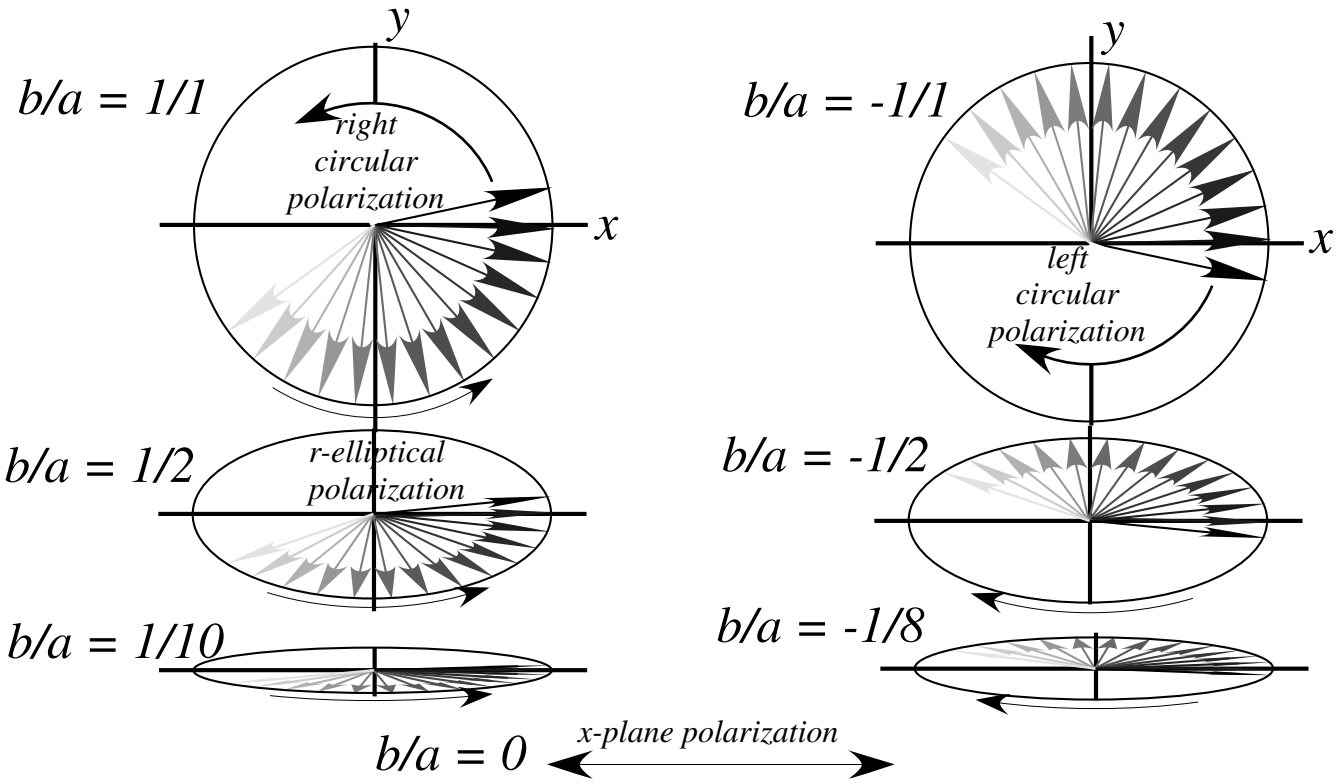

Fig. 6.12 Elliptical polarization states of varying aspect ratio a/b or standing wave ratio SWR. This figure is analogous to Fig. 6.10 according to the Keplerian geometry of Fig. 6.11.

(e) Taming the phase: Wavepackets and pulse trains

In each of Fig. 6.9 or Fig. 6.10 real wave $\mathrm{Re}\Psi(x,t)$ is plotted in spacetime. If the intensity $\Psi^*\Psi$ or envelope $|\Psi|$ is plotted, the part of the wave having the fast and wild phase velocity disappears leaving only its envelope moving constantly at the slow and tame group velocity.

For example, the complicated dynamics of the *(SWR=-1/8)* galloping in Fig. 6.10(d) is reduced to parallel grooves by a $|\Psi|$-plot in Fig. 6.13(a). The grooves follow the group envelope motion that has only a steady group velocity. The lower part of Fig. 6.10 is thus tamed. Pure plane wave states Fig. 6.10 (a) and Fig. 6.10 (f) are tamed even more in a $|\Psi|$-plot to become featureless and flat like their envelopes.

One gets a glimpse of phase behavior in an envelope or $\Phi^*\Phi$ plot by adding the lowest scalar DC fundamental *(m=0)*-wave $\Psi_{0=1}$ to a galloping combination wave such as $\Psi = a\,\Psi_{+4} + b\,\Psi_{-1}$. The result

$$\begin{aligned}\Phi^*\Phi &= \left(1 + a\Psi_{+4} + b\Psi_{-1}\right)^* \left(1 + a\Psi_{+4} + b\Psi_{-1}\right) = \left(1 + a\Psi_{+4} + b\Psi_{-1} + a^*\Psi_{+4}^* + b^*\Psi_{-1}^* + \Psi^*\Psi\right) \\ &= 1 + 2\,\mathrm{Re}\Psi + \Psi^*\Psi\end{aligned} \tag{6.25}$$

is plotted in the upper part of Fig. 6.13(b). The DC bias keeps the phase part from canceling itself, and the probability distribution shows signs of, at least half-heartedly, following the fast phase motion of the $\mathrm{Re}\Psi$ wave plotted underneath it. (Dashed lines showing phase and group paths are superimposed on $\Phi^*\Phi$.)

Indeed, (6.25) shows that if the *(1+Ψ*Ψ)* background could be subtracted, then the real wave $\mathrm{Re}\Psi$ plots of Fig. 6.13 would emerge double-strength! However, such a subtraction, while easy for the theorist, is more problematic for the experimentalist. More often one must be content with results more like the upper than the lower portions of Fig. 6.13. It's a bit like watching an orgy going on under a thick rug.

However, such censorship can be a welcome feature. As more participating Fourier components enter the fray, a simpler view can help to sort out important effects that might otherwise be hidden in the milieu. We consider examples of this with regard to sharper wavepackets such as pulse trains and Gaussian wavepackets.

Continuous Wave (CW) versus Optical Pulse Trains (OPT): colorful versus colorless

Optical pulse train (OPT) waves are Fourier series of *N* continuous wave (CW) ω_1-harmonics.

$$\begin{aligned}\Phi_N(x,t) &= 1 + e^{i(k_1x-\omega_1t)} + e^{i(-k_1x-\omega_1t)} + e^{i(k_2x-\omega_2t)} + e^{i(-k_2x-\omega_2t)} + \ldots + e^{i(k_Nx-\omega_Nt)} + e^{i(-k_Nx-\omega_Nt)} \\ &= 1 + \quad 2e^{-i\omega_1t}\cos k_1x \quad + \quad 2e^{-i\omega_2t}\cos k_2x \quad + \ldots + \quad 2e^{-i\omega_Nt}\cos k_Nx\end{aligned} \tag{6.26a}$$

The fundamental OPT or *(N=0-1)* beat wave in Fig. 6.14(b) is a rest-frame view of Fig. 6.13(b)

$$\Phi_1(x,t) = 1 + \quad 2e^{-i\omega_1t}\cos k_1x \tag{6.26b}$$

Φ_1 should be compared to the pure or unbiased fundamental *(m=±1)*-standing wave Ψ_1 in Fig. 6.14(a).

$$\Psi_1(x,t) = 2e^{-i\omega_1t}\cos k_1x \tag{6.26c}$$

The real part Re Ψ_1 is discussed in connection with the Cartesian spacetime wave grid in Fig. 3.2.3(a). The modulus $|\Psi_1|$, unlike $|\Phi_1|$, is constant in time as indicated by the vertical time-grooves at the extreme upper right of Fig. 6.14(a). In contrast, the magnitude $|\Phi_1|$ of the DC-biased beat wave makes an "H" or "X" in its spacetime plot of Fig. 6.14(b) thereby showing the beats. The width of the fundamental *(0-1)* beat is one fundamental wavelength $\Delta x=2\pi/k_0$ of space and one fundamental period $\Delta t=2\pi/\omega_0$ of time.

Including *N=2,3,…* terms in (6.26) reduces the pulse width by a factor of *1/N* as seen in Fig. 6.14 (c-e) below. The spatial $^{\sin N x}/_{x}$ wave shape is the same as is had by adding *N=2,3,…* slits to an elementary optical diffraction experiment. Adding more frequency harmonics makes the pulse narrower in time, as well as space. Using *12* terms with *11* harmonics reduces the pulse width to *1/11* of a fundamental period. A pico-period pulse would have a trillion harmonics!

Reducing pulse width or spatial uncertainty Δx and temporal duration Δt of each pulse requires increased wavevector and frequency bandwidth Δk and $\Delta\omega$. The widths obey Heisenberg relations $\Delta x\Delta k\sim 2\pi$ or $\Delta t\Delta\omega\sim 2\pi$. The sharper the pulses the more white or colorless they become. Finally, the spacetime plots will simplify to simple equilateral diamonds or *45*°-tipped squares shown in the *N=11* plots of Fig. 6.14(e). (They resemble the sketched pulse paths of Fig. 6.7(b).)

As *N* increases there is much less distinction between the Re Φ and $|\Phi|$ plots than there is for the cases of *N=1,2,* or *3* shown in the preceding plots of Fig. 6.14(a-d). However, as in Fig. 6.13, there is a considerable distinction between Re Φ and $|\Phi|$ plots with all Re Φ plots being sharper than $|\Phi|$ plots in all cases including the high-*N* cases. Having phase information increases precision particularly for low *N*.

The sharpest set of zeros, somewhat paradoxically, are found in the *N=1* case of Fig. 6.14(a) and for the unbiased Re Ψ plot of the Cartesian wave grid. However, plotting zeros by graphics shading is one thing. Finding experimental phase zeros using $\Psi^*\Psi$ or $|\Psi|$ *squared*, is quite another thing.

A close look at the center of the Re Φ plot for N=11 in Fig. 6.14(e) reveals a tiny Cartesian spacetime grid. It is surrounded by "gallop-scallops" similar to the faster-and-slower-than-light paths shown in Fig. 6.7. It is due to the interference of counter-propagating ringing wavelets that surround each counter propagating $^{\sin N x}/_{x}$ –pulse. In contrast the $|\Phi|$ plots for which the ringing leaves only vertical grooves like those that occupy the entire *N=1* plot of $|\Psi|$ in Fig. 6.14(a).

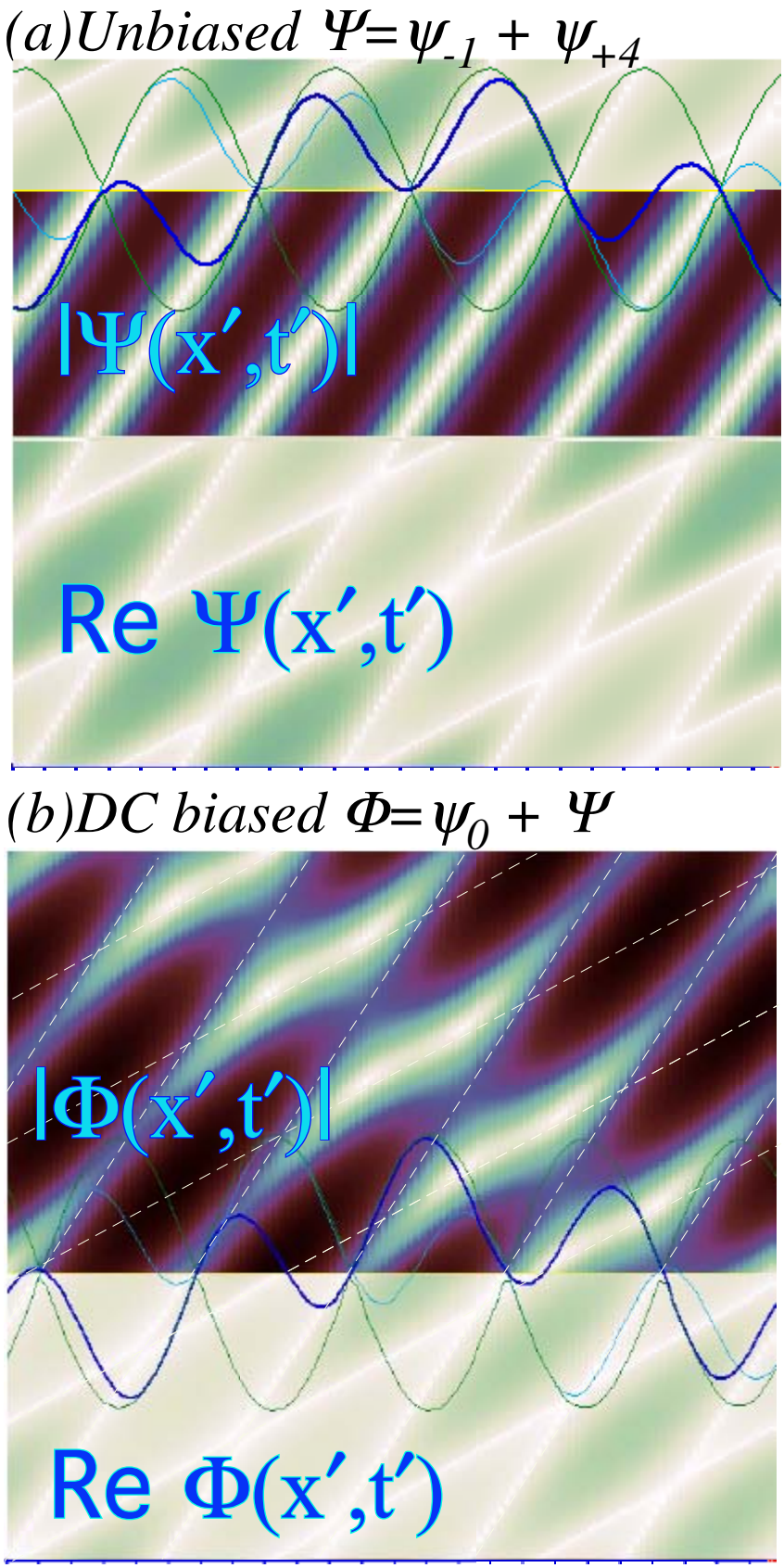

Fig. 6.13 Examples of group envelope plots of galloping waves (a) Unbiased. (b) DC biased.

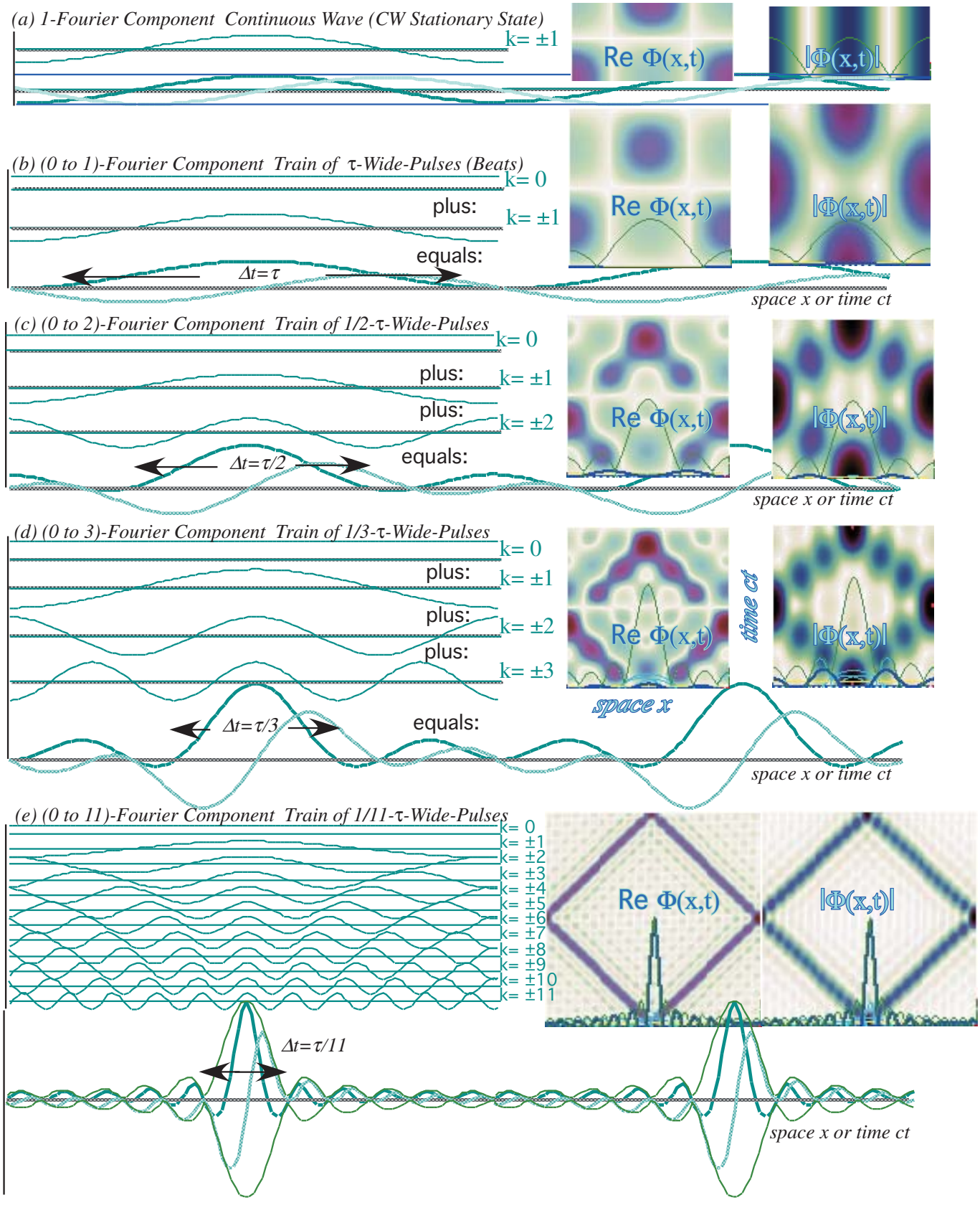

Fig. 6.14 Optical Pulse Trains (OPT) and Continuous Wave (CW) Fourier components

Wave ringing: m_{Max}-term cutofft effects

An analysis of wave pulse ringing reveals it may be blamed on the last Fourier component added. There are *11* zeros in the ringing wave envelope in Fig. 6.14(e), the same number as in the 11^{th} and last Fourier component. An integral over $k = m2\pi/N$ approximatea a Fourier sum $S(m_{Max})$ up to a maximum $m_{Max}=11$. The unit sum interval $\Delta m=1$ is replaced by a smaller *k*-differential *dk* multiplied by $\frac{\Delta m}{dk} = \frac{N}{2\pi}$.

$$S(m_{Max}) = \sum_{m=-m_{Max}}^{m_{Max}} e^{im(\phi-\alpha)} = \sum_{m=-m_{Max}}^{m_{Max}} \Delta m\, e^{im(\phi-\alpha)} \cong \int_{-k_{Max}}^{k_{Max}} dk \frac{\Delta m}{dk} e^{ik\frac{N}{2\pi}(\phi-\alpha)}$$
$$\cong \frac{e^{i\frac{k_{Max}N}{2\pi}(\phi-\alpha)} - e^{-i\frac{k_{Max}N}{2\pi}(\phi-\alpha)}}{i(\phi-\alpha)} = 2\frac{\sin\frac{k_{Max}N(\phi-\alpha)}{2\pi}}{(\phi-\alpha)} = 2\frac{\sin m_{Max}(\phi-\alpha)}{\phi-\alpha} \qquad (6.27)$$

This geometric sum verifies our suspect's culpability. The sum rings according to the highest m_{Max}-terms while lesser *m*-terms seem to experience an interference cancellation. The last-one-in is what shows.

Ringing supressed: m_{Max}-term Gaussian packets

Ringing is reduced by tapering off higher-*m* waves so they cancel each other's ringing and no single wave dominates. A Gaussian $e^{-(m/\Delta m)^2}$ taper makes cleaner "particle-like" pulses in Fig. 6.15.

$$S_{Guass}(m_{Max}) = \frac{1}{2\pi}\sum_{m=-\infty}^{\infty} e^{-\frac{m^2}{\Delta m^2}} e^{im\phi} = \frac{1}{2\pi}\sum_{m=-\infty}^{\infty} e^{-\pi\left(\frac{m}{m_{Max}}\right)^2} e^{im\phi}, \text{ where: } \Delta m = \frac{m_{Max}}{\sqrt{\pi}} \qquad (6.28a)$$

Completing the square of the exponents extracts a Gaussian ϕ-angle wavefunction $e^{-(\Delta m\phi/2)^2}$ with an angular uncertainty $\Delta\phi$ that is twice the inverse of the momentum quanta uncertainty Δm. *($\Delta\phi = 2/\Delta m$).*

$$S_{Guass}(m_{Max}) = \frac{1}{2\pi}\sum_{m=-\infty}^{\infty} e^{-\left(\frac{m}{\Delta m} - i\frac{\Delta m}{2}\phi\right)^2 - \left(\frac{\Delta m}{2}\phi\right)^2} = \frac{A(\Delta m,\phi)}{2\pi} e^{-\left(\frac{\Delta m}{2}\phi\right)^2} \qquad (6.28b)$$

Definition $\Delta m = m_{Max}/\sqrt{\pi}$ of momentum uncertainity relates *half-width-($^1/_e$)th-maximum Δm* to the value $m=m_{Max}$ for which the taper $e^{-(m/\Delta m)^2}$ is $e^{-\pi}$. ($e^{-\pi} = 0.04321$ is an easy-to-recall number near *4%*. Waves $e^{im\phi}$ beyond $e^{im_{Max}\phi}$ have $e^{-(m/\Delta m)^2}$ amplitudes below $e^{-\pi}$.) Amplitude $A(\Delta m,\phi)$ becomes an integral for large m_{Max} as does (6.27). Then $A(\Delta m,\phi)$ approaches a Gaussian integral whose value itself is m_{Max}.

$$A(\Delta m,\phi) = \sum_{m=-\infty}^{\infty} e^{-\left(\frac{m}{\Delta m} - i\frac{\Delta m}{2}\phi\right)^2} \xrightarrow[\Delta m >> 1]{} \int_{-\infty}^{\infty} dk\, e^{-\left(\frac{k}{\Delta m}\right)^2} = \sqrt{\pi}\Delta m = m_{Max} \qquad (6.28c)$$

The resulting Gaussian wave $e^{-(\phi/\Delta\phi)^2}$ has angular uncertainty $\Delta\phi = \phi_{Max}/\sqrt{\pi}$ defined analogously to Δm.

$$S_{Guass}(m_{Max}) \cong \frac{1}{2\pi}\sum_{m=-m_{Max}}^{m_{Max}} e^{-\left(\frac{m}{\Delta m}\right)^2} e^{im\phi} = \frac{m_{Max}}{2\pi} e^{-\left(\frac{\Delta m}{2}\phi\right)^2} = \frac{m_{Max}}{2\pi} e^{-\left(\frac{\phi}{\Delta\phi}\right)^2} \text{ where: } \Delta\phi = \frac{\phi_{Max}}{\sqrt{\pi}} \qquad (6.28d)$$

Uncertainty relations in Fig. 6.15 are stated using Δm and $\Delta\phi$ or in terms of *4%* limits m_{Max} and ϕ_{Max}.

$$\Delta m \cdot \Delta\phi = 2 \qquad (6.29a) \qquad\qquad m_{Max} \cdot \phi_{Max} = 2\pi \qquad (6.29b)$$

In Fig. 6.14, the number of pulse widths in interval 2π is the the number m_{Max} of *(>4%)*-Fourier terms.

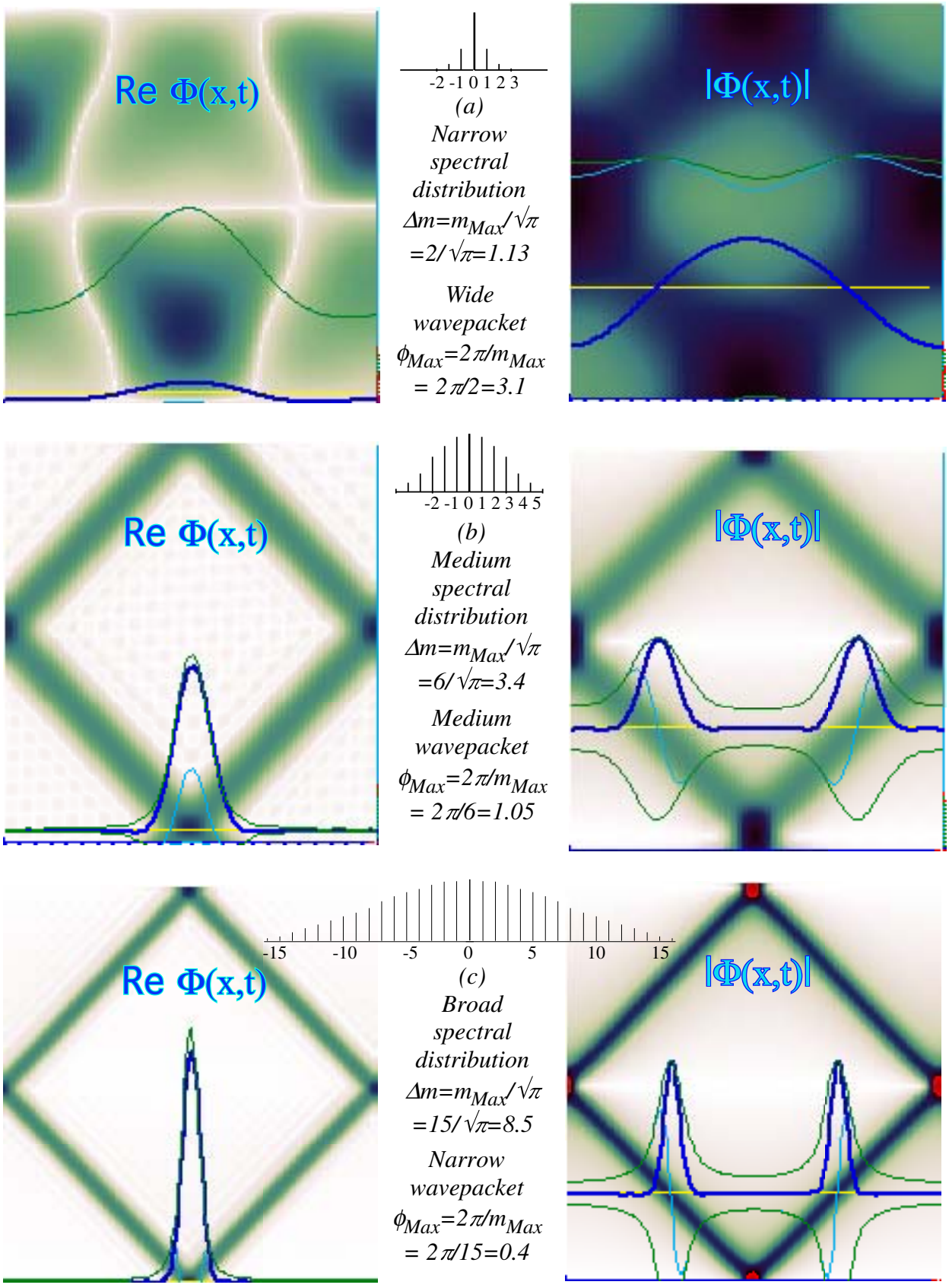

Fig. 6.15 Gaussian wavepackets. (Ringing is reduced compared to Fig. 6.14.)